UNIVERSITY OF CALIFORNIA

Los Angeles

Molecular and Genetic Study of Human Liposarcoma

A dissertation submitted in partial satisfaction of the

requirements for the degree of Doctor of Philosophy

in Molecular and Medical Pharmacology

by

Kathleen Barzan Smith

2012

ABSTRACT OF THE DISSERTATION

Molecular and Genetic Study of Human Liposarcoma

by

Kathleen Barzan Smith

Doctor of Philosophy in Molecular and Medical Pharmacology

University of California, Los Angeles, 2012

Professor Frederick C. Eilber, Co-chair

Professor Hong Wu, Co-chair

Sarcomas are cancers of connective tissue, such as bone, nerves, and muscle. Liposarcoma, a neoplasm arising within adipose tissue, is the most common soft tissue sarcoma. Although most commonly found in the retroperitoneum or thighs, liposarcomas can arise throughout the body and are often large when found. Current treatment is limited to surgery and radiation, with chemotherapy doing little to improve prognosis in advanced cases. Due to the large size of tumors and their proximity to organs and healthy tissue, complete surgical removal is difficult and recurrence rates remain high. Liposarcoma can be divided into three histological subtypes: pleomorphic, myxoid/round cell, and well-/dedifferentiated. Here we demonstrate the generation of three novel dedifferentiated liposarcoma xenograft models from freshly resected patient tissue. These xenograft models and their derived cultured cells successfully recapitulate the morphological and gene expression profiles of their patient tumors throughout serial passage in mice. Interestingly, the patients whose tumors could engraft and be serially passaged had significantly shorter survival than patients whose tumors did not engraft. These

tumors carried gene expression signatures with more aggressive and less differentiated features. We then show the use of these newly developed xenografts in pre-clinical studies of the mTOR inhibitor rapamycin and the multi-kinase inhibitor sorafenib as potential therapies for dedifferentiated liposarcoma. Although only one of the three xenografts responded to treatment with slowed tumor growth, all three tumors show distinct morphological changes in response to combination treatment with rapamycin and sorafenib, such as increased necrosis and decreased cell density. Interestingly, combination treatment also elicited a partial differentiation response as demonstrated by changes in lipid content and gene expression signatures. Taken together, these studies have created a flexible xenograft model that successfully recapitulates the human disease and will serve as a useful tool to further understand this complex disease and screen potential therapies.

The dissertation of Kathleen Barzan Smith is approved.

Peter J. Tontonoz

Heather R. Christofk

Frederick C. Eilber, Committee Co-chair

Hong Wu, Committee Co-chair

University of California, Los Angeles

2012

Dedicated to the sarcoma community and Connie and Phil Smith:

for giving me perspective and motivation for my research

TABLE OF CONTENTS

LIST OF FIGURES AND TABLES

Chapter 1:

Chapter 2:

Chapter 3:

ACKNOWLEDGEMENTS

I would first like to acknowledge the funding I received from the UCLA Tumor Cell Biology USHHS Ruth L. Kirchstein Institutional National Research Service Award #T32-34 CA009056 from 2007-2010, the Dissertation Year Fellowship from the Graduate Division received in 2011-2012, and the Travel Award from the Department of Molecular and Medical Pharmacology the fall of 2011. This work is supported by in part by seed grants from UCLA Institute for Molecular Medicine, Jonsson Comprehensive Cancer Center, and grant from National Institutes of Health (P50 CA086306 to H Wu and FC Eilber).

Chapter 2 is a version of a manuscript that has been submitted for publication, and I would like to acknowledge the co-authors: LM Tran, BM Tam, Y Li, EM Shurell, D Braas, HR Christofk, WD Tap, SM Dry, FC Eilber, and H Wu. K.B.S., H.W., F.C.E., and S.M.D. conceived of and designed the experiments. F.C.E., E.M.S., W.D.T., and S.M.D. provided the surgical specimens and clinical history and pathological evaluation; and K.B.S. and B.M.T. conducted the animal studies. Y.L. performed immunohistochemistry and slide scanning. K.B.S. and S.M.D. performed histopathological analysis. D.B. and H.C. conducted cell culture studies. L.M.T. and W.D.T. conducted the genetic and statistical analysis for the microarrays. K.B.S., L.M.T and H.W. compiled data and wrote the manuscript, and all authors revised the manuscript and agreed on the contents and conclusions.

The appendices are reprints of previous publications, which appear in the following journals:

Appendix 1: *Genes Chromosomes Cancer.* 2011 Feb;50(2):95-112. Copyright permission to reprint has been granted by John Wiley and Sons. I would like to acknowledge the contribution of the co-authors: WD Tap, FC Eilber, C Ginther, SM Dry, N Reese, HW Chen, H Wu, FR Eilber, DJ Slamon, and L Anderson.

Appendix 2: *Proc Natl Acad Sci* U S A. 2009 Oct 21. Reprint allowed for dissertations. I would like to acknowledge the co-authors: C Gregorian, J Nakashima, SM Dry, PL Nghiemphu, Y Ao, J Dang, G Lawson, IK Mellinghoff, PS Mischel, M Phelps, LF Parada, X Liu, MV Sofroniew, FC Eilber, and H Wu.

First and foremost, I would like to thank the patients and their families for participating in this research. I would not have a project without their donation, and I truly appreciate their gift to science.

Much of my gratitude goes to my advisor, Hong Wu, who taught me how to ask the right questions and be a good scientist. She took a chance on a project that was not the typical area of study or methodology for the lab, and I will forever be grateful for that opportunity. She never asked anything of me that I could not do and often gave me the confidence to do it.

To the members of my committee: Peter Tontonoz, Heather Christofk, and Fritz Eilber. Peter's paper from 1997 regarding the differentiation of liposarcoma cell lines truly inspired me, and became something I referred to often. Heather and her lab were our collaborators in studying liposarcoma and helped tremendously with the cell culture studies. Fritz gave me a project - he brought in all of the fresh patient samples and taught me about liposarcoma as a clinical

disease. He also always kept me connected to the “bed-side” part of the research, which has now become my favorite part.

To the sarcoma squad: Bill Tap, Sarah Dry, Brenna Tam, Liz Shurell, Linh Tran, Yunfeng Li, and Jonathan Nakashima. Bill provided samples, microarray services, and sorafenib. In addition, he has been a wonderful scientific and medical mind who has helped me greatly with understanding the treatment side of oncology. Sarah helped me value what I was looking at under the microscope, always answered my questions, and shared in my joy when the xenografts looked like the patient tumors. Brenna taught me how to properly plan experiments. She brought her experience and helped me with the xenograft system. She also became a good friend, which was even more fun with Liz around. Liz is my key to the clinical world and my connection to the Midwest – and I feel like my twin sometimes. Linh did all of the microarray analysis, and she even patiently described it to me so I could understand. Yunfeng is the IHC guru who saved me from being afraid of it. Jonathan was the first person I truly got to know in the lab during my rotation, and he taught me the ropes.

To team pancreas – for always being willing to have a little fun. To all members of the Hong Wu lab, past and present, it has always been fun and you truly have become like a family to me.

To the members of ACCESS 13 for always having fun and making my first year memorable! To the members of the Molecular and Medical Pharmacology family, past and present, who threw the best retreats, pubs, and Halloween parties, and who have the best administrative staff a graduate student could ever dream of. To the UCLA Masters Swim Team, for maintaining my sanity and introducing me to some of the greatest people I’ve ever met who helped keep me going the last few years.

To my family – my sister for always being a wonderful role model and a good friend; my parents for always believing in me, letting me blow bubbles on the kitchen table, and encouraging me to follow my dreams; my Aunt Gin, Grandma Jeanne, and Pop for being supportive; and my Grandma Gloria and Grandpa Leu for good memories and giving me perspective on my work.

Last but not least, thank you to my husband, who moved across the country so I could pursue my dreams. Thank you for putting up with me, having patience, cooking, picking me up when I worked late, and always making me laugh.

VITA

2004	B.S. in Biology, minor in Psychology Purdue University, West Lafayette, IN
Summers 2002-2003	Intern Shedd Aquarium, Chicago, IL
2003-2004	Teaching Intern Purdue University, West Lafayette, IN
Summer 2004	Intern Florida Program for Shark Research Gainesville, FL
2005-2006	Research Technician Lab of Dr. James Fleet Purdue University, West Lafayette, IN
2006-2012	Graduate student researcher Department of Molecular and Medical Pharmacology University of California, Los Angeles
2007-2010	Training grant recipient Tumor Cell Biology University of California, Los Angeles
2008-2009	Teaching assistant Department of Molecular, Cell, and Developmental Biology University of California, Los Angeles
2009	Graduate student representative Department of Molecular and Medical Pharmacology University of California, Los Angeles
2011	Travel award recipient Department of Molecular and Medical Pharmacology University of California, Los Angeles
2011-2012	Dissertation year fellowship recipient Graduate Division University of California, Los Angeles

PUBLICATIONS AND PRESENTATIONS

Publications:

Tap WD, Eilber FC, Ginther C, Dry SM, Reese N, **Barzan-Smith K,** Chen HW, Wu H, Eilber FR, Slamon DJ, Anderson L. (2011) Evaluation of well-differentiated/de-differentiated liposarcomas by high-resolution oligonucleotide array-based comparative genomic hybridization. *Genes Chromosomes Cancer.* 2011 Feb;50(2):95-112.

Gregorian C, Nakashima J, Dry SM, Nghiemphu PL, **Smith KB**, Ao Y, Dang J, Lawson G, Mellinghoff IK, Mischel PS, Phelps M, Parada LF, Liu X, Sofroniew MV, Eilber FC, Wu H. (2009) PTEN dosage is essential for neurofibroma development and malignant transformation. *Proc Natl Acad Sci* U S A. 2009 Nov 17;106(46):19479-84. PMCID: PMC2765459

Gregorian C, Nakashima J, Le Belle J, Ohab J, Kim R, Liu A, **Smith KB**, Groszer M, Garcia AD, Sofroniew MV, Carmichael ST, Kornblum HI, Liu X, Wu H. (2009) Pten deletion in adult neural stem/progenitor cells enhances constitutive neurogenesis. *J Neurosci*. 2009 Feb 11; 29(6):1874-86. PMCID: PMC2754186

Fleet JC, Gliniak C, Zhang Z, Xue Y**, Smith KB**, McCreedy R, Adedokun SA. (2008) Serum Metabolite Profiles and Target Tissue Gene Expression Define the Effect of Cholecalciferol Intake on Calcium Metabolism in Rats and Mice. *Journal of Nutrition.* 2008; *138*, 1114-1120.

Poster presentations:

Smith KB, Tran L, Tam BM, Braas D, Li Y, Tap WD, Christofk H, Dry SM, Eilber FC, Wu H. Patient-derived xenograft models of human liposarcomas. *Connective Tissue Oncology Society Annual Meeting.* Chicago, IL, October 2011.

Smith KB, Nakashima J, Tam B, Tap WD, Eilber, FC, and Wu H. Understanding liposarcoma metabolism. *Keystone Symposia on Molecular and Cellular Biology: Metabolism and Cancer Progression.* Vancouver, BC, March 2010.

Chapter 1:

Introduction

Clinical characteristics of liposarcoma

Sarcoma is a rare subset of cancers that arises within connective tissue, such as bone, muscle, and nerves. There are more than 50 subtypes of sarcoma that can be categorized into two basic groups: soft tissue sarcoma or bone and joint sarcoma. Soft tissue sarcomas comprise about 1% of all cancers diagnosed in the United States, with approximately 10,980 new cases per year (Jemal, Siegel et al. 2009). Liposarcoma, a neoplasm arising within adipose tissue, is the most frequently occurring soft tissue sarcoma, accounting for approximately 20% of all cases (Dalal, Antonescu et al. 2008). Liposarcoma can be divided into three histological subtypes: pleomorphic, myxoid/round cell, and well-/dedifferentiated. The morphology of the cells and extent of differentiation determine the subtype and grade of the tumor. Well-differentiated and myxoid liposarcomas are low grade, slow growing tumors, while pleomorphic, round cell, and dedifferentiated liposarcomas are high grade, aggressive tumors with a risk of metastasis (Dalal, Antonescu et al. 2008; Conyers, Young et al. 2011). The well-/dedifferentiated subtypes comprise the majority of liposarcomas, accounting for 46% and 18% respectively, with myxoid/round cell accounting for 28%. Pleomorphic liposarcoma is rare, accounting for only 8% of liposarcoma, and will not be the focus of this paper (Dalal, Antonescu et al. 2008).

Liposarcoma can occur throughout the body, but they most frequently arise within the thigh and retroperitoneum. Prognosis of liposarcoma is dependent on many factors, including age, gender, presentation status, histological subtype, location, depth, and tumor burden (Dalal, Kattan et al. 2006). Patients with extremity tumors have a better disease specific survival than patients with tumors in the retroperitoneum (Fig. 1-1A). Regardless of primary location, histological subtype plays a large role in survival as well (Fig. 1-1B). 5-year disease specific survival ranges from 44% for dedifferentiated liposarcoma to 93% for well-differentiated (Dalal, Kattan et al. 2006). While low grade tumors have very little chance of metastasizing, there is a

32% chance of local recurrence within 3 years of diagnosis – the risk increasing with each recurrence. High grade tumors have an 80% chance of local recurrence and 30% chance of distance recurrence or metastasis within 3 years of diagnosis (Singer, Antonescu et al. 2003).

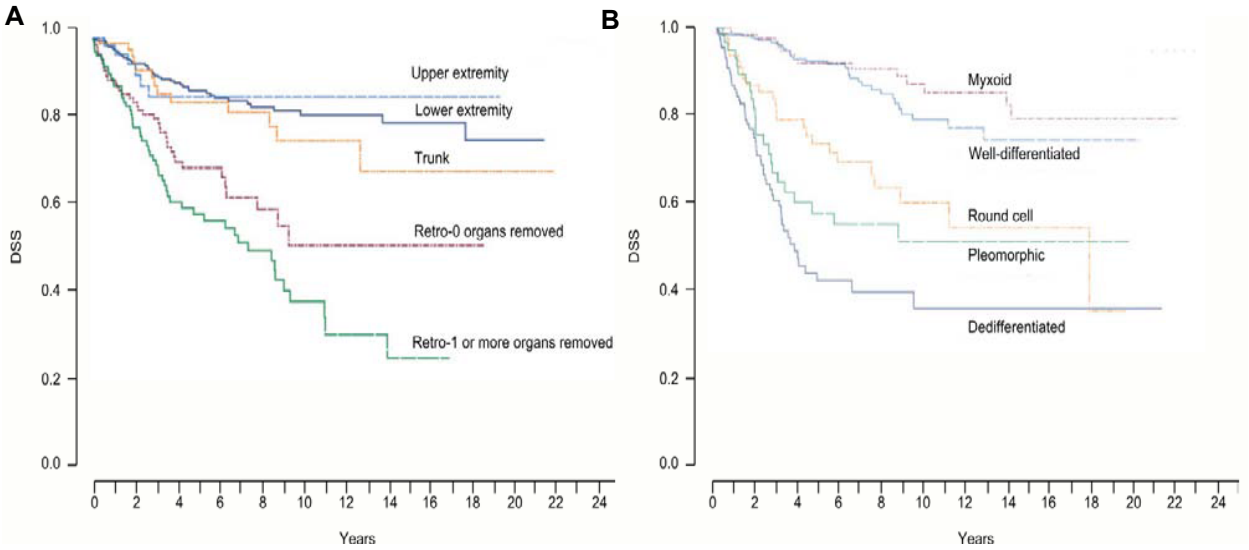

Figure 1-1. Disease specific survival (DSS) of liposarcoma patients stratified by tumor site (**A**) and histological subtype (**B**). Modified from (Dalal, Kattan et al. 2006).

The main treatment options for liposarcoma are still limited to surgery and radiation. Surgery is the only known curative treatment, but tumors are often difficult to remove with clean margins due to their large size and proximity to organs and muscle. Radiation is often effective in high-grade extremity liposarcoma to decrease chances of local recurrence, but it is difficult to deliver to retroperitoneal liposarcoma without damaging healthy tissue and vital organs. Response to chemotherapy in advanced disease is dependent on histological subtype, such that myxoid/round cell and pleomorphic liposarcomas show higher response rates than dedifferentiated liposarcomas (Dalal, Antonescu et al. 2008). Overall, 50% of patients with liposarcoma will die of disease, accentuating a great need to study the molecular mechanisms driving liposarcomagenesis to design better treatment options (Crago and Singer 2011).

Molecular biology of liposarcoma

Liposarcoma is thought to arise from mesenchymal stem cells (MSCs) that have been interrupted during differentiation to become adipocytes. One study shows a correlation between histological subtypes and stages of developmental progression of MSCs into adipocytes. In this study, human MSCs were differentiated into adipocytes *in vitro* and gene expression was analyzed at various steps throughout the process. The gene expression of the different stages of differentiation was compared to gene expression from liposarcomas divided into histological subtypes. The results showed that each liposarcoma subtype corresponded to a different stage of adipogenesis. Dedifferentiated liposarcomas were most like the MSCs, followed by pleomorphic, myxoid/round cell, and well-differentiated was most like normal adipocytes (Fig. 1-2) (Matushansky, Hernando et al. 2008).

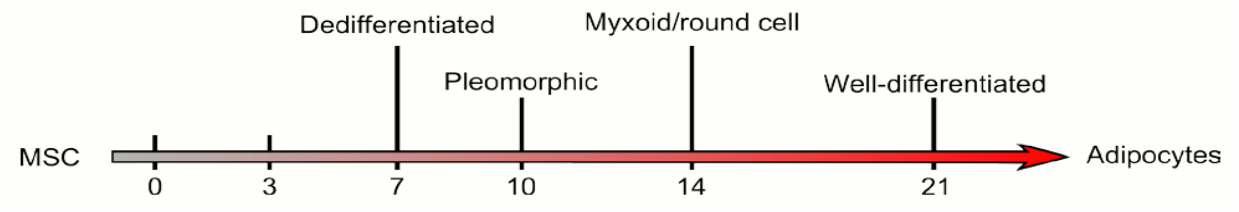

Figure 1-2. Histological subtypes of liposarcoma as they correspond to different stages of adipocyte differentiation. Number indicates day of *in vitro* differentiation. Modified from (Matushansky, Hernando et al. 2008).

Genetically, sarcomas can be di vided into two main groups: simple and complex karyotypes. Those with simple karyotypes harbor a disease-specific chromosomal translocation, while sarcomas with complex karyotypes show severe genomic disturbance and instability. Myxoid/round cell liposarcomas have a simple karyotype, caused by a chromosomal translocation between chromosome 12 and either 16 or 22, creating the *FUS-DDIT3* or *EWSR1-DDIT3* fusion gene (Helman and M eltzer 2003). DDIT3, also known as CHOP, is stress-

induced mediator of cell death and negative regulator of the transcription factor C/EBP. While the exact function of the fusion protein is not fully understood, it is thought to inhibit adipogenesis, thereby allowing the cells to continually proliferate (Conyers, Young et al. 2011; Hoffman, Lazar et al. 2011). Well-differentiated and dedifferentiated liposarcomas are considered to have complex karyotypes, showing many chromosomal rearrangements and mutations (Fig. 1-3A). The most characteristic mutation found in more than 90% of well-differentiated and dedifferentiated liposarcoma tumors is amplification within the long arm of chromosome 12 (12q13-23) (Fig. 1-3B). This locus carries genes such as *MDM2*, *HMGA2*, and *CDK4* (Barretina, Taylor et al. 2010). While the chromosome 12q amplicons are the most characterized, amplifications of areas on chromosomes 1 and 6q have also been described in well-differentiated and dedifferentiated liposarcoma (Fig. 1-3A) (Tap, Eilber et al. 2011).

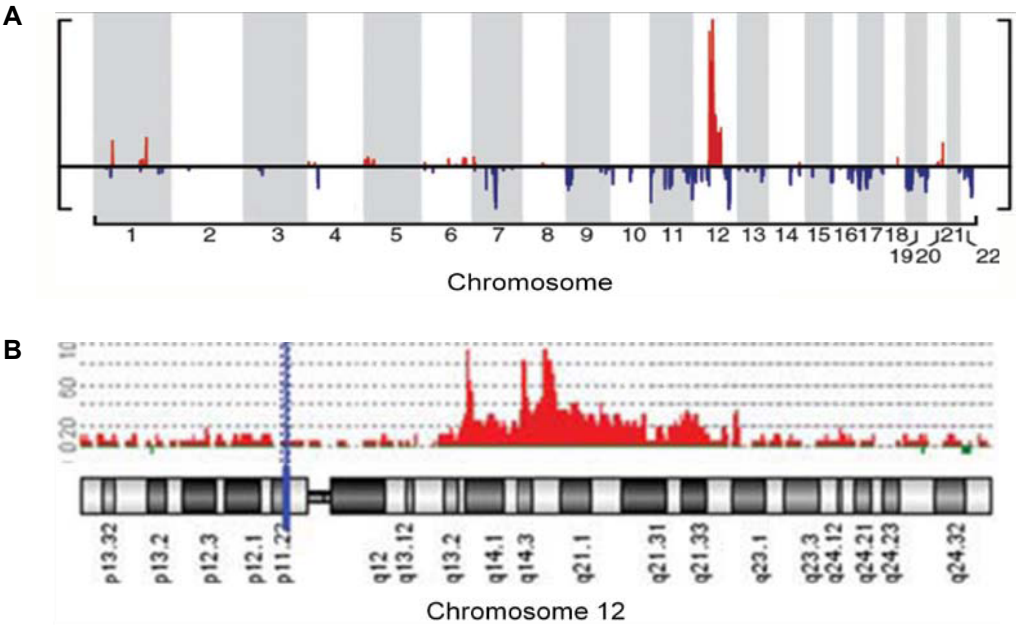

Figure 1-3. Chromosomal abnormalities common in dedifferentiated liposarcoma. A) Genome-wide map of chromosomal amplifications (red, above bar) and deletions (blue, below bar). **B)** Map of chromosome 12, which has the most common amplifications in dedifferentiated liposarcoma. Modified from (Barretina, Taylor et al. 2010; Tap, Eilber et al. 2011).

Model systems for studying liposarcoma

As we learn more about the genetic lesions present in liposarcoma, it is important to distinguish which aberrations are driving malignant transformation, such as with a model system. An ideal model system recapitulates the human disease, adds to the understanding of the disease, and allows for testing potential therapies. Genetically engineered animal models are often used to study diseases such as cancer. Two such mouse models exist for myxoid liposarcoma, in which mice express the *FUS-CHOP* fusion gene (Perez-Losada, Pintado et al. 2000; Charytonowicz, Terry et al. 2012). Recently, a mouse that develops spontaneous well-differentiated liposarcoma was discovered. In this model, IL-22 was over expressed in adipose tissue under the aP2 promoter. When fed a normal chow diet, the mice did not develop any tumors. However, when fed a high fat diet for 4 months, the mice developed well-differentiated liposarcomas (Wang, Yang et al. 2011). Another model recently created is a zebrafish model expressing a transactivation-defective p53 protein and a constitutively active Akt2 protein. Although *p53* mutation alone was not enough to induce tumor formation, 29% of the *p53* homozygous mutants with Akt2 activation developed well-differentiated liposarcoma (Gutierrez, Snyder et al. 2011). Taken together, these genetic models help identify potential driving mutations and conditions for liposarcomagenesis.

Another common method for modeling cancer is a xenograft system. This system utilizes an immune compromised mouse host to grow human tissue either directly from a tissue sample or from cultured cells. Xenografts generated directly from human tissue, also known as tumorgrafts, have been shown to be predictive of clinical response to drug treatment (Kerbel 2003; Garber 2009). One group demonstrated consistent genetic, morphologic, and pharmacologic features of myxoid liposarcoma patient tumors and their resulting xenografts (Frapolli, Tamborini et al. 2010). Other groups have used xenograft models to study

chromosomal changes in sarcomas and find potential therapeutic targets for liposarcomas (Peng, Zhang et al. 2011; Kresse, Meza-Zepeda et al. 2012).

Perhaps the most common way to study cancer is with cell lines. While several liposarcoma cell lines have been created, only one is commercially available (Wabitsch, Bruderlein et al. 2000; Nishio, Iwasaki et al. 2003; Hugo, Brandebourg et al. 2006; Ariizumi, Ogose et al. 2011). Cell lines are useful for studying the mechanisms behind disease, such as the finding that *ZIC1*, a transcription factor involved in neuronal development, is overexpressed in liposarcoma. Upon knockdown in liposarcoma cell lines, proliferation and invasion were reduced, and apoptosis was increased (Brill, Gobble et al. 2010). Cell lines are also useful for screening potential therapeutics, such as the MDM2 inhibitor Nutlin-3A (Ambrosini, Sambol et al. 2007; Muller, Paulsen et al. 2007).

Potential therapies for liposarcoma

As the field of cancer biology expands, we learn more about the mechanisms underlying the cause of the disease and therefore can design more effective therapies. Drugs are designed to effect specific pathways known to be aberrantly regulated in the cancer of interest. These therapies typically have much fewer side effects than traditional chemotherapy and radiation and are often easier to take. Because liposarcomas are thought to be MSCs interrupted along their differentiation to becoming adipocytes, one proposed therapy has been to restart the differentiation process. One study was able to accomplish this *in vitro* using an agonist for the nuclear receptor PPARγ. PPARγ (peroxisome proliferator-activated receptor γ) is considered to be the master regulator of adipogenesis. After adding an artificial ligand of PPARγ to liposarcoma cell lines, the cells reached terminal differentiation and withdrawal from cell cycle (Tontonoz, Singer et al. 1997). Even though initial clinical results with similar

compounds were disappointing, this type of therapy is still being studied (Demetri, Fletcher et al. 1999; Debrock, Vanhentenrijk et al. 2003). Trabectedin, a cytotoxic chemotherapy, has been shown to induce differentiation in myxoid liposarcomas *in vitro* and *in vivo*, an effect that is further enhanced by the addition of a PPARγ ligand (Forni, Minuzzo et al. 2009; Charytonowicz, Terry et al. 2012).

Because *MDM2* is amplified in most well-differentiated and dedifferentiated liposarcomas, it is an attractive target for small molecule therapies. MDM2 is an E3 ubiquitin ligase that negatively regulates the tumor suppressor p53. Preventing the interaction between MDM2 and p53 would reactivate p53 signaling and allow the cells to restore the DNA damage response. The MDM2 antagonist, Nutlin-3a, has shown promising results *in vitro* for several liposarcoma cell lines by inducing apoptosis (Ambrosini, Sambol et al. 2007; Muller, Paulsen et al. 2007). A clinical trial for the MDM2 inhibitor, RO5045337, is currently ongoing in patients with liposarcoma (ClinicalTrials.gov identifier: NCT01143740).

Another commonly targeted pathway is the PI3K/AKT/mTOR pro-survival pathway. This pathway is frequently upregulated in cancers by one or more mechanisms, including mutations to the regulating subunits of PI3K or its negative regulator *PTEN*. Dual inhibition of PI3K and AKT with small molecules slowed *in vitro* proliferation, induced cell cycle arrest and apoptosis, and decreased xenograft growth of several soft tissue sarcoma cell lines, including liposarcoma (Zhu, Ren et al. 2008). Inhibition of mTOR with rapamycin or its derivatives has been shown to have clinical benefit in soft tissue sarcomas, as well as radiosensitizing cultured cells and reducing angiogenesis in mouse models (Murphy, Spalding et al. 2009). A recently published clinical trial of ridaforolimus, a rapamycin analog and inhibitor of mTOR, showed a 29.5% clinical benefit response in the liposarcoma patients tested (Chawla, Staddon et al. 2012). The information presented here shows that while the understanding of liposarcoma and its mechanisms are expanding, there is still much to be learned to allow for more potential therapies and better modeling of this complex disease.

Specific aims of the dissertation

The first objective of these studies was to develop *in vivo* and *in* vitro model systems for liposarcoma that successfully recapitulate the human disease. After creating xenograft models from freshly resected human samples, we sought to determine genetic and biological properties of these tumors that allowed them to engraft in a murine host. Most importantly, we used the newly created xenograft models for testing small molecule inhibitors alone and in combination as potential therapeutic options for liposarcoma.

References

Ambrosini G, Sambol EB, Carvajal D, Vassilev LT, Singer S and Schwartz GK. (2007) Mouse double minute antagonist Nutlin-3a enhances chemotherapy-induced apoptosis in cancer cells with mutant p53 by activating E2F1. *Oncogene.* 26(24): 3473-3481.

Ariizumi T, Ogose A, Kawashima H, Hotta T, Li G, Xu Y, et al. (2011) Establishment and characterization of a novel dedifferentiated liposarcoma cell line, NDDLS-1. *Pathol. Int.* 61(8): 461-468.

Barretina J, Taylor BS, Banerji S, Ramos AH, Lagos-Quintana M, Decarolis PL, et al. (2010) Subtype-specific genomic alterations define new targets for soft-tissue sarcoma therapy. *Nat. Genet.* 42(8): 715-721.

Brill E, Gobble R, Angeles C, Lagos-Quintana M, Crago A, Laxa B, et al. (2010) ZIC1 overexpression is oncogenic in liposarcoma. *Cancer Res.* 70(17): 6891-6901.

Charytonowicz E, Terry M, Coakley K, Telis L, Remotti F, Cordon-Cardo C, et al. (2012) PPARgamma agonists enhance ET-743-induced adipogenic differentiation in a transgenic mouse model of myxoid round cell liposarcoma. *J. Clin. Invest.* 122(3): 886-898.

Chawla SP, Staddon AP, Baker LH, Schuetze SM, Tolcher AW, D'Amato GZ, et al. (2012) Phase II study of the mammalian target of rapamycin inhibitor ridaforolimus in patients with advanced bone and soft tissue sarcomas. *J. Clin. Oncol.* 30(1): 78-84.

Conyers R, Young S and Thomas DM. (2011) Liposarcoma: molecular genetics and therapeutics. *Sarcoma.* 2011.

Crago AM and Singer S. (2011) Clinical and molecular approaches to well differentiated and dedifferentiated liposarcoma. *Curr. Opin. Oncol.* 23(4): 373-378.

Dalal KM, Antonescu CR and Singer S. (2008) Diagnosis and management of lipomatous tumors. *J. Surg. Oncol.* 97(4): 298-313.

Dalal KM, Kattan MW, Antonescu CR, Brennan MF and Singer S. (2006) Subtype specific prognostic nomogram for patients with primary liposarcoma of the retroperitoneum, extremity, or trunk. *Ann. Surg.* 244(3): 381-391.

Debrock G, Vanhentenrijk V, Sciot R, Debiec-Rychter M, Oyen R and Van Oosterom A. (2003) A phase II trial with rosiglitazone in liposarcoma patients. *Br. J. Cancer.* 89(8): 1409-1412.

Demetri GD, Fletcher CDM, Mueller E, Sarraf P, Naujoks R, Campbell N, et al. (1999) Induction of solid tumor differentiation by the peroxisome proliferator-activated receptor-g ligand troglitazone in patients with liposarcoma. *Proceedings of the National Academy of Sciences.* 96: 3951-3956.

Forni C, Minuzzo M, Virdis E, Tamborini E, Simone M, Tavecchio M, et al. (2009) Trabectedin (ET-743) promotes differentiation in myxoid liposarcoma tumors. *Mol. Cancer Ther.* 8(2): 449-457.

Frapolli R, Tamborini E, EmanuelaVirdis, Bello E, Tarantino E, Marchini S, et al. (2010) Novel models of Myxoid Liposarcoma Xenografts mimicking the biological and pharmacological features of human tumors. *Clin. Cancer. Res.* 16: 4958-4967.

Garber K. (2009) From human to mouse and back: 'tumorgraft' models surge in popularity. *J. Natl. Cancer Inst.* 101(1): 6-8.

Gutierrez A, Snyder EL, Marino-Enriquez A, Zhang YX, Sioletic S, Kozakewich E, et al. (2011) Aberrant AKT activation drives well-differentiated liposarcoma. *Proc. Natl. Acad. Sci. U. S. A.* 108(39): 16386-16391.

Helman LJ and Meltzer P. (2003) Mechanisms of sarcoma development. *Nat Rev Cancer.* 3(9): 685-694.

Hoffman A, Lazar AJ, Pollock RE and Lev D. (2011) New frontiers in the treatment of liposarcoma, a therapeutically resistant malignant cohort. *Drug Resist Updat.* 14(1): 52-66.

Hugo ER, Brandebourg TD, Comstock CE, Gersin KS, Sussman JJ and Ben-Jonathan N. (2006) LS14: a novel human adipocyte cell line that produces prolactin. *Endocrinology.* 147(1): 306-313.

Jemal A, Siegel R, Ward E, Hao Y, Xu J and Thun MJ. (2009) Cancer statistics, 2009. *CA. Cancer J. Clin.* 59(4): 225-249.

Kerbel RS. (2003) Human tumor xenografts as predictive preclinical models for anticancer drug activity in humans: better than commonly perceived-but they can be improved. *Cancer biology & therapy.* 2(4 Suppl 1): S134-139.

Kresse SH, Meza-Zepeda LA, Machado I, Llombart-Bosch A and Myklebost O. (2012) Preclinical xenograft models of human sarcoma show nonrandom loss of aberrations. *Cancer.* 118(2): 558-570.

Matushansky I, Hernando E, Socci ND, Matos T, Mills J, Edgar MA, et al. (2008) A developmental model of sarcomagenesis defines a di fferentiation-based classification for liposarcomas. *Am. J. Pathol.* 172(4): 1069-1080.

Muller CR, Paulsen EB, Noordhuis P, Pedeutour F, Saeter G and Myklebost O. (2007) Potential for treatment of liposarcomas with the MDM2 antagonist Nutlin-3A. *Int. J. Cancer.* 121(1): 199-205.

Murphy JD, Spalding AC, Somnay YR, Markwart S, Ray ME and Hamstra DA. (2009) Inhibition of mTOR radiosensitizes soft tissue sarcoma and tumor vasculature. *Clin. Cancer. Res.* 15(2): 589-596.

Nishio J, Iwasaki H, Ishiguro M, Ohjimi Y, Fujita C, Ikegami H, et al. (2003) Establishment of a novel human dedifferentiated liposarcoma cell line, FU-DDLS-1: conventional and m olecular cytogenetic characterization. *Int. J. Oncol.* 22(3): 535-542.

Peng T, Zhang P, Liu J, Nguyen T, Bolshakov S, Belousov R, et al. (2011) An experimental model for the study of well-differentiated and dedifferentiated liposarcoma; deregulation of targetable tyrosine kinase receptors. *Lab. Invest.* 91(3): 392-403.

Perez-Losada J, Pintado B, Gutierrez-Adan A, Flores T, Banares-Gonzalez B, del Campo JC, et al. (2000) The chimeric FUS/TLS-CHOP fusion protein specifically induces liposarcomas in transgenic mice. *Oncogene.* 19(20): 2413-2422.

Singer S, Antonescu CR, Riedel E and Brennan MF. (2003) Histologic subtype and margin of resection predict pattern of recurrence and survival for retroperitoneal liposarcoma. *Ann. Surg.* 238(3): 358-370; discussion 370-351.

Tap WD, Eilber FC, Ginther C, Dry SM, Reese N, Barzan-Smith K, et al. (2011) Evaluation of well-differentiated/de-differentiated liposarcomas by high-resolution oligonucleotide array-based comparative genomic hybridization. *Genes Chromosomes Cancer.* 50(2): 95-112.

Tontonoz P, Singer S, Forman BM, Sarraf P, Fletcher JA, Fletcher CDM, et al. (1997) Terminal differentiation of human liposarcoma cells induced by ligands for peroxisome proliferator-activated receptor g and the retinoid X receptor. *Proceedings of the National Academy of Sciences.* 94: 237-241.

Wabitsch M, Bruderlein S, Melzner I, Braun M, Mechtersheimer G and Moller P. (2000) LiSa-2, a novel human liposarcoma cell line with a high capacity for terminal adipose differentiation. *Int. J. Cancer.* 88: 889-894.

Wang Z, Yang L, Jiang Y, Ling ZQ, Li Z, Cheng Y, et al. (2011) High fat diet induces formation of spontaneous liposarcoma in mouse adipose tissue with overexpression of interleukin 22. *PLoS One.* 6(8): e23737.

Zhu QS, Ren W, Korchin B, Lahat G, Dicker A, Lu Y, et al. (2008) Soft tissue sarcoma cells are highly sensitive to AKT blockade: a role for p53-independent up-regulation of GADD45 alpha. *Cancer Res.* 68(8): 2895-2903.

Chapter 2:

Development and validation of liposarcoma xenograft models

Abstract

Liposarcoma is the most common type of soft tissue sarcoma. Other than surgery and radiation, there are few effective treatments available for locally advanced or metastatic liposarcomas. Recent progress has been made toward identification of molecular and genetic alterations involved in liposarcoma development. However, few models of liposarcoma exist that accurately reflect the human disease and are amenable to testing of potential therapeutic agents. Here we describe the generation of liposarcoma xenograft models from freshly-resected liposarcoma samples. We show that xenograftability is directly correlated with pathological grade and disease specific survival of liposarcoma patients. Importantly, all xenografts recapitulate morphological and gene expression characteristics of the primary tumors even after continuous *in vivo* passages. Gene expression analyses highlight the association between xenograftability and upregulation of signaling pathways important in cellular proliferation and invasion. Furthermore, tumors that could be xenografted and serially passaged had a less-differentiated, more progenitor-like phenotype.

Introduction

Liposarcoma (LPS), a neoplasm arising within adipose tissue thought to originate from mesenchymal stem cells , is the most common type of soft tissue sarcoma and is associated with poor outcome (Skubitz and D'Adamo 2007; Dalal, Antonescu et al. 2008; Matushansky, Hernando et al. 2008; Snyder, Sandstrom et al. 2009). LPS is classified into 3 histological subtypes: well-differentiated/dedifferentiated (WD/DD), pleomorphic, and myxoid/round cell. The extent of differentiation, as reflected by histological grade, remains the most important determinant of outcome. The myxoid/round cell LPS typically have a characteristic chromosomal translocation creating the *TLS-CHOP* fusion gene, and WD/DD LPS have complex karyotypes, generally including two amplicons within chromosome 12q13–15 carrying genes such as *MDM2* and *CDK4*. However, there are likely additional pathway alterations associated with the malignancy that have yet to be identified (Dalal, Antonescu et al. 2008). The main treatment options for LPS are surgery and radiation. Chemotherapy for locally advanced or metastatic disease has little effect on the overall prognosis for patients with LPS (Eilber, Eilber et al. 2004; Kasper, Gil et al. 2007). This emphasizes the urgent need to understand the molecular mechanisms responsible for LPS development.

The establishment of a clinically relevant disease model is vital for studying the molecular mechanisms underlying LPS malignant transformation and evaluating emerging targeted therapies. Currently there are two genetic mouse models for myxoid liposarcoma (Rodriguez, Rubio et al. 2011; Charytonowicz, Terry et al. 2012) and a mouse model and zebra fish model for WD (Gutierrez, Snyder et al. 2011; Wang, Yang et al. 2011), but no genetic models exist for DD LPS. Given our limited knowledge of the cell-of-origin and major pathway alterations associated with LPS, it may take years to establish genetically engineered DD LPS mouse models. While xenograft models are commonly used, only one group has demonstrated

myxoid liposarcoma xenografts to successfully recapitulate the human disease (Frapolli, Tamborini et al. 2010).

In this study, we develop a direct LPS xenograft method by implanting and serially passaging freshly resected LPS samples from patients into immune deficient mice. Our analysis of the tumors identifies clinical and biological features associated with the ability to engraft. We demonstrate through histological and gene expression analysis that the xenografts and their subsequently derived cell lines recapitulate the human disease. These human xenograft models may facilitate LPS research and accelerate the generation of readily translatable preclinical data that will ultimately influence patient care.

METHODS

Collection of tumor samples

Patients with a suspected liposarcoma (LPS) who underwent surgery at UCLA were enrolled in an Institutional Review Board (IRB) approved tissue procurement protocol and gave informed consent. A sample of each tumor was sliced into sections with a sterile razor blade or scalpel and divided for genomic and gene expression analyses, histology, and the remaining xenograft implantation and tissue culture studies (described below). Histological review by a sarcoma pathologist (S.M.D.) confirmed diagnosis, subtype, and grade of tumors used in this study.

Xenograft implantation and passage

Mouse studies were performed using NOD.CB17-*Prkdc*^{scid}/J (common name NOD-*scid*) or NOD.Cg-*Prkdc*^{scid} *Il2rg*^{tm1Wjl}/SzJ (common name NSG) immune deficient mice acquired from in-house bred colonies at UCLA. For the initial xenograft, approximately 100 mg of the patient tumor was divided into approximately 1 cm^3 fragments and implanted subcutaneously in mice. Mice were maintained in barrier cages, on standard chow diet with food and water available *ad libitum*. Mice were maintained on sulfamethoxazole and trimethoprim (TMS, added to drinking

water) to prevent infection. All studies were performed in accordance with the Division of Laboratory Animal Medicine at the University of California Los Angeles.

Implanted samples were allowed a six month incubation period to form a palpable tumor. When successful engraftment occurred, tumors were collected before reaching 1.5 cm in diameter. Tumor fragments were then isolated for histology, gene expression analysis, and further passaged into additional mice. In some cases, tissue was collected for tissue culture or cryopreservation.

Single cell suspensions from tumors were generated using either mechanical dissociation or cell straining. For mechanical dissociation, the gentleMACS dissociator (Miltenyi Biotec Inc.) was used. Approximately 2 mg of tumor was added to a gentleMACS C tube containing enzymatic solution (collagenase (Gibco) in Dulbecco's Modified Eagle's Media (DMEM), 10% fetal bovine serum (FBS), 1% penicillin/streptomycin). The C tube was placed upside down onto the sleeve of the dissociator, and gentleMACS programs C and D were run in succession. The tube was removed from the machine and the material was applied to a 70 µm cell strainer, without force, into a 50 ml tube. The cell strainer was rinsed with Dulbecco's Phosphate Buffered Saline (DPBS), and the resulting solution was centrifuged, aspirated, and resuspended in DPBS. Another dissociation method involved cutting the tumor into 2–4 mm pieces and manual straining through a 100 µm cell filter into DPBS. The cells were centrifuged, aspirated, and resuspended in DPBS.

For cryopreservation, tissue was manually strained through a 100 µm cell into freezing media (10% dimethyl sulfoxide and 90% FBS). Cells were then gradually frozen in a –80 °C freezer and cryopreserved for at least 24 hours before being rapidly thawed in a 37 °C water bath. After adding DPBS, the cells were centrifuged, supernatant discarded, and resuspended in DPBS. Cells were counted on a hemocytometer using trypan blue exclusion and concentration was adjusted to $5x10^6$ cells ml^{-1}. Approximately $0.5–1.0x10^6$ cells were injected subcutaneously into mice with a 28 gauge needle on a 0.5 ml insulin syringe.

Tissue culture

Tumor tissue samples (200–300 mg) were minced with a scalpel and subsequently dissociated by carefully passing them in complete medium (basal media supplemented with 10% FBS and 1% penicillin/streptomycin) through a 40 µm cell strainer. Three basal media were tested: DMEM, DMEM in an equal ratio with Ham's F12 nutrient mixture (DMEM/F12), and Roswell Park Memorial Institute media (RPMI) 1640. Cells were centrifuged, resuspended in red cell lysis buffer (150 mM ammonium chloride, 1 mM potassium bicarbonate, 0.1 mM EDTA) and incubated at room temperature for 10 minutes. After centrifuging the cells, they were resuspended in complete medium and plated onto 6-well dishes (10^6 cells per well). Cell adhesion was observed 24 hours post plating, and confluent plates were expanded. Cells were maintained in a 37 °C incubator with 5% carbon dioxide and monitored for cell adhesion.

For inoculation in mice, 70% confluent cells were rinsed with DPBS and treated with 0.25% trypsin-EDTA (Invitrogen) until the cells separated from the dish. Complete media was added to quench the trypsin reaction, and the cells were centrifuged. The supernatant was aspirated and cells were resuspended in DPBS, counted on a hemocytometer using trypan blue exclusion, and adjusted to a concentration of $5x10^6$ cells ml^{-1}. $0.5–1.0x10^6$ cells were injected subcutaneously with a 28 gauge needle on a 0.5 ml insulin syringe.

Histology

In the case of either a patient tumor or a xenograft, a slice from the center of the tumor sample was saved for histological analysis, avoiding necrotic areas. The sample was fixed in 10% phosphate buffered formalin overnight and transferred into 50–70% ethanol. The tissue was then paraffin embedded with standard protocols, cut into 4 µm sections, and stained with hematoxylin and eosin (H&E) by the UCLA Translational Pathology Core Laboratory. Slides were digitally scanned at 400x with the Aperio XL system and images analyzed with

ImageScope software and Adobe Photoshop CS4. All slides were reviewed by a sarcoma pathologist (S.M.D).

For immunohistochemistry, formalin-fixed, paraffin-embedded patient tumor or xenograft tumor sections were deparaffinized in xylene and rehydrated in graded ethanol. Endogenous peroxidase activity was blocked with 3% hydrogen peroxide (H_2O_2). Antigen retrieval was performed by boiling the sections in 0.01 M citric acid buffer (pH 6.0) for 15 minutes. Sections were first blocked with 5% normal donkey serum in PBS, and then incubated with primary antibody against Ki67 (Vector laboratories, VP-RM04, 1:500) overnight at 4 °C. Sections were then incubated with biotinylated secondary antibody (1:500, Jackson ImmunoResearch Laboratories) for one hour at room temperature. Antibody binding was detected with Vectastain ABC Elite Kit (Vector Laboratories, PK-6100) and visualized with DAB (3,3'-diaminobenzidine, Vector Laboratories). Sections were counterstained in Gill's hematoxylin. Digital images of sections were obtained using a ScanScope XT System (Aperio Technologies Inc) at 200X magnification courtesy of the UCLA Translational Pathology Core Laboratory.

Proliferative activity was quantified as the percentage of positively stained Ki67 tumor cells relative to total tumor cells within the section. Five snapshots were taken from non-necrotic, representative areas of each slide. Positive and negative nuclei were tallied using the cell counter on ImageJ software, and a mean ± standard error (s.e.m.) positive index was calculated for each slide.

Oil red O staining

Frozen sections of liposarcomas were stained in a 0.3% oil red O/isopropyl alcohol solution for 7–10 minutes at room temperature. Excess stain was washed out in 60% isopropyl alcohol, followed by washes in 30% isopropyl alcohol and distilled water. Slides were counterstained with Harris hematoxylin, rinsed with two changes of tap water, and coverslips were mounted with glycerol. Slides were subsequently stored at 4° C.

Bodipy 493/503 staining

Bodipy 493/503 solid was dissolved in ethanol to reach a concentration of 1 mg ml^{-1}. Cells were grown on a coverslip placed in a cell culture dish. Upon reaching 70% confluence, cells were rinsed with PBS, fixed for 20 minutes in 4% paraformaldehyde, and rinsed again with PBS. Bodipy 493/503 was diluted in PBS to 1 µg ml^{-1} and added to the cells. Cells were incubated with shaking at room temperature for at least 15 minutes, washed 3 times with PBS, and mounted onto a slide with mounting media containing 4',6-diamidino-2-phenylindole (DAPI) to stain the nucleus.

Microarray

Procedures for sample preparation, RNA isolation, DNA isolation, array hybridization, and arrays were all as described in our previous paper (Tap, Eilber et al. 2011).

CGH and gene expression analysis

CGH Analytics software v.4.0 (Agilent Technologies) was used for copy number analysis, employing the ADM2 algorithm (threshold 5) with Fuzzy Zero and Centralization corrections to minimize background noise. A minimum of three consecutive probes were required to define a region as amplified or deleted.

In gene expression analysis, two-tail t-test was used for comparing expression between the xenograftable tumors and other high-grade LPS. For a gene represented by multiple probes, its representative p-value was the lowest p-value among the probes. Gene ontology analysis was conducted using pathway databases downloaded from Gene Ontology and Broad Institute Molecular Signature Database (Ashburner, Ball et al. 2000). Fisher's exact test was used to identify which gene ontology or biological pathway was significantly enriched by differentially expressed (t-test $P<0.05$ and fold-change>1.5) genes between unsuccessfully and successfully grafted high grade LPS groups. Cluster 3.0 and TreeView were used in hierarchical clustering analysis in which the expression profile of each gene was first

transformed to z-scores, and then samples were clustered by using average linkage method based on un-centered correlation coefficients as distance metric among samples.

Rank-rank hypergeometric overlap (http://systems.crump.ucla.edu/rankrank/)(Plaisier, Taschereau et al. 2010) was used to compare gene expression data from our samples versus gene expression of pre-adipocytes collected after 0, 3, and 7 days of induction in differentiation media (GEO accession ID: GSE28628) (Sohle, Machuy et al. 2012).

Statistical analysis

Multiple regression analysis was performed on clinical data from all 22 patients. Multiple predictors for engraftment and passage capability were tested, including disease status, gender, location of tumor, sample type (from primary, recurrent, or metastatic tumor), number of organs with tumor burden, margin status, presence of post-operative complications, chemotherapy prior to tumor sample collection, radiation therapy prior to tumor sample collection, grade, size of tumor, presence of multifocal disease, patient history of other cancer type, presence and/or development of metastasis, and histological subtype. Regression analysis was performed using STATA 11.0 (StataCorp). All statistical assessments were considered significant if $P<0.05$. Other statistical analyses were conducted with GraphPad Prism v.5.04 (GraphPad Software, Inc.).

RESULTS

Grade and disease specific survival are associated with xenograftability

To generate clinically relevant LPS models for investigating the molecular etiology of LPS and evaluating response to targeted therapies, we took a xenotransplantation approach by subcutaneously implanting fresh surgically resected LPS samples into immune compromised mice (Fig. 2-1A). Over a two year period, we implanted 22 tumors corresponding to two of the major subtypes of LPS [myxoid/round cell (n=5), WD (n=7) and DD (n=10)]. These tumors

varied in grade, site of origin, size, and treatment history (Table 2-1). Of the 10 DD samples, 8 came from tumors that had both well-differentiated and dedifferentiated components (as indicated by DD* in Table 2-1), but all DD areas were pathologically diagnosed as high grade and selected for xenografting. Within 6 months of implantation, 2/5 myxoid/round cell, 0/7 WD, and 5/10 DD samples produced palpable tumors, resulting in a 32% engraftment rate. Three of the DD xenografts, LPSX1, LPSX2 and LPSX3 (Table 2-1), could be serially passaged in mice (14% of all tumors, 43% of engrafted tumors), suggesting that the xenograft procedure may select tumors with specific biological features.

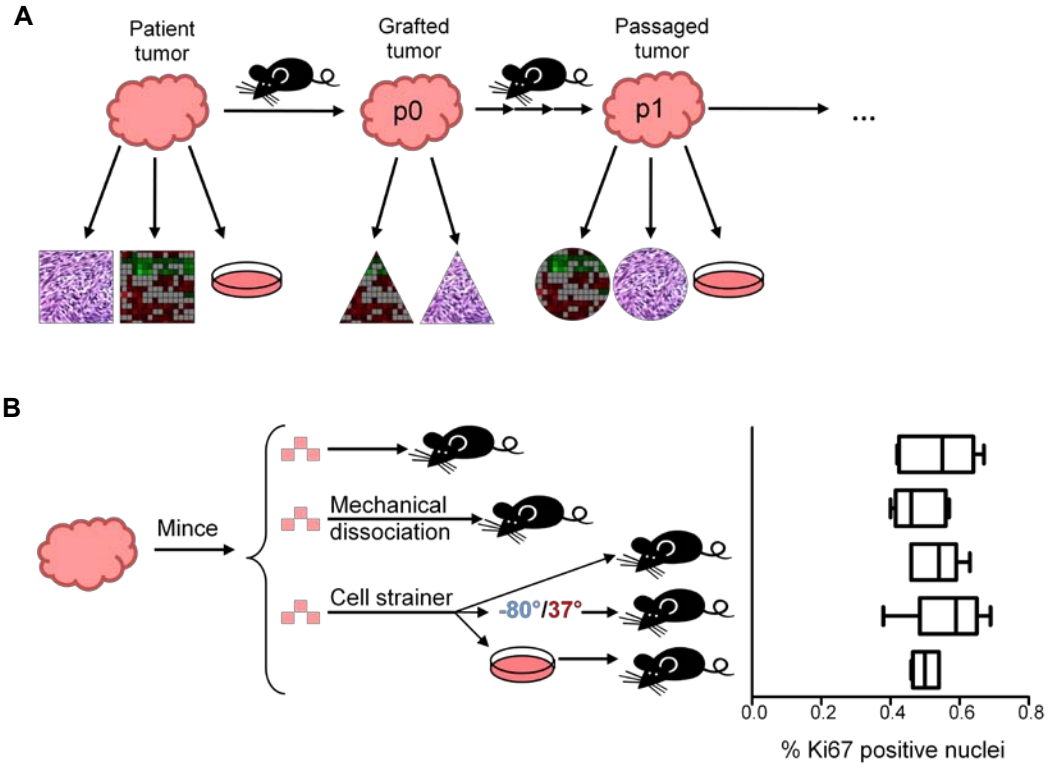

Figure 2-1. Schematic representation of study. A) Surgically resected liposarcoma and xenografted tumors were portioned for gene expression analysis, histopathological analysis, *in vitro*, and *in vivo* studies. **B)** Various tissue dissociation methods tested did not affect the proliferation of the xenografted tumors, as indicated by Ki67 index (± s.e.m., *n*=5 per technique; P=0.79, Friedman test).

Table 2-1. Description of liposarcoma study samples

ID	Histology	Grade	Origin of sample	Site	Size (cm)	Treatment	Gender	Age	Patient status	Growth *in vitro*?
Tumors that did not engraft										
1	Myxoid	low	Primary	Thigh	29	XRT	M	39	NED	
2	Myxoid/RC	Intermed.	Primary	Thigh	16	XRT	M	28	NED	
3	Myxoid/RC	high	Primary	Thigh	9	XRT	M	47	NED	no
4	WD	low	Primary	RP	15		F	58	NED	
5	Cellular WD	low	Primary	RP	41	XRT	F	51	NED	no
6	WD	low	Primary	RP	32	AC	M	61	AWD	
7	WD	low	Recurrent	RP	15		M	72	NED	
8	Cellular WD	low	Recurrent	RP	3	XRT	M	49	NED	no
9	Cellular WD	low	Recurrent	RP	20	XRT	M	54	AWD	no
10	WD	low	Recurrent	RP	22	XRT	M	43	NED	no
11	DD*	high	Primary	RP	31	XRT	F	57	NED	no
12	DD*	high	Primary	RP	30		M	86	DOD	no
13	DD*	high	Primary	Abdomen	13	XRT	M	66	NED	no
14	DD*	high	Recurrent	RP	20	XRT	F	60	NED	no
15	DD*	high	Recurrent	RP	5	XRT	F	86	DOD	
Tumors that engrafted only										
16	Myxoid/RC	high	Primary	Gluteal	16	AC, XRT	F	29	NED	
17	Myxoid/RC	high	Metastatic	Abdomen	22	AC	M	66	AWD	
18	DD	high	Recurrent	RP	5	AC, XRT	F	58	AWD	
19	DD*	high	Metastatic	Flank	4	NC, XRT	F	61	DOD	no
Tumors that engrafted and could be passaged										
LPSX1	DD	high	Recurrent	Abdomen	12	NC, XRT	F	51	DOD	YES(x)
LPSX2	DD*	high	Recurrent	Thigh	15	XRT	M	90	DOD	YES(x)
LPSX3	DD*	high	Primary^	RP	27	NC	M	75	DOD	YES(x)

Clinical and pathological data for study samples. ^This patient presented with metastatic lesions, but the sample came from the primary tumor. Growth in vitro for tumors LPSX1, LPSX2, and LPSX3 was only attempted on xenografted tumors, not the patients' tumors, as indicated by (x). RC: round cell; WD: well-differentiated; DD: dedifferentiated; DD*: dedifferentiated arising from a well-differentiated tumor; RP: retroperitoneum; XRT: radiation therapy; AC: adjuvant chemotherapy; NC: neoadjuvant chemotherapy; NED: no evidence of disease; AWD: alive with disease; DOD: died of disease.

Multiple regression analysis was conducted to examine clinical correlates to tumor engraftment ability. The presence or development of metastases (P=0.024) and patient disease status (P=0.005) positively correlated to xenograftability. All 7 engrafted LPS tumors were high grade, while the low grade tumors did not establish growth in mice (Table 2-1). Furthermore, those DD LPS patients whose samples could be xenografted and serially passaged died of disease within 200 days of tumor removal and therefore had significantly worse disease specific survival (DSS) than patients whose tumors did not engraft (Fig. 2-2, red and black lines, *n*=3, *n*=15, P<0.0001, Mantel-Cox test). Patients whose samples engrafted but could not be passaged also had a significantly better survival than those whose tumors could be passaged (Fig. 2-2, blue line, *n*=4, P=0.01, Mantel-Cox test). Such a correlation is consistent with our recent grade-associated DSS study on 46 independent LPS patients showing that patients with high grade DD LPS had statistically significant shortened survival compared to patients with low grade tumors (Evans 2007; Chopra 2011).

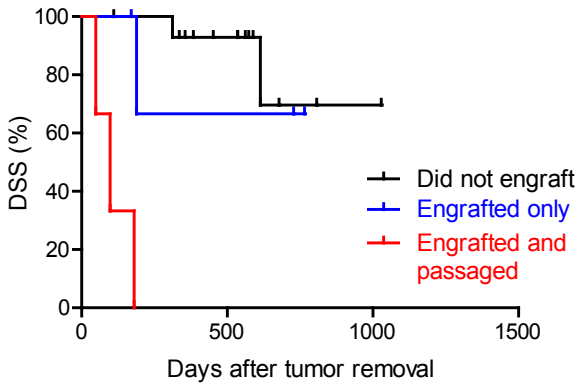

Figure 2-2. Xenograftability as it correlates with patient survival. Patients whose tumors could be serially passaged (red line, *n*=3) had significantly shortened median survival rate than patients whose tumors engrafted but could not be passaged (blue line, *n*=4, P=0.01) and those that did not engraft at all (black line, P<0.0001, *n*=15, Mantel-Cox test). For surviving patients, tick marks represent latest follow up.

Xenografted tumors, but not primary tumors, can be cultured in vitro

With recent progress in the identification of molecular and genetic alterations involved in liposarcoma development, a system that is amenable to genetic interrogation and biochemical analysis is urgently needed. While several labs have been able to culture liposarcomas *in vitro,* only one cell line is commercially available (Singer, Socci et al. 2007; Peng, Zhang et al. 2011). We therefore attempted to generate stable LPS cell lines in parallel with *in vivo* xenograft models from ten human LPS tumors, including one myxoid/round cell, 4 WD, and 5 DD tumors (Table 2-1, right column). While these cells adhered to tissue culture plates within 24 hours, they did not proliferate and soon died out. In contrast, cells from all three xenografted tumors could be successfully cultured and serially passaged *in vitro* for 10–17 passages. Importantly, all three stable cultures could be implanted *in vivo* as xenografts and maintained the histopathologic and gene expression characteristics of the patient tumors (see below). The cultured cells also maintained characteristic small lipid droplets that were present in the patient samples and xenografted tumors (Fig. 2-3). These studies suggest that a xenograft model system may also help create better *in vitro* models.

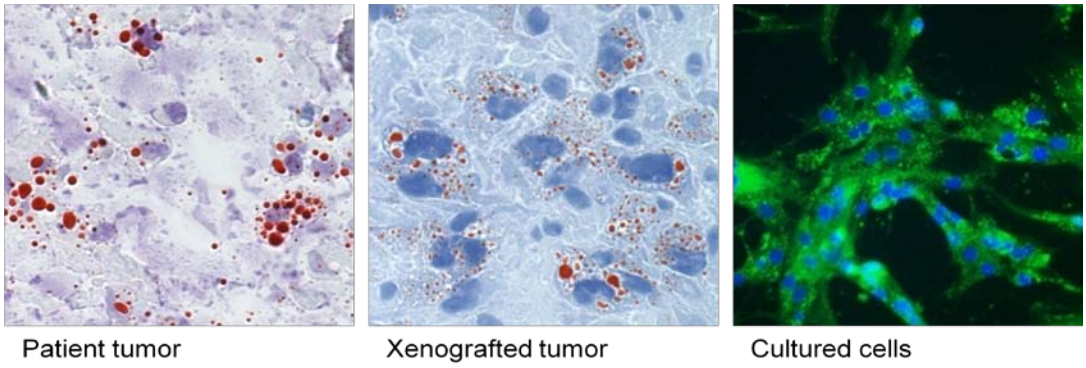

Figure 2-3. ***In vitro*** **cultured cells maintain lipid droplets present in patient and xenografted tumors.** Oil red O (left two panels) and bodipy 493/503 (right panel) staining highlights small lipid droplets in the original LPSX3 patient tumor (left), passage 9 of the xenograft (middle), and cells isolated from the xenograft for *in vitro* culture (right). In all panels, blue indicates the nucleus, and red or green indicates lipid.

Xenografted tumors successfully recapitulate human LPS

To ensure that the xenografts and xenograft-derived primary cell cultures recapitulate the human disease, we compared surgically resected tumors with their derivatives, i.e., xenograft tumors that had been passaged *in vivo* and xenografts generated from cultured cells. Representative histological images from the patient tumor LPSX3 and its resulting xenografts passaged *in vivo* for 1–9 passages demonstrate no major morphological changes (Fig. 2-4). We also compared tissue dissociation strategies and found no resulting histopathological differences (Fig. 2-1B, 2-4B). Proliferation index, as measured by Ki67 quantification, is also consistent regardless of dissociation method (Fig. 2-1B, right panel). These analyses demonstrate that *in vivo* passaged and culture-derived xenografts maintain the histological features of the patient tumors.

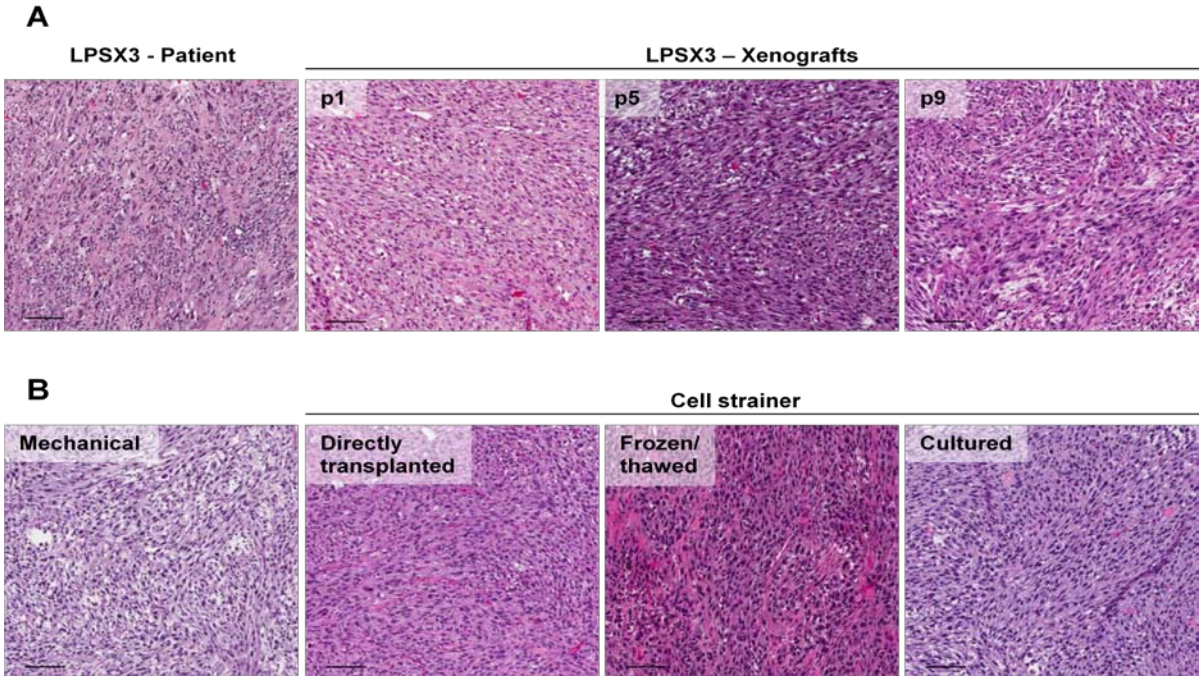

Figure 2-4. Histological features of the patient tumors are well maintained in serially transplanted xenografts. **A)** Histological features are maintained in xenografts over serial passages, shown by H&E staining of patient sample LPSX3 and serial passages of its resulting xenografts. **B)** Tissue dissociation method does not affect the tumor histology, as shown by LPSX3 passage 9. Scale bar 100 μm.

We also looked at specific genetic alterations associated with LPS to confirm that the xenograft model accurately reflects molecular characteristics of the human disease. Previous work published by us and others identified characteristic amplicons on chromosome 12q in most WD and DD LPS tumors (Fletcher, Akerman et al. 1996; Willen, Akerman et al. 1998; Singer, Socci et al. 2007; Taylor, Barretina et al. 2011). Our CGH array analysis shows that the xenograftable patient tumors indeed carry amplifications in this region (Fig. 2-5A). Amplicon-associated genes, e.g. *MDM2* and *CDK4*, show similarly upregulated gene expression in the patient tumors and their xenografts (Fig. 2-5B). These analyses indicate that the xenograft models recapitulate both histopathological and molecular features of the primary disease and are therefore suitable models for studying LPS.

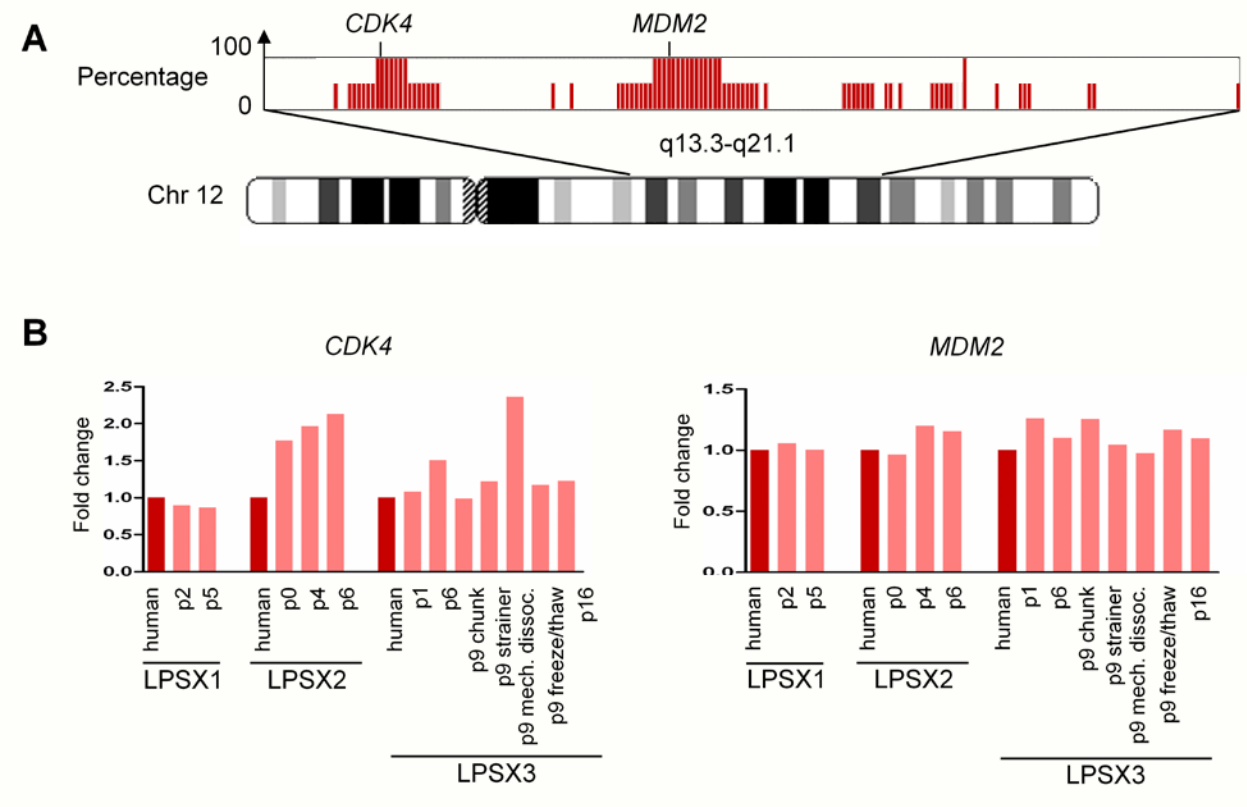

Figure 2-5. Xenografts mimic genetic features of the patient tumors. A) CGH analysis shows areas of chromosome 12 amplified in xenograftable tumors. **B)** Genes amplified in patient tumors, such as *CDK4* and *MDM2*, are expressed at similar levels in the patient tumors and corresponding xenografted tumors (fold change compared to patient sample).

Xenograftability is associated with aggressive and undifferentiated gene expression signatures

To understand the mechanisms underlying xenograftability and associated decreased DSS, we conducted genome-wide gene expression analysis. Our unsupervised cluster analysis shows that the patient tumors (marked with +) cluster alongside their xenografts and xenograft-derived cultured cells (Fig. 2-6A). The analysis also shows closer association of the patient tumors and their xenograft derivatives to other high grade patient LPS tumors in our database. We then narrowed our gene expression analysis to chromosome 12q13.3–23.1, which includes commonly detected amplicons, and found that the patient tumors, xenografts, and xenograft-derived cultured cells maintain their own cluster and carry a unique gene expression signature (Fig. 2-6B highlighted in yellow box). We conducted further global transcriptome analysis and identified approximately 1,000 genes with expression levels that are significantly different between the xenograftable LPS tumors that could be passaged and those that could not be passaged (2-tail t-test, P<0.05, fold-change >1.5, *n=3* each group). Further analysis highlighted several signaling pathways relating to cell proliferation and invasion that were specifically altered in passaged samples (Table 2-2).

Table 2-2. Gene ontology analysis of xenograft signature genes

Pathway	FETpv
Packaging of telomere ends	2.56E-11
Nucleosome assembly	7.61E-06
Insulin receptor signaling pathway	0.000161
Cell cycle	0.00135
Extracellular matrix	0.00137
p53 signaling pathway	0.00673
Cell adhesion	0.00719
Rho guanyl-nucleotide exchange factor activity	0.00793
mTOR signaling pathway	0.0201
ERBB signaling pathway	0.0224
Regulation of cell growth	0.0238

Gene ontology analysis of pathways whose genes are significantly (P<0.05) enriched in xenograftable tumors that can be passaged compared to tumors that engrafted only. FETpv: p-value of Fisher's exact.

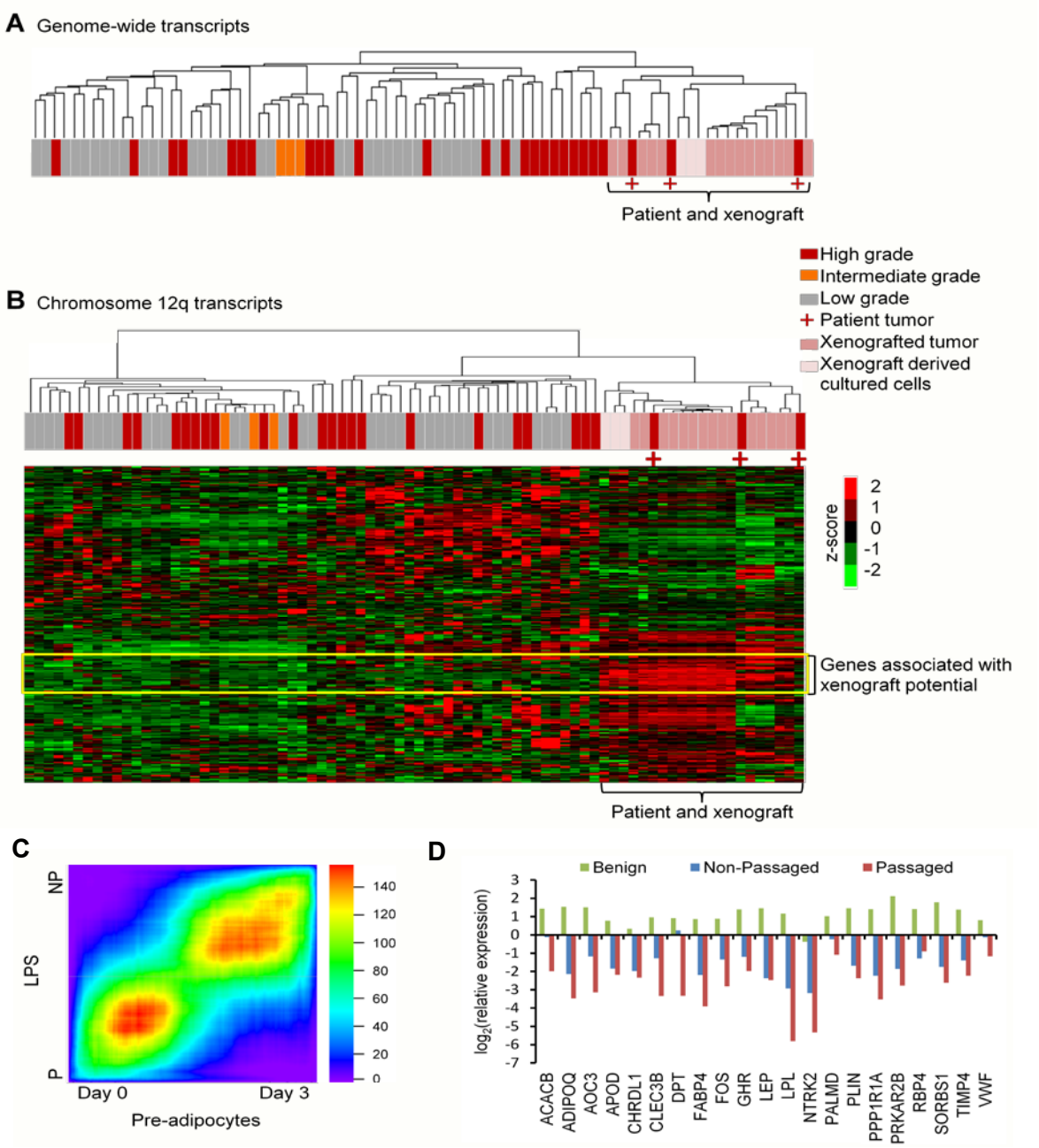

Figure 2-6. Xenograftable tumors have a unique, less-differentiated gene expression profile. A) Unsupervised hierarchical cluster analysis based on 41,000 transcripts separates the xenograftable patient tumors (+) and several passages of their xenografts (pink, right most cluster) from other LPS samples. **B)** Further analysis of transcripts of the chromosome 12q amplicons (q13.3–q23.1) reveals a set of genes specifically associated with the xenograftable primary tumors and their xenografts (highlighted in yellow box). **C)** This heat maps compares the gene expression signatures of patient tumors that were passaged (P) versus non-passaged (NP) on the Y-axis to the signature of pre-adipocytes after induction of differentiation at day 0 versus day 3 on the X-axis. The color indicates the $\log_{10}$ value of the hypergeometric enrichment P-value between the two signature gene sets. The high heat areas show high correlation between the genes upregulated in day 0 (undifferentiated) pre-adipocytes and the passaged (P) tumors, while the non-passaged (NP) tumors are most similar to pre-adipocytes at day 3 after induction of differentiation. *n=3* for all groups. **D)** Expression of genes involved in adipogenesis.

Accumulated evidence suggests that different subtypes of LPS may represent developmental blockages of adipocyte differentiation of mesenchymal stem cells (Matushansky, Hernando et al. 2008). We therefore wanted to determine if the patient tumors that generated serially-passaged xenografts were more progenitor-like. For this, we used the Rank-Rank Hypergeometric Overlap algorithm to compare the overlap of differentially expressed genes in passaged (P) versus non-passaged (NP) patient tumors (Y-axis) with pre-adipocytes 0 days versus 3 days post differentiation (X-axis) (Sohle, Machuy et al. 2012). The heat map generated from these comparisons (Fig. 2-6C) shows greatest similarity between the passaged tumors and day 0 undifferentiated pre-adipocytes, while the non-passaged tumors show highest similarity to pre-adipocytes day 3 post differentiation. These results suggest that the passaged tumors are less-differentiated and more stem/progenitor-like than the tumors that engrafted only. Additionally, when we compare the expression levels of genes known to be important in adipogenesis (Matushansky, Hernando et al. 2008), the grafted but non-passaged tumors show much lower expression compared to benign tumors, with the passaged tumors expressing even lesser amounts (Fig. 2-6D). Taken together, our genetic and gene expression analyses demonstrate the close association of xenografted tumors with aggressive/malignant and stem/progenitor signatures.

DISCUSSION

Liposarcoma represents the most common type of soft tissue sarcomas (Skubitz and D'Adamo 2007; Dalal, Antonescu et al. 2008); however, it remains poorly understood and difficult to study due to the lack of available *in vivo* and *in vitro* model systems. The xenograft system demonstrated in this study successfully recapitulates the human disease and creates a flexible and useful model for studying the molecular mechanisms underlying LPS. This model

also provides a foundation upon which new targets can be developed and novel therapeutics tested.

The xenograft model system developed in our study has both prognostic and therapeutic values. Treatment response in xenograft systems has been shown to be predictive for clinical outcome (Garber 2009). Out of the many clinical variables we tested, including disease status, gender, location of the tumor, number of organs involved, margin status, post-operation complications, prior treatment history, etc., only presence or development of metastasis and patient status correlated with graftability. Moreover, the capability of the tumor to engraft and survive serial passaging is related to higher grade and shorter DSS. Thus, the ability for a patient's tumor to engraft may help identify patients who will benefit from more aggressive treatment regimens. Additionally, since the median interval to disease recurrence is approximately 16 months for patients with high grade LPS, xenografts generated from patient biopsies or resected tumors at the time of initial presentation can be molecularly profiled and interrogated with targeted therapies (Eilber, Brennan et al. 2005). This would allow physicians to define appropriate treatment paradigms and institute personalized therapies that could be used as preventive measurements or promptly initiated upon disease recurrence.

We validated that the xenograft model system recapitulates the human disease at histopathologic, genetic, and gene expression levels, and allows for the maintenance of tumor characteristics across serial *in vivo* passages in immune deficient mice. We also tested the outcomes of different dissociation strategies in parallel and found that grafted tumors can sustain complete dissociation and freeze and thaw without loss of growth potential and integrity, making these xenograft models more easily maintained and shared/distributed by investigators. Our method allows for the generation of a single cell suspension, permitting accurate cell counting and xenograft tumor seeding. Our ability to revive tumor cells from cryopreservation is also critical to avoid the requirement of continuous maintenance of the tumors in mice, keeping passage number low and preventing the potential risk of genotypic/phenotypic drift.

Previous studies demonstrated that freshly resected LPS samples can be dissociated and cultured as primary cells (Singer, Socci et al. 2007; Peng, Zhang et al. 2011); however, generation of stable cell lines directly from the surgical specimens has been difficult. Over the past 6 years, we attempted to generate LPS lines from over 20 patient samples without success (our unpublished observation). Although the cells from the 10 patient samples we tested can adhere to the culture dishes, none could be passaged *in vitro*. We have attempted to generate xenograft models and primary cell lines from the same patient tumor samples in parallel but found that although the DD LPS sample can be grafted and passaged in the NSG mice, cells dissociated from the same primary tumor cannot be passaged *in vitro*. In contrast, cells dissociated from the xenografted tumors can be easily cultured, passaged, and used for generating secondary xenografts, allowing for detailed mechanistic studies and genetic manipulation. Importantly, cells derived from these xenograft tumors maintain the gene expression profiles of the primary tumors. These data suggest that the use of the xenograft system may also help create cell lines more readily than patient tissue alone.

Finally, our gene expression analysis identified alterations unique to the patient tumors that could be xenografted and serially passaged, as well as suggesting that these tumors are more progenitor-like than the non-passaged xenografts. These data will be useful to identify malignant drivers of liposarcomas, new therapeutic targets, and novel prognostic markers.

References

Ashburner M, Ball CA, Blake JA, Botstein D, Butler H, Cherry JM, et al. (2000) Gene ontology: tool for the unification of biology. The Gene Ontology Consortium. *Nat. Genet.* 25(1): 25-29.

Charytonowicz E, Terry M, Coakley K, Telis L, Remotti F, Cordon-Cardo C, et al. (2012) PPARgamma agonists enhance ET-743-induced adipogenic differentiation in a transgenic mouse model of myxoid round cell liposarcoma. *J. Clin. Invest.* 122(3): 886-898.

Chopra S, Li, Y., Gui, D., Eilber, F.C. and Dry S.M. (2011) Primary Retroperitoneal Liposarcomas: Mitoses in Non-Adipogenic Zones Correlate with Survival. *Mod. Pathol.* 24(suppl 1): 11A.

Dalal KM, Antonescu CR and S inger S. (2008) Diagnosis and management of lipomatous tumors. *J Surg Oncol.* 97(4): 298-313.

Dalal KM, Antonescu CR and Singer S. (2008) Diagnosis and management of lipomatous tumors. *J. Surg. Oncol.* 97(4): 298-313.

Eilber FC, Brennan MF, Riedel E, Alektiar KM, Antonescu CR and Singer S. (2005) Prognostic factors for survival in patients with locally recurrent extremity soft tissue sarcomas. *Ann. Surg. Oncol.* 12(3): 228-236.

Eilber FC, Eilber FR, Eckardt J, Rosen G, Riedel E, Maki RG, et al. (2004) The impact of chemotherapy on the survival of patients with high-grade primary extremity liposarcoma. *Ann. Surg.* 240(4): 686-695; discussion 695-687.

Evans HL. (2007) Atypical lipomatous tumor, its variants, and its combined forms: a study of 61 cases, with a minimum follow-up of 10 years. *Am J Surg Pathol.* 31(1): 1-14.

Fletcher CD, Akerman M, Dal Cin P, de Wever I, Mandahl N, Mertens F, et al. (1996) Correlation between clinicopathological features and karyotype in lipomatous tumors. A report of 178 cases from the Chromosomes and Morphology (CHAMP) Collaborative Study Group. *Am. J. Pathol.* 148(2): 623-630.

Frapolli R, Tamborini E, EmanuelaVirdis, Bello E, Tarantino E, Marchini S, et al. (2010) Novel models of Myxoid Liposarcoma Xenografts mimicking the biological and pharmacological features of human tumors. *Clin. Cancer. Res.* 16: 4958-4967.

Garber K. (2009) From human to mouse and back: 'tumorgraft' models surge in popularity. *J. Natl. Cancer Inst.* 101(1): 6-8.

Gutierrez A, Snyder EL, Marino-Enriquez A, Zhang YX, Sioletic S, Kozakewich E, et al. (2011) Aberrant AKT activation drives well-differentiated liposarcoma. *Proc. Natl. Acad. Sci. U. S. A.* 108(39): 16386-16391.

Kasper B, Gil T and Awada A. (2007) Treatment of patients with advanced soft tissue sarcoma: disappointment or challenge? *Curr. Opin. Oncol.* 19(4): 336-340.

Matushansky I, Hernando E, Socci ND, Matos T, Mills J, Edgar MA, et al. (2008) A developmental model of sarcomagenesis defines a di fferentiation-based classification for liposarcomas. *Am. J. Pathol.* 172(4): 1069-1080.

Peng T, Zhang P, Liu J, Nguyen T, Bolshakov S, Belousov R, et al. (2011) An experimental model for the study of well-differentiated and dedifferentiated liposarcoma; deregulation of targetable tyrosine kinase receptors. *Lab. Invest.* 91(3): 392-403.

Plaisier SB, Taschereau R, Wong JA and Graeber TG. (2010) Rank-rank hypergeometric overlap: identification of statistically significant overlap between gene-expression signatures. *Nucleic Acids Res.* 38(17): e169.

Rodriguez R, Rubio R, Gutierrez-Aranda I, Melen GJ, Elosua C, Garcia-Castro J, et al. (2011) FUS-CHOP Fusion Protein Expression Coupled to p53 D eficiency Induces Liposarcoma in Mouse but Not in Human Adipose-Derived Mesenchymal Stem/Stromal Cells. *Stem Cells.* 29(2): 179-192.

Singer S, Socci ND, Ambrosini G, Sambol E, Decarolis P, Wu Y, et al. (2007) Gene expression profiling of liposarcoma identifies distinct biological types/subtypes and pot ential therapeutic targets in well-differentiated and dedifferentiated liposarcoma. *Cancer Res.* 67(14): 6626-6636.

Skubitz KM and D'Adamo DR. (2007) Sarcoma. *Mayo Clin. Proc.* 82(11): 1409-1432.

Snyder EL, Sandstrom DJ, Law K, Fiore C, Sicinska E, Brito J, et al. (2009) Jun amplification and overexpression are oncogenic in liposarcoma but not always sufficient to inhibit the adipocytic differentiation programme. *The Journal of Pathology.* 218(3): 292-300.

Sohle J, Machuy N, Smailbegovic E, Holtzmann U, Gronniger E, Wenck H, et al. (2012) Identification of new genes involved in human adipogenesis and fat storage. *PLoS One.* 7(2): e31193.

Tap WD, Eilber FC, Ginther C, Dry SM, Reese N, Barzan-Smith K, et al. (2011) Evaluation of well-differentiated/de-differentiated liposarcomas by high-resolution oligonucleotide array-based comparative genomic hybridization. *Genes Chromosomes Cancer.* 50(2): 95-112.

Taylor BS, Barretina J, Maki RG, Antonescu CR, Singer S and Ladanyi M. (2011) Advances in sarcoma genomics and new therapeutic targets. *Nat Rev Cancer.*

Wang Z, Yang L, Jiang Y, Ling ZQ, Li Z, Cheng Y, et al. (2011) High fat diet induces formation of spontaneous liposarcoma in mouse adipose tissue with overexpression of interleukin 22. *PLoS One.* 6(8): e23737.

Willen H, Akerman M, Dal Cin P, De Wever I, Fletcher CD, Mandahl N, et al. (1998) Comparison of chromosomal patterns with clinical features in 165 lipomas: a report of the CHAMP study group. *Cancer Genet. Cytogenet.* 102(1): 46-49.

Chapter 3:

Pre-clinical studies of rapamycin and sorafenib as therapy for dedifferentiated liposarcoma

Abstract

Liposarcoma treatment options are currently limited to surgery and radiation, with chemotherapy having little effect on advanced disease. Small molecule inhibitors are commonly used in cancer therapy, but patients treated with single agents often develop resistance. Therefore, we proposed to test combination therapy of the mTOR inhibitor rapamycin with the multi-tyrosine kinase inhibitor sorafenib on our newly developed xenograft models of dedifferentiated liposarcoma. We found that although the growth rate of tumors was not always affected, combination treatment induced necrosis and morphological changes. Lipid staining and gene expression analysis of the combination-treated tumors is consistent with more differentiated, less-aggressive cells as compared to vehicle treatment. Rapamycin and sorafenib combination treatment is a promising avenue to explore for future targeted and differentiation therapy of dedifferentiated liposarcoma.

Introduction

Liposarcomas (LPS) can arise throughout the body, but most frequently occurs in the lower extremities and the retroperitoneum. LPS tumors rarely cause symptoms and therefore grow undetected until mass-effect occurs; one large institutional study found the median liposarcoma tumor burden to be 15 cm (Dalal, Kattan et al. 2006). Many factors are important in the prognosis of LPS patients, including tumor size, depth, location, and histological subtype (Dalal, Kattan et al. 2006). Surgery is the only known curative treatment, and although patients are often treated with radiation and chemotherapy, the impact on disease-free survival is often minimal (Eilber, Eilber et al. 2004; Dalal, Antonescu et al. 2008). It is often difficult to achieve negative margins in retroperitoneal LPS resection due to the large size of the tumor and proximity to vital organs. As such, local recurrence rates remain high, with 50% probability of local recurrence within 3 years for all LPS subtypes and 83% probability for dedifferentiated LPS (Singer, Antonescu et al. 2003).

Due to the rarity of liposarcoma and all soft tissue sarcomas, these cancers are often grouped together for clinical trials, which may mask LPS-specific therapeutic benefit. (Conyers, Young et al. 2011). However, identification of genetic and pathway alterations are allowing for targeted therapy with small molecular inhibitors. One of the molecular hallmarks of well-differentiated (WD) and dedifferentiated (DD) LPS is chromosomal amplification of the 12q13-15 region, which includes genes such as *MDM2* and *CDK4*. MDM2 negatively regulates the tumor suppressor p53, and CDK4 plays a key role in regulating the transition from G1 to S phase of the cell cycle, making both proteins attractive targets for therapy. MDM2 and CDK4 inhibitors have shown promising results in lab studies and are currently undergoing clinical trials (Crago and Singer 2011; Hoffman, Lazar et al. 2011).

Another strategy for treatment of LPS is to induce re-differentiation through activation of the nuclear receptor peroxisome proliferator activated receptor-γ (PPARγ). PPARγ is a ligand-activated transcription factor considered to be the master regulator of adipogenesis (Tontonoz

and Spiegelman 2008). PPARγ agonists have been shown to induce differentiation of LPS cells *in vitro* and in a mouse model of myxoid round cell LPS (Tontonoz, Singer et al. 1997; Charytonowicz, Terry et al. 2012). Initial clinical results from a pilot study were very promising (Demetri, Fletcher et al. 1999), but a follow-up study showed little response in patients treated with similar therapy (Debrock, Vanhentenrijk et al. 2003). While these results have been disappointing, active study of the molecular mechanisms of the liposarcomagenesis may provide insight into other methods of differentiation therapy.

Rapamycin and sorafenib are both small molecule inhibitors currently used as cancer therapy. Rapamycin was initially described as an anti-fungal agent and later found to slow tumor growth through inhibition of the mTOR pathway (Vezina, Kudelski et al. 1975; Eng, Sehgal et al. 1984; Koltin, Faucette et al. 1991), and sorafenib is a multi-kinase inhibitor shown to target RAF, VEGFR-2, Flt-3, c-KIT, and FGFR-1 (Wilhelm, Carter et al. 2004). While both have shown promising results for treatment of sarcoma, many patients treated with single-agent therapies develop resistance, suggesting that combination therapy may be a better option (Maki, D'Adamo et al. 2009; Vemulapalli, Mita et al. 2011; von Mehren, Rankin et al. 2011; Woodcock, Griffin et al. 2011).

Xenograft models have been shown to be predictive of clinical response, making them a useful tool for the screening of potential therapies (Voskoglou-Nomikos, Pater et al. 2003; Garber 2009). We therefore sought to use our newly developed xenograft model to test the combination of rapamycin and sorafenib as a potential therapy for DD LPS. We hypothesized that LPS, which often have disruption of the mTOR pathway, would have increased sensitivity to rapamycin treatment, an effect that would be further enhanced by combination therapy with sorafenib. Only one of three DD LPS xenografts responded to treatment with slowed tumor growth, however all three showed marked histological response. Most notably, there were changes in morphology suggestive of re-differentiation. Gene expression analysis confirmed that tumors treated with a combination of rapamycin and sorafenib became more differentiated

than vehicle-treated tumors. Taken together, these results suggest that combination treatment with rapamycin and sorafenib is a potential therapeutic option for dedifferentiated liposarcoma.

Materials and Methods

Xenografts

All three tumors were isolated from freshly resected human dedifferentiated liposarcomas as previously described (Smith et al, manuscript submitted). Tissue from an established xenograft was dissociated with a 100 µm mesh cell strainer into DPBS. Cells were then counted with trypan blue exclusion, centrifuged, and resuspended in equal portions of DPBS and Matrigel (BD Biosciences). The flank regions of NOD.Cg-*Prkdc*^{scid} *Il2rg*^{tm1Wjl}/SzJ (common name NSG) mice were shaved with electric clippers, the area prepped with an iodophor followed by alcohol, and $5x10^5$ cells were injected subcutaneously. When tumors reached approximately 5 mm in diameter, tumors were measured with calipers, and mice were divided into groups such that each group had similar variance in tumor volume. Tumor volume was calculated with the equation: Volume = $0.52*a^2*b$, where *a* represents the shorter diameter.

Mouse treatment

Rapamycin powder (LC Laboratories) was reconstituted in 100% ethanol to a stock solution of 10 mg/ml and stored at -20°C. Fresh working solution was made each day by diluting the stock solution to 1 mg/ml with vehicle (5.68% Tween-80, 5.68% polyethylene glycol 400 in water). Rapamycin (4 mg/kg) or an equal amount of vehicle was administered via intraperitoneal injection daily. Sorafenib powder was dissolved into freshly made vehicle (12.5% ethanol, 12.5% cremaphor in water) to 20 mg/ml. Sorafenib (70 mg/kg) or an equal amount of vehicle was administered via oral gavage daily. Mice were treated daily with one of the following combinations: rapamycin vehicle and sorafenib vehicle, rapamycin drug and sorafenib vehicle, sorafenib drug and rapamycin vehicle, or rapamycin drug and sorafenib drug. Mice

were weighed and tumors measured every three to four days. Drug dosage was adjusted appropriately based on the new weight measurements. Mice were sacrificed and tumors collected if the tumors reached 1.5 cm in diameter, or if they lost more than 10% of their bodyweight within one week. Mice were maintained in barrier cages, on standard chow diet with food and water available *ad libitum*. Mice were maintained on 2 mg ml^{-1} sulfamethoxazole and 0.4 mg ml^{-1} trimethoprim (TMS, added to drinking water) to prevent infection. All studies were performed in accordance with the Division of Laboratory Animal Medicine at the University of California Los Angeles.

Immunohistochemistry

A slice from the center of the tumor sample was saved for histological analysis, avoiding necrotic areas. The sample was fixed in 10% phosphate buffered formalin overnight and transferred into 50–70% ethanol. The tissue was then paraffin embedded with standard protocols, cut into 4 µm sections, and stained with hematoxylin and eosin (H&E) by the UCLA Translational Pathology Core Laboratory. Formalin-fixed, paraffin-embedded sections were deparaffinized in xylene and rehydrated in graded alcohol. Endogenous peroxidase activity was blocked with 3% (vol/vol) hydrogen peroxide (H_2O_2). Antigen retrieval was performed by boiling the sections in 0.01 M citric acid buffer (pH 6.0) for 15 minutes. Sections were first blocked with 5% (vol/vol) normal donkey serum in PBS, and then incubated with primary antibody against Ki67 (1:500, Vector Laboratories), PTEN (1:100), phospho-S6 (Ser240/244, 1:100), phospho-ERK (Thr202/Tyr204, 1:300), or cleaved caspase 3 (Asp175, 1:200, all from Cell Signaling Technology) overnight at 4 °C. Sections were then incubated with biotinylated secondary antibody (1:500, Jackson ImmunoResearch Laboratories) for one hour at room temperature. Antibody binding was detected with Vectastain ABC Elite Kit (Vector Laboratories, PK-6100) and visualized with DAB (3,3'-diaminobenzidine, Vector Laboratories). Sections were counterstained in Gill's hematoxylin.

Oil red o staining

Frozen sections of liposarcomas were stained in a 0.3% oil red O/isopropyl alcohol solution for 7–10 minutes at room temperature. Excess stain was washed out in 60% isopropyl alcohol, followed by washes in 30% isopropyl alcohol and distilled water. Slides were counterstained with Harris hematoxylin, rinsed with two changes of tap water, and coverslips were mounted with glycerol. Slides were subsequently stored at 4° C. Slides were digitally scanned at 200x with the Aperio XL system and images analyzed with ImageScope software, ImageJ, and Adobe Photoshop CS4.

Gene expression microarray

All microarray preparation was completed by the UCLA Clinical Microarray Core. Frozen tissue from LPS X1 and LPS X3 vehicle and combination treatment groups was homogenized with a MagNa lyser (Roche) and RNA extracted with MagNa Pure Compact nucleic isolation system (Roche). LowInput QuickAmp One Color labeling kit (Agilent) was used for first strand, second strand, and in vitro transcription reactions. Samples were analyzed on Agilent SurePrint Human GE 8x60k microarrays and scanned on an Agilent DNA microarray scanner.

In gene expression analysis, two-tail t-test was used for comparing expression between the vehicle and combination groups. For a gene represented by multiple probes, its representative P-value was the lowest P-value among the probes. Gene ontology analysis was conducted using pathway databases downloaded from Gene Ontology and Broad Institute Molecular Signature Database (Ashburner, Ball et al. 2000). Fisher's exact test was used to identify which gene ontology or biological pathway was significantly enriched by differentially expressed (t-test $P<0.05$ and fold-change>1.5) genes between unsuccessfully and successfully grafted high grade LPS groups.

Rank-rank hypergeometric overlap was used to compare gene expression data from our samples versus gene expression of pre-adipocytes collected after 0, 3, and 7 days of induction

in differentiation media (GEO accession ID: GSE28628) (Plaisier, Taschereau et al. 2010; Sohle, Machuy et al. 2012).

Statistics

Statistical analyses were conducted with GraphPad Prism v.5.04 (GraphPad Software, Inc.). All statistical assessments were considered significant if $P<0.05$.

Results

Xenografts express low levels of PTEN

Based on previous results that our three LPS xenograft models had altered mTOR signaling, we hypothesized that *PTEN,* a tumor suppressor upstream of the mTOR signaling pathway, would also be deregulated. CGH analysis of the original patient tumors showed no genetic alterations at the *PTEN* locus (Tap, Eilber et al. 2011). However, expression analysis revealed low *PTEN* gene expression in all DD LPS patient samples tested, and a significantly lower expression level in the xenograft samples and the original tumors from which they were derived (Fig. 3-1A). As expected, PTEN protein was not expressed in tumor cells, but expressed in surrounding stroma and blood vessels (Fig. 3-1B).

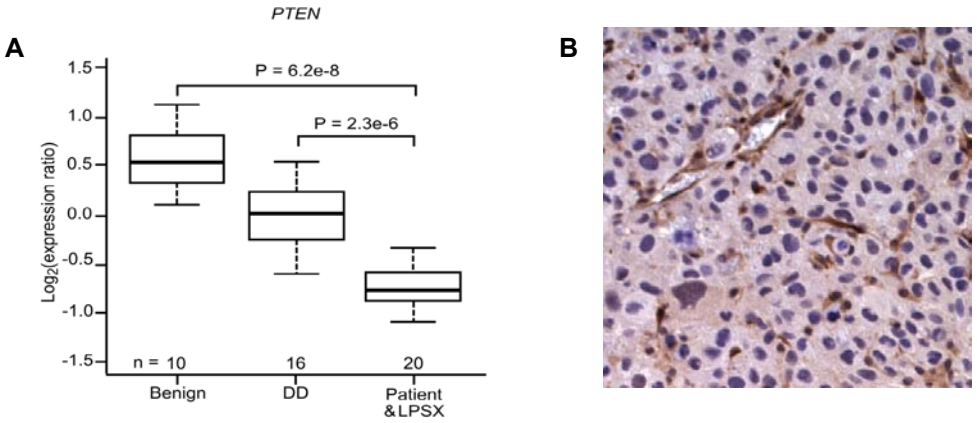

Figure 3-1. LPS xenografts show low gene and protein expression levels of PTEN. A) Gene expression of *PTEN* is lower in DD LPS compared to benign fatty tumors, but patient tumors and their derived xenograft tumors show even lower gene expression. **B)** A representative image of LPSX1 staining for PTEN is negative in tumor cells. The cells showing positive stain are blood vessels and stroma.

Tumor size does not predict treatment response

Although rapamycin and sorafenib have both been used clinically for soft tissue sarcoma treatment, there have not been any formal studies to evaluate either drug alone or in combination for LPS. Because PTEN-deficient tumors show enhanced sensitivity to mTOR inhibition (Neshat, Mellinghoff et al. 2001), and our sample tumors showed disruption of several receptor tyrosine kinase pathways, we sought to use our patient-derived LPS xenograft system for pre-clinical evaluation of rapamycin and sorafenib treatment for DD LPS. Three LPS xenografts (LPSX1, LPSX2, LPSX3) were treated daily with no drug (vehicle), rapamycin only, sorafenib only, or rapamycin and sorafenib, and tumor growth was monitored over the course of their treatment. Figure 3-2 depicts the tumor growth curves of all three xenografts as a percentage of their starting size. LPSX1 treated with rapamycin alone or the combination treatment showed much slower tumor growth than either the vehicle or sorafenib groups. However, neither LPSX2 nor LPSX3 had the same response in tumor growth. The doubling times of the tumors, as calculated from the growth curve, shows significantly slowed growth in LPSX1 treated with rapamycin or combination treatment (Fig. 3-2). While LPSX2 and LPSX3 trended toward the same growth effect, the differences did not reach statistical significance.

Additionally, we examined the histology to check for necrosis and any morphological changes. At low magnification, it was easy to identify the tumors that had been treated with combination treatment. Figure 3-3 shows a low magnification view of LPSX3 tumors from each treatment group. While the vehicle and sorafenib tumors looked similar in cellular density, the rapamycin- and combination-treated tumors had lower cellular density and more necrotic areas. Higher magnification revealed morphological changes including thinning of cytoplasm in the rapamycin group, and lipid droplets in the sorafenib group. Both changes were observed in the combination treatment group (Fig. 3-4). These histopathological changes suggest that, although the tumor size and growth rate did not differ among treatment groups, the tumors responded to treatment.

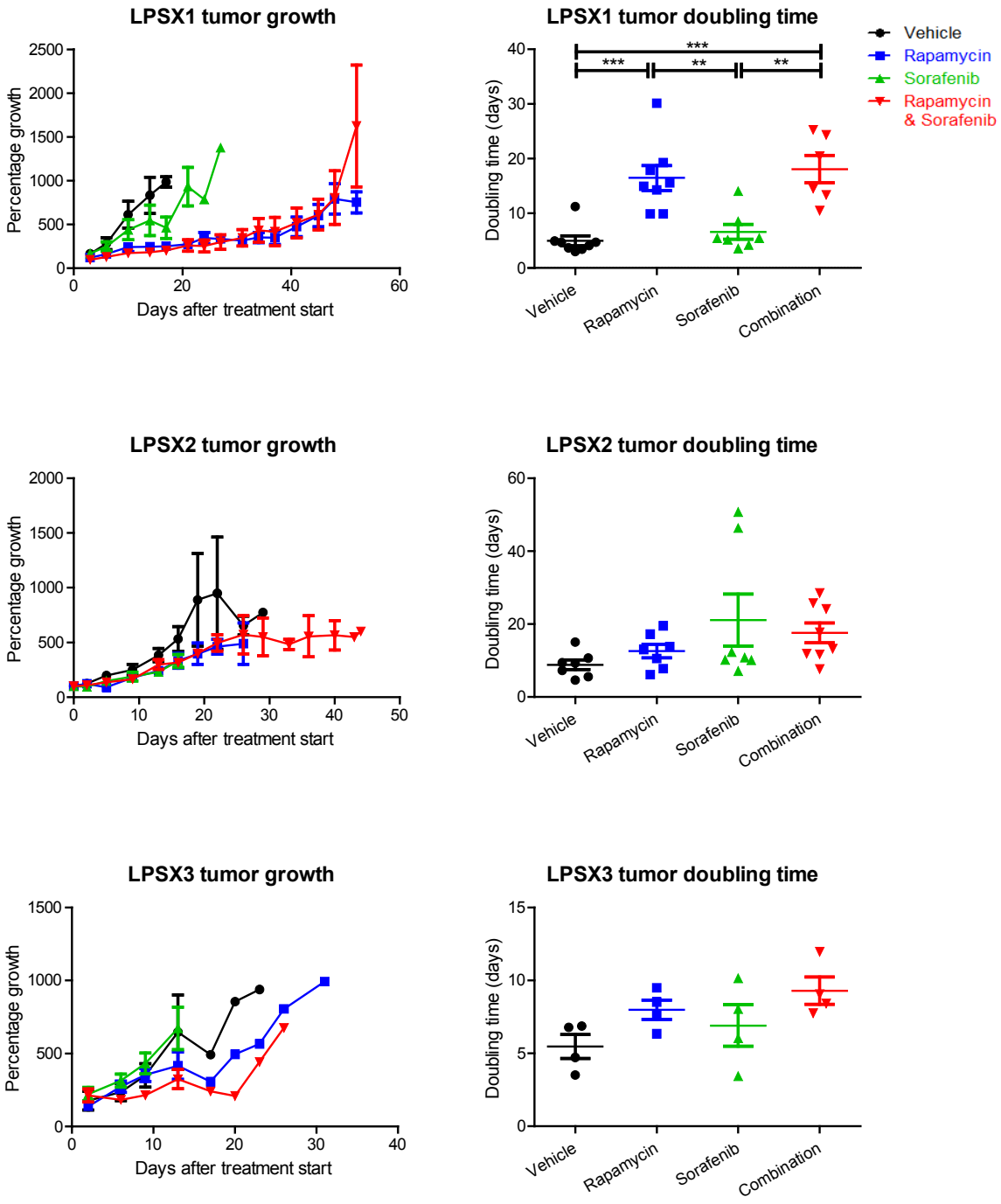

Figure 3-2. Growth curves and doubling times of treated xenografts. Only LPSX1 (top panel) showed a significant difference in the tumor doubling time when treated with rapamycin or combination treatment. LPSX2 and LPSX3 showed a similar trend, but the difference did not reach statistical significance. Data are presented as mean ± sem.

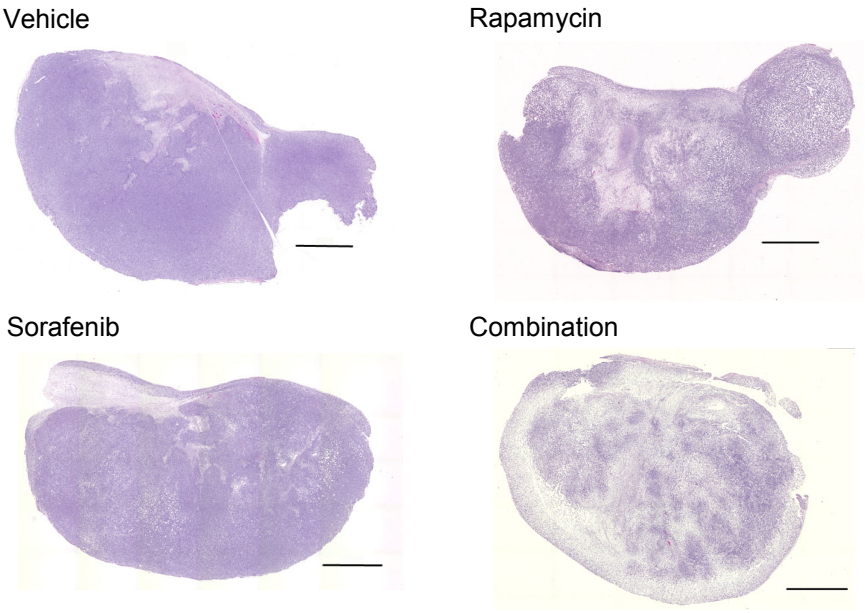

Figure 3-3. Combination treatment causes morphological changes. Low magnification view of LPSX3 exemplifies marked changes in morphology in response to rapamycin and combination treatment, such as increased necrosis and decreased cell density. Scale bar = 2.5mm.

Monitoring intracellular pathway targets

In addition to evaluating histopathological changes, we aimed to evaluate the intended pathway targets of the drugs. Phospho-S6 was chosen as a surrogate marker of mTOR activity and phospho-MAPK was chosen as a downstream marker of Raf activity to monitor response to rapamycin and sorafenib, respectively. As would be expected, the levels of phospho-S6 decreased in response to rapamycin and combination treatment, while the levels of phospho-MAPK decreased in response to sorafenib and combination treatment (Fig. 3-4). We also measured the rate of proliferation and apoptosis, which were evaluated by Ki67 and cleaved caspase 3 staining, respectively. As might be expected by the growth rate of the tumors, the percentage of Ki67 and cleaved caspase 3 stained cells did not change between the treatment groups (Fig. 3-4). As such, we began to explore additional pathways that could explain the morphological changes observed between treatment groups.

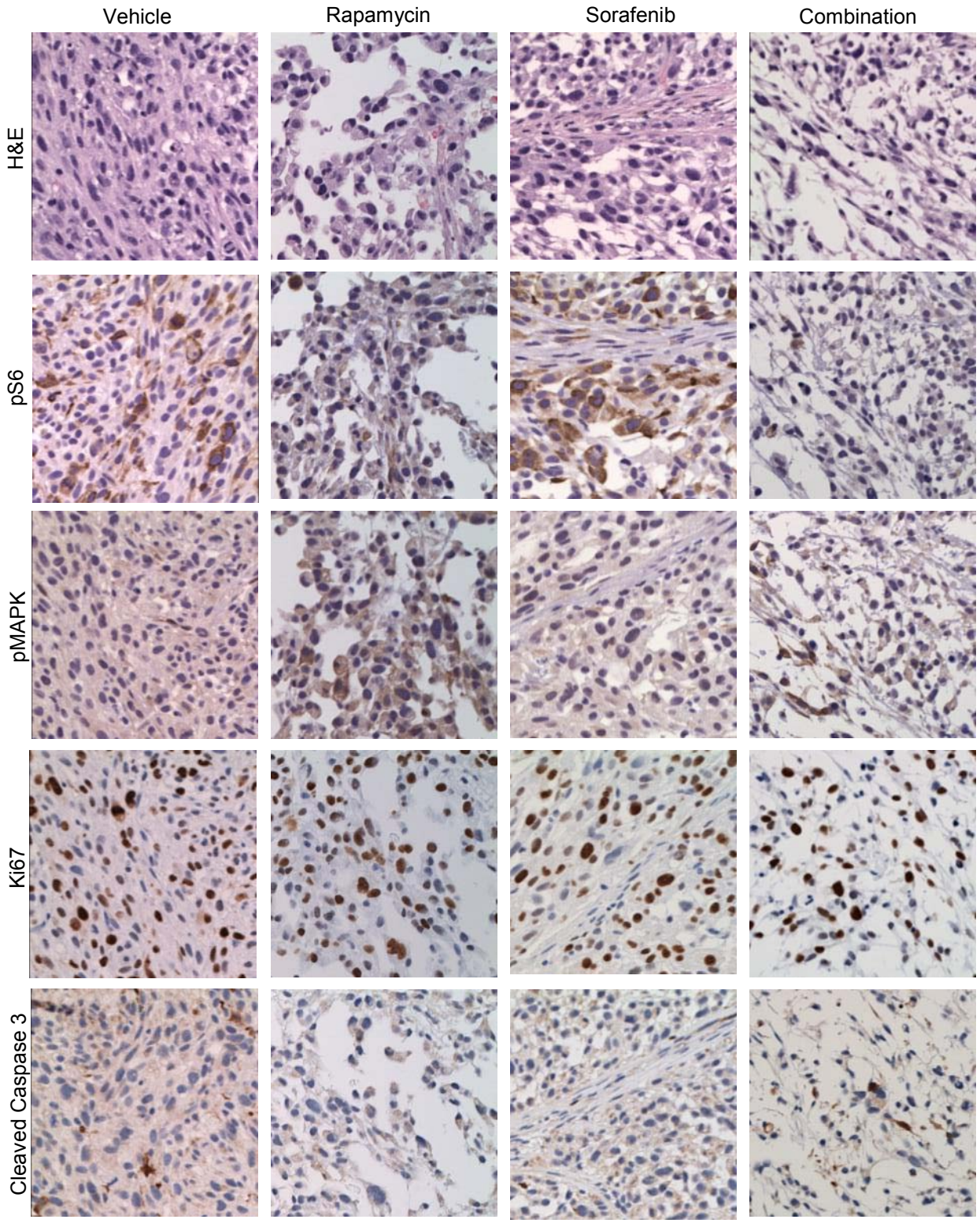

Figure 3-4. Intracellular targets of rapamycin and sorafenib. Representative images from consecutive sections of LPSX3 show down regulation of pS6 and pMAPK in response to rapamycin and sorafenib treatment, respectively. Ki67 and cleaved caspase 3 levels did not change regardless of treatment.

Evaluating markers of adipogenesis

One of the morphological changes we observed after treatment was the presence of cells that more closely resembled adipocytes. Because liposarcomas are thought to be derived from mesenchymal stem cells interrupted along the differentiation pathway toward adipocytes (Mariani, Brennetot et al. 2007; Matushansky, Hernando et al. 2008; Snyder, Sandstrom et al. 2009), our hypothesis was that the treatment allowed the cells to re-start their differentiation. To test our hypothesis, we first looked for the presence of lipid droplets by staining with oil red o. The treated LPS xenografts had increased number and size of lipid droplets when compared to vehicle (Fig. 3-5). Although the vehicle treated tumors had a higher percent of cells containing lipid droplets, the rapamycin and combination treated tumors had significantly larger lipid droplets (Fig. 3-6).

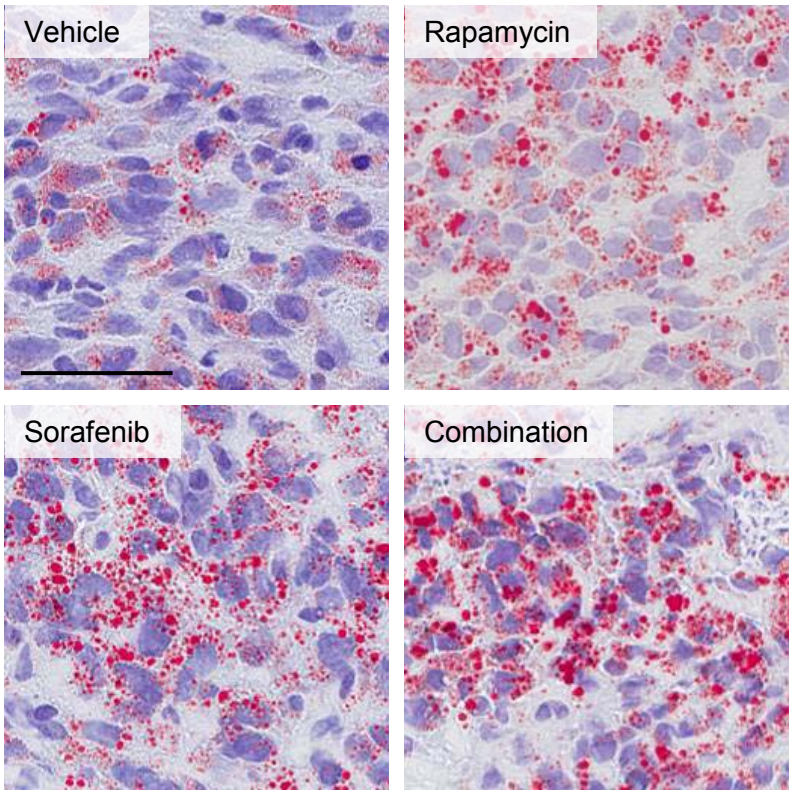

Figure 3-5. Oil red o staining of treated tumors reveals changes in lipid droplets. Tumors treated with all therapies show slightly larger lipid droplets than vehicle alone. Images are representative from LPSX3, scale bar = 50μm.

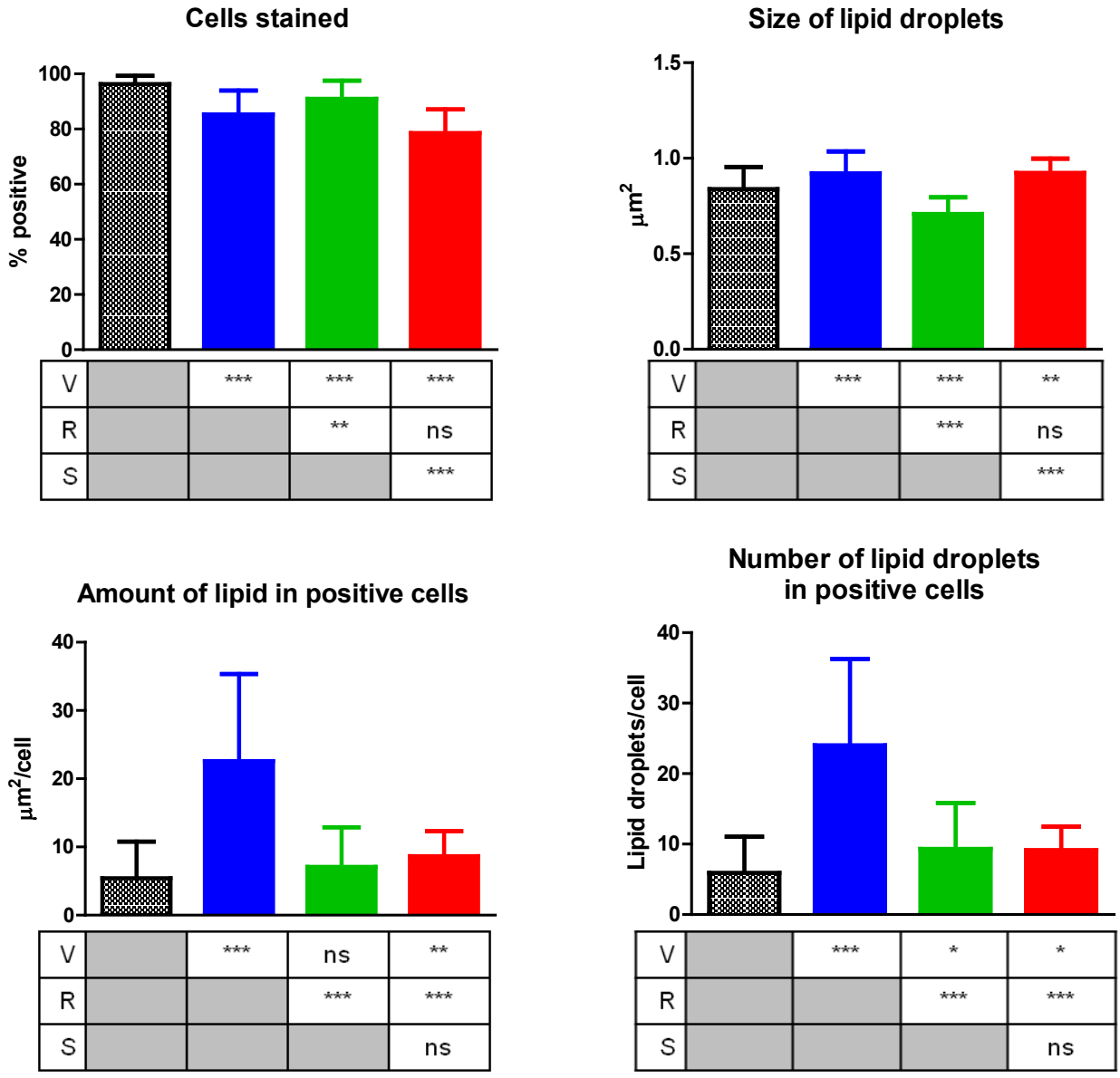

Figure 3-6. Quantification of oil red o staining. Quantification of oil red o staining determined that although a smaller percent of rapamycin and combination treated cells were positively stained, the lipid droplets were larger. Rapamycin treated tumors also had the largest amount of lipid and number of lipid droplets per positively stained cell. Data are represented as mean ± sd. Table depicts range of P value for comparison between the groups indicated by row and data column above. V=vehicle, R=rapamycin, S=sorafenib. *** indicates P<0.001, ** indicates 0.001<P<0.01, * indicates 0.01<P<0.05, "ns" indicates not significant P>0.05.

For an unbiased assessment of how the tumors were responding to treatment, we analyzed gene expression across the whole genome from vehicle and combination treated samples. To

determine if the combination treatment induced tumor re-differentiation, we used the Rank-Rank Hypergeometric Overlap algorithm to compare the overlap of differentially expressed genes in vehicle (V) versus combination (C) treated tumors with pre-adipocytes 0 days versus 3 days post differentiation (Sohle, Machuy et al. 2012). The heat map generated from this comparison shows high similarity between the vehicle treated tumors and the pre-adipocytes 0 days post differentiation, whereas the combination treated tumors are more similar to the pre-adipocytes 3 days after induction of differentiation (Fig. 3-7). Gene set enrichment analysis of genes commonly altered in both expression signatures yielded 167 genes that were consistently enriched. Pathway analysis of these genes suggests that combination treatment affects cellular interactions with the extracellular matrix and the G1/S transition of cell cycle (Table 3-1). Taken together, these results show that combination treatment may be initiating re-differentiation and preventing entry into S phase, rendering the tumors less-aggressive.

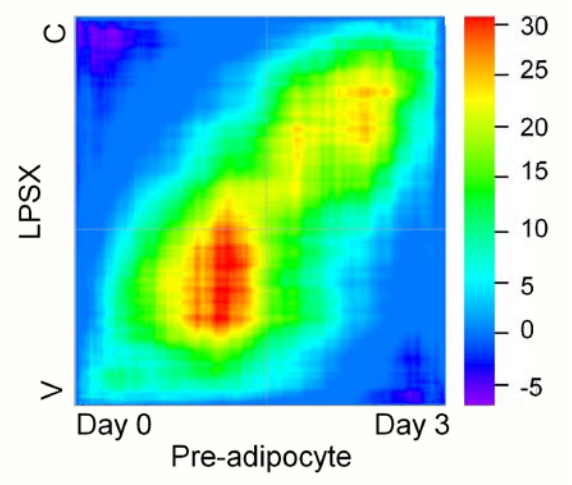

Figure 3-7. Tumors treated with combination therapy are more differentiated and less aggressive. This heat map compares the gene expression signatures of xenograft tumors that were treated with vehicle (V) versus combination therapy (C) on the Y-axis to the signature of pre-adipocytes after induction of differentiation at day 0 versus day 3 on the X-axis. The color indicates the $\log_{10}$ value of the hypergeometric enrichment P-value between the two signature gene sets. The high heat areas show high correlation between the genes upregulated in day 0 (undifferentiated) pre-adipocytes and the vehicle treated (V) tumors, while the combination treated (C) tumors are most similar to pre-adipocytes at day 3 after induction of differentiation. *n=3* for pre-adipocytes, *n=6* for LPSX.

Table 3-1. Gene ontology analysis of combination treatment signature genes.

Pathway	FETpv
ECM-receptor interaction	1.80E-05
Focal adhesion	5.65E-05
G alpha (q) signaling events	0.000953
Drug metabolism - other enzymes	0.000981
Regulation of actin cytoskeleton	0.00222
Calcium signaling pathway	0.00306
Metabolism of vitamins and cofactors	0.00321
Fc gamma R-mediated phagocytosis	0.00338
G1/S transition	0.00618
Downstream events in GPCR signaling	0.00619
Hematopoietic cell lineage	0.00647
Class A/1 (Rhodopsin-like receptors)	0.00737
Cell cycle	0.0109
HIV infection	0.0109
Cell junction organization	0.0144
Regulation of APC/C activators between G1/S and early anaphase	0.0168

Gene ontology analysis of pathways whose genes are significantly ($P<0.05$) enriched in xenograftable tumors that can be passaged compared to tumors that engrafted only. FETpv: p-value of Fisher's exact.

Discussion

As the mechanisms of liposarcomagenesis become better understood, improved treatment options will become available for patients who are currently limited to surgery and radiation. Microarray data from DD LPS patient samples showed abnormal regulation of the mTOR pathway and low *PTEN* expression. PTEN protein levels were also low, suggesting these tumors may have increased sensitivity to the mTOR inhibitor rapamycin. We therefore sought to test rapamycin and sorafenib as a potential combination therapy for DD LPS using our newly generated xenograft models. While there was a trend toward slower tumor growth in the rapamycin and combination treatment groups, only tumor volume change in DD LPSX1 reached statistical significance. Currently, one of the criteria upon which tumor response to therapy is measured is tumor size. (Eisenhauer, Therasse et al. 2009). Based on this criterion, we would have assumed that LPSX2 and LPSX3 did not respond to treatment. However, histological evaluation of the tumors revealed a noticeable response in all three xenografts. The greatest response was to the combination therapy, which showed increased necrosis, decreased cellular density, and changes in cell morphology. Evaluation of intracellular targets with IHC revealed both drugs successfully targeted the pathways of interest, although the rates of proliferation and apoptosis did not drastically change. Interestingly, further analysis of lipid content and gene expression revealed that tumors treated with a combination of rapamycin and sorafenib became more differentiated. These results are particularly intriguing because they suggest that differentiation therapy may still be possible.

The results presented here show that combination therapy with rapamycin and sorafenib could be an effective therapy for dedifferentiated liposarcoma. Although the differentiation of the treated tumors was incomplete, this may be resolved with more efficient mTOR inhibition. Rapamycin has been shown to create a feedback loop resulting in increased levels of activated AKT (O'Reilly, Rojo et al. 2006). Additionally, other mTOR inhibitors have increased ability to inhibit mTORC1 activity as compared to rapamycin (Peterson, Sengupta et al. 2011). Drugs are

currently being developed that can inhibit both mTOR and PI3K to prevent the AKT feedback loop, which may engage the treated tumors to fully differentiate (Mazzoletti, Bortolin et al. 2011). Another option is to include PPARγ ligands as a treatment modality. A recent study on a myxoid liposarcoma mouse model found that addition of PPARγ agonists enhanced tumor differentiation achieved by treating with trabectedin (Charytonowicz, Terry et al. 2012). With our xenograft model, we have demonstrated that combination therapy with rapamycin and sorafenib has a moderate therapeutic effect on LPS tumors. Using this established protocol, the testing of novel drugs, such as the dual mTOR/PI3K and PPARγ ligands, will further strengthen the repertoire of targeted therapeutic options for patients with DD LPS.

References

Ashburner M, Ball CA, Blake JA, Botstein D, Butler H, Cherry JM, et al. (2000) Gene ontology: tool for the unification of biology. The Gene Ontology Consortium. *Nat. Genet.* 25(1): 25-29.

Charytonowicz E, Terry M, Coakley K, Telis L, Remotti F, Cordon-Cardo C, et al. (2012) PPARgamma agonists enhance ET-743-induced adipogenic differentiation in a transgenic mouse model of myxoid round cell liposarcoma. *J. Clin. Invest.* 122(3): 886-898.

Conyers R, Young S and T homas DM. (2011) Liposarcoma: molecular genetics and therapeutics. *Sarcoma.* 2011.

Dalal KM, Antonescu CR and S inger S. (2008) Diagnosis and management of lipomatous tumors. *J. Surg. Oncol.* 97(4): 298-313.

Dalal KM, Kattan MW, Antonescu CR, Brennan MF and S inger S. (2006) Subtype specific prognostic nomogram for patients with primary liposarcoma of the retroperitoneum, extremity, or trunk. *Ann. Surg.* 244(3): 381-391.

Debrock G, Vanhentenrijk V, Sciot R, Debiec-Rychter M, Oyen R and Van Oosterom A. (2003) A phase II trial with rosiglitazone in liposarcoma patients. *Br. J. Cancer.* 89(8): 1409-1412.

Demetri GD, Fletcher CDM, Mueller E, Sarraf P, Naujoks R, Campbell N, et al. (1999) Induction of solid tumor differentiation by the peroxisome proliferator-activated receptor-g ligand troglitazone in patients with liposarcoma. *Proceedings of the National Academy of Sciences.* 96: 3951-3956.

Eilber FC, Eilber FR, Eckardt J, Rosen G, Riedel E, Maki RG, et al. (2004) The impact of chemotherapy on the survival of patients with high-grade primary extremity liposarcoma. *Ann. Surg.* 240(4): 686-695; discussion 695-687.

Eisenhauer EA, Therasse P, Bogaerts J, Schwartz LH, Sargent D, Ford R, et al. (2009) New response evaluation criteria in solid tumours: revised RECIST guideline (version 1.1). *Eur. J. Cancer.* 45(2): 228-247.

Eng CP, Sehgal SN and Vezina C. (1984) Activity of rapamycin (AY-22,989) against transplanted tumors. *J. Antibiot.* 37(10): 1231-1237.

Garber K. (2009) From human to mouse and back: 'tumorgraft' models surge in popularity. *J. Natl. Cancer Inst.* 101(1): 6-8.

Koltin Y, Faucette L, Bergsma DJ, Levy MA, Cafferkey R, Koser PL, et al. (1991) Rapamycin sensitivity in Saccharomyces cerevisiae is mediated by a pept idyl-prolyl cis-trans isomerase related to human FK506-binding protein. *Mol. Cell. Biol.* 11(3): 1718-1723.

Maki RG, D'Adamo DR, Keohan ML, Saulle M, Schuetze SM, Undevia SD, et al. (2009) Phase II study of sorafenib in patients with metastatic or recurrent sarcomas. *J. Clin. Oncol.* 27(19): 3133-3140.

Mariani O, Brennetot C, Coindre JM, Gruel N, Ganem C, Delattre O, et al. (2007) JUN oncogene amplification and overexpression block adipocytic differentiation in highly aggressive sarcomas. *Cancer Cell.* 11(4): 361-374.

Matushansky I, Hernando E, Socci ND, Matos T, Mills J, Edgar MA, et al. (2008) A developmental model of sarcomagenesis defines a di fferentiation-based classification for liposarcomas. *Am. J. Pathol.* 172(4): 1069-1080.

Mazzoletti M, Bortolin F, Brunelli L, Pastorelli R, Di Giandomenico S, Erba E, et al. (2011) Combination of PI3K/mTOR Inhibitors: Antitumor Activity and Molecular Correlates. *Cancer Res.* 71(13): 4573-4584.

Neshat MS, Mellinghoff IK, Tran C, Stiles B, Thomas G, Petersen R, et al. (2001) Enhanced sensitivity of PTEN-deficient tumors to inhibition of FRAP/mTOR. *Proc. Natl. Acad. Sci. U. S. A.* 98(18): 10314-10319.

O'Reilly KE, Rojo F, She QB, Solit D, Mills GB, Smith D, et al. (2006) mTOR inhibition induces upstream receptor tyrosine kinase signaling and activates Akt. *Cancer Res.* 66(3): 1500-1508.

Peterson T R, Sengupta SS, Harris T E, Carmack A E, Kang S A, Balderas E, et al. (2011) mTOR Complex 1 Regulates Lipin 1 Localization to Control the SREBP Pathway. *Cell.* 146(3): 408-420.

Plaisier SB, Taschereau R, Wong JA and Graeber TG. (2010) Rank-rank hypergeometric overlap: identification of statistically significant overlap between gene-expression signatures. *Nucleic Acids Res.* 38(17): e169.

Singer S, Antonescu CR, Riedel E and Brennan MF. (2003) Histologic subtype and margin of resection predict pattern of recurrence and survival for retroperitoneal liposarcoma. *Ann. Surg.* 238(3): 358-370; discussion 370-351.

Snyder EL, Sandstrom DJ, Law K, Fiore C, Sicinska E, Brito J, et al. (2009) Jun amplification and overexpression are oncogenic in liposarcoma but not always sufficient to inhibit the adipocytic differentiation programme. *The Journal of Pathology.* 218(3): 292-300.

Sohle J, Machuy N, Smailbegovic E, Holtzmann U, Gronniger E, Wenck H, et al. (2012) Identification of new genes involved in human adipogenesis and fat storage. *PLoS One.* 7(2): e31193.

Tap WD, Eilber FC, Ginther C, Dry SM, Reese N, Barzan-Smith K, et al. (2011) Evaluation of well-differentiated/de-differentiated liposarcomas by high-resolution oligonucleotide array-based comparative genomic hybridization. *Genes Chromosomes Cancer.* 50(2): 95-112.

Tontonoz P, Singer S, Forman BM, Sarraf P, Fletcher JA, Fletcher CDM, et al. (1997) Terminal differentiation of human liposarcoma cells induced by ligands for peroxisome proliferator-activated receptor g and the retinoid X receptor. *Proceedings of the National Academy of Sciences.* 94: 237-241.

Tontonoz P and Spiegelman BM. (2008) Fat and beyond: the diverse biology of PPARgamma. *Annu. Rev. Biochem.* 77: 289-312.

Vemulapalli S, Mita A, Alvarado Y, Sankhala K and Mita M. (2011) The emerging role of mammalian target of rapamycin inhibitors in the treatment of sarcomas. *Targeted oncology.* 6(1): 29-39.

Vezina C, Kudelski A and Sehgal SN. (1975) Rapamycin (AY-22,989), a new antifungal antibiotic. I. Taxonomy of the producing streptomycete and isolation of the active principle. *J. Antibiot.* 28(10): 721-726.

von Mehren M, Rankin C, Goldblum JR, Demetri GD, Bramwell V, Ryan CW, et al. (2011) Phase 2 Southwest Oncology Group-directed intergroup trial (S0505) of sorafenib in advanced soft tissue sarcomas. *Cancer.*

Voskoglou-Nomikos T, Pater JL and Seymour L. (2003) Clinical predictive value of the in vitro cell line, human xenograft, and mouse allograft preclinical cancer models. *Clin. Cancer. Res.* 9(11): 4227-4239.

Wilhelm SM, Carter C, Tang L, Wilkie D, McNabola A, Rong H, et al. (2004) BAY 43-9006 exhibits broad spectrum oral antitumor activity and targets the RAF/MEK/ERK pathway and receptor tyrosine kinases involved in tumor progression and angiogenesis. *Cancer Res.* 64(19): 7099-7109.

Woodcock J, Griffin JP and Behrman RE. (2011) Development of novel combination therapies. *New Engl. J. Med.*

Chapter 4:

Concluding Remarks

An ideal model system reproducibly recapitulates the desired human disease, allows for better understanding of that disease, and serves as a tool for screening potential therapeutics. The most commonly used model systems are genetic models, xenografts, and cell lines. While there are currently genetic models for myxoid and well-differentiated liposarcomas, none exist for dedifferentiated liposarcoma (Perez-Losada, Pintado et al. 2000; Charytonowicz, Terry et al. 2012). While xenograft models are commonly used, we are only aware of one group who has validated that their myxoid liposarcoma model successfully recapitulates the human disease (Frapolli, Tamborini et al. 2010). We and others have found primary cells difficult to culture, and the reliability of cell lines has recently been called into question (Gillet, Calcagno et al. 2011).

Because of the lack of dedifferentiated liposarcoma models, we sought to create a patient-derived xenograft model. Histological and gene expression analysis of serial passages in mice are consistent with patient tumors, demonstrating successful recapitulation of the human disease. The cultured cells derived from the xenografted tumors were also consistent with the patient tumor, which will allow for mechanistic studies and genetic manipulation. Finally, we have been able to use the xenograft models to test rapamycin and sorafenib combination therapy as a potential treatment option for dedifferentiated liposarcoma. We will also use dual PI3K/mTOR inhibitors and PPARγ agonists to see if more complete differentiation is possible.

With rare diseases such as sarcoma, it is often difficult to accrue enough patients to run a clinical trial. Tools such as the liposarcoma xenografts are a valuable screen for potential therapies so only the most promising therapies can be tested clinically. The xenograft derived cultured cells will also allow for genetic manipulation and mechanistic studies, which is part of our future studies. These studies will help determine which genes or pathways are critical for malignancy and identify new targets for therapies.

Another critical element of cancer care is tumor imaging and monitoring treatment response. While FDG-PET/CT is often used to determine tumor grade and response to treatment, one third of high grade liposarcomas do not have high FDG uptake (our own

unpublished observation). Through the studies described here and others, tumor size is not always indicative of response to treatment (Evilevitch, Weber et al. 2008). The xenograft derived cultured cells can help identify potential new imaging targets or PET-probes, which can then be tested on the xenograft models.

The main goal of these studies was to create a model system that could easily go from "bench to bedside" and "bedside to bench." It allows simultaneous study of basic biological and clinical questions – true translational research.

References

Charytonowicz E, Terry M, Coakley K, Telis L, Remotti F, Cordon-Cardo C, et al. (2012) PPARgamma agonists enhance ET-743-induced adipogenic differentiation in a transgenic mouse model of myxoid round cell liposarcoma. *J. Clin. Invest.* 122(3): 886-898.

Evilevitch V, Weber WA, Tap WD, Allen-Auerbach M, Chow K, Nelson SD, et al. (2008) Reduction of glucose metabolic activity is more accurate than change in size at predicting histopathologic response to neoadjuvant therapy in high-grade soft-tissue sarcomas. *Clin. Cancer. Res.* 14(3): 715-720.

Frapolli R, Tamborini E, EmanuelaVirdis, Bello E, Tarantino E, Marchini S, et al. (2010) Novel models of Myxoid Liposarcoma Xenografts mimicking the biological and pharmacological features of human tumors. *Clin. Cancer. Res.* 16: 4958-4967.

Gillet J-P, Calcagno AM, Varma S, Marino M, Green LJ, Vora MI, et al. (2011) Redefining the relevance of established cancer cell lines to the study of mechanisms of clinical anti-cancer drug resistance. *Proceedings of the National Academy of Sciences.* 108(46): 18708-18713.

Perez-Losada J, Pintado B, Gutierrez-Adan A, Flores T, Banares-Gonzalez B, del Campo JC, et al. (2000) The chimeric FUS/TLS-CHOP fusion protein specifically induces liposarcomas in transgenic mice. *Oncogene.* 19(20): 2413-2422.

Appendix 1:

Evaluation of well-differentiated/de-differentiated liposarcomas by high-resolution oligonucleotide array-based comparative genomic hybridization.

Evaluation of Well-Differentiated/De-Differentiated Liposarcomas by High-Resolution Oligonucleotide Array-Based Comparative Genomic Hybridization

William D. Tap,[1]* Fritz C. Eilber,[2,3] Charles Ginther,[1] Sarah M. Dry,[4] Nicholas Reese,[5] Kate Barzan-Smith,[3] Hsiao-Wang Chen,[1] Hong Wu,[3] Frederick R. Eilber,[2] Dennis J. Slamon,[1] and Lee Anderson[1]

[1]Division of Hematology/Oncology, Department of Medicine, David Geffen School of Medicine, University of California Los Angeles, Los Angeles, CA 90095
[2]Division of Surgical Oncology, Department of Surgery, David Geffen School of Medicine, University of California Los Angeles, Los Angeles, CA 90095
[3]Department of Molecular and Medical Pharmacology, David Geffen School of Medicine, University of California Los Angeles, Los Angeles, CA 90095
[4]Department of Pathology, David Geffen School of Medicine, University of California Los Angeles, Los Angeles, CA 90095
[5]Department of Medicine, David Geffen School of Medicine, University of California Los Angeles, Los Angeles, CA 90095

Well-differentiated/de-differentiated liposarcomas (WDLS/DDLS) encompass an intriguing disease model in which a temporal intersection occurs between the malignant transformation of mesenchymal cells and the process of adipogenesis. Deciphering the molecular events that trigger and are characteristic of the intersection of these oncogenic and normal processes is critical to affect the often morbid and lethal consequences of malignant tumors of fat. High-resolution genome-wide oligonucleotide array-based comparative genomic hybridization (aCGH) with matched gene expression analyses was performed on seven lipomas, one hibernoma, and 38 WD and DDLS to define and compare the genomic events associated with these tumors. WD and DDLS had complex karyotypes. On average, WDLS had 11.1 and DDLS had 22.7 chromosomal copy number aberrations. All of the liposarcomas had 12q13-q15 amplifications with varying peaks at *CDK4* (12q14.1), *HMGA2* (12q14.3), and *MDM2* (12q15); 24% of the DDLS and no WDLS had 1p32.2 (*JUN*) amplifications; 33% WDLS and 35% DDLS had 1q24.3 amplifications involving *DNM3* and miR-214/miR-199a2; 24% of the liposarcomas had 6q23-q24 amplifications (including *MAP3K5*). Amplifications in *GLI1* (12q13.3), *JUN*, and *MAP3K5* (6q23.3) were mutually exclusive and occurred predominately in the DDLS. 6q amplifications occurred primarily in retroperitoneal tumors and females represented the majority of those patients who developed fatty tumors prior to the age of 50 years old. This detailed genetic mapping provides insight into the heterogeneity of WD and DDLS and the chromosomal and genetic abnormalities that are present in and distinguish these mesenchymal malignancies.

INTRODUCTION

Liposarcomas (LSs) are a diverse group of adipocyte neoplasms that are subclassified into three distinct subsets [well-differentiated/de-differentiated (WD/DD), myxoid/round cell, and pleomorphic] based on morphology and cytogenetics (Fletcher et al., 1996; Eilber et al., 2004b). In each of these tumors, the extent of de-differentiation, as reflected by histological grade, remains the most important determinant of clinical course and prognosis (Eilber et al., 2004b; Dalal et al., 2006). Of the three groups, WD/DD is the most common (Kattan et al., 2002; Eilber et al., 2004a; Coindre et al., 2009). This subtype represents an intriguing disease which is thought to encompass the malignant transformation of mesenchymal cells at various points along the continuum of adipogenesis (Mariani et al., 2007; Matushansky et al., 2008; Snyder et al., 2009). In practice though, the linearity associated with this process is less clear. Clinically, there are WD tumors that never develop a DD component, DD tumors that develop de novo without a documented preceding or concurrent WD phase, WD and DD tumors that present synchronously, and WD and DD tumors that present metachronously (Henricks et al., 1997; Horvai et al., 2009). The variable clinical presentations of these tumors call into question temporal points of transformation

Additional Supporting Information may be found in the online version of this article.

Supported by: The Jonsson Comprehensive Cancer Center Sarcoma Program.

*Correspondence to: William D. Tap, UCLA, Division of Hematology/Oncology, 2825 Santa Monica Blvd., Suite 200, Santa Monica, CA 90404. E-mail: wtap@mednet.ucla.edu

Received 6 August 2010; Accepted 11 October 2010

DOI 10.1002/gcc.20835

Published online 29 November 2010 in Wiley Online Library (wileyonlinelibrary.com).

and highlight the importance of understanding the molecular cues and events that trigger the development and further de-differentiation of LSs.

Current research has sought to identify the genetic factors that distinguish WDLS and DDLS (Singer et al., 2007; Horvai et al., 2009; Snyder et al., 2009). This has prognostic implications, affords insight into the biology of fat and tumor development, and could identify new therapeutic targets. As a group, WD and DDLS are known to have characteristic, but not categorical, cytogenetic abnormalities that have diagnostic but uncertain functional, prognostic, and therapeutic significance. The most common cytogenetic abnormalities found in WD and DDLS are supernumerary rings and giant chromosomes, which frequently contain amplifications in the long arm of chromosome 12 (12q13-q15) (Sreekantaiah et al., 1992; Dal Cin et al., 1993). Although the significance of these amplicons has yet to be evaluated, genes of interest [e.g., *MDM2* (Mdm2 p53 binding protein homolog), *CDK4* (cyclin-dependent kinase 4), *HMGA2* (high-mobility group AT-hook 2), and *TSPAN31* (tetraspanin 31)] have been identified (Singer et al., 2007; Italiano et al., 2008; Horvai et al., 2009; Trombetta et al., 2009). These genes have a theoretical role in LS development and the amplifications are thought to be initiating factors in fat tumorigenesis. However, the presence of marker chromosomes or specific amplifications in genes such as *MDM2* or *CDK4* do not allow for the risk stratification of WDLS or entirely explain the molecular triggers that promote de-differentiation.

Gain, rather than loss, of genetic material appears to be the hallmark of WD and DDLS. Amplifications in 1p32, 1q21-q24, and/or 6q23 have also been identified as frequent areas of interest in these tumors (Mariani et al., 2007; Horvai et al., 2009). *JUN* (Jun oncogene) and *MAP3K5* (mitogen-activated protein kinase kinase kinase 5) are upregulated through amplifications in 1p32 and 6q23, respectively. These findings, as well as noted gains in 19q13.2 (*FOSB*, FBJ murine osteosarcoma viral oncogene homolog B), have implicated the JNK (JUN N-terminal protein kinase) signaling pathway in the formation of DDLS (Horvai et al., 2009). However, the true role of these amplifications in the pathogenesis and propagation of WD and DDLS, as well as a target area in 1q21-24, has yet to be determined.

A recent body of work has begun to dissect the complexity of WD and DDLS. Immunohistochemical studies have shown that proteins such as JUN are often expressed in WD and DD components of synchronously presenting tumors but not WD tumors alone, unless they are of the inflammatory subtype (Snyder et al., 2009). Bacterial artificial chromosome (BAC)-based CGH arrays comparing paired WD and DDLS have also shown that amplifications of 12q, 1p, and 6q are often present in both the WD and DD components of the same tumor (Horvai et al., 2009). cDNA array analyses of synchronous WD and DDLS tumors have found that the paired WD and DD components of the same tumor clustered together more closely than the WD and DD components derived from different tumors (Shimoji et al., 2004).

In this study, we sought to investigate the intra and inter cytogenetic abnormalities that define a clinically annotated cohort of WD and DDLS. We performed high-resolution genome-wide oligonucleotide array-based CGH with matched gene expression analyses on 46 fatty tumors (7 lipomas, 1 hibernoma, 21 WDLS, 17 DDLS). Oligonucleotide array-based comparative genomic hybridization (aCGH) studies have been performed on LS cell lines (Persson et al., 2008) and DDLS (Barretina et al., 2010). Analyses utilizing metaphase CGH, fluorescent in situ hybridization, and BAC-based arrays have also been performed on LSs (Chibon et al., 2002; Mariani et al., 2007; Italiano et al., 2008; Horvai et al., 2009; Rieker et al., 2009). However, to our knowledge, this is the first high-resolution oligonucleotide array-based CGH analysis that compares well-differentiated (WDLS) and de-differentiated liposarcomas (DDLS).

MATERIALS AND METHODS

Tumor Specimens

Patients with soft tissue sarcomas who required surgery were prospectively enrolled onto an Institutional Review Board (IRB) approved tissue procurement protocol in which sarcoma samples were stored for molecular and genetic analyses (UCLA IRB#99-05-085). In each case, informed consent was obtained preoperatively. A representative sample of tumor was sectioned for banking after sufficient tissue was obtained for pathological review. Tumor samples were immediately snap frozen in liquid nitrogen and maintained at −80°C until selected for analysis. Definitive histologic subtype was confirmed by a sarcoma pathologist at the time of tissue acquisition. All

pertinent patient information was prospectively maintained in the UCLA sarcoma database (UCLA IRB#08-12-050). Evaluation of the sarcoma tissue bank yielded 46 tumor samples that were appropriate for this analysis. Selection criteria included a diagnosis of a benign fatty tumor (lipoma or hibernoma) or a WDLS and/or DDLS that was histologically reconfirmed by a sarcoma pathologist and the isolation of sufficient (quantity and quality) DNA and RNA for CGH and microarray analyses, respectively.

RNA Isolation and Microarrays

Tumor specimens were trimmed of excess adipose tissue on dry ice and divided in half for RNA and DNA extraction. Total RNA was isolated from ~25 mg of fresh frozen tissue using the QIAzol RNA Kit (Qiagen, Germantown, MD). Work surfaces, instruments, and pipetters were cleaned with RNaseZap® (Ambion, Austin, TX). After addition of the QIAzol Lysis Reagent, the samples were disrupted and homogenized in a rotor-stator homogenizer (Polytron PT-3100, Kinematica, Lucerne, Switzerland) for 15 sec at maximum speed, then extracted according to the QIAzol protocol. The purified RNA was eluted in 30–60 μl diethylpyrocarbonate (DEPC)-treated sterile water (EMD, Gibbstown, NJ). The quantity of RNA was measured by spectral analysis using the NanoDrop ND-1000 Spectrophotometer (NanoDrop Technologies, Wilmington, DE). RNA quality was determined by separation of the RNA via capillary electrophoresis using the Agilent 2000 Bioanalyzer (Agilent Technologies, Santa Clara, CA).

Characterization of individual LS transcripts was performed by comparison with a cRNA mixed reference pool of labeled fatty tumors. The mixed reference pool included 8 benign fatty tumors (7 lipomas, 1 hibernoma), 33 WDLS, 15 DDLS, 2 pleomorphic LSs, and 11 myxoid LSs. cRNA from the individual tumors was labeled with Cy5-UTP using the Agilent Quick Amp Labeling Kit (Agilent Technologies). The mixed reference cRNA pool consisted of equal amounts of cRNA from all of the fatty tumors and was labeled with Cy3-UTP. Equal amounts of labeled tumor and reference were mixed and hybridized to Agilent Human 44K microarray slides at 63°C for 24 hr. After washing, microarray slides were read using an Agilent Scanner. Agilent Feature Extraction software v.7.5 was used to calculate gene expression values. The feature extracted files were imported into the Rosetta Resolver® system v.7.1 for gene expression data analysis (Rosetta Biosoftware, Seattle, WA). The intensity ratios between the tumor sample and mixed reference pool calculated for each sequence were computed according to the Agilent error model. A particular sequence was considered differentially expressed if the calculated *P*-value of change was ≤ 0.01.

The Rosetta Array Search Tool (ROAST) was used to compute the correlation of the expression probe for miRNAs 214 and 199a2 (AK021543) in the LSs with all other expression probes in the Agilent microarray. The ROAST conducts a statistically weighted expression profile similarity search using a cosine correlation, with an arbitrary *P*-value cutoff (set at 0.01).

DNA Isolation

Genomic DNA was extracted from fresh frozen tissue using the DNeasy Blood and Tissue Kit (Qiagen) with the following modifications to remove excess adipose tissue. Briefly, 25–50 mg of tissue was homogenized in 720 μl of Buffer ATL using a rotor-stator homogenizer (Polytron PT-3100) for 15 sec. After a quick foam reducing spin, 80 μl of proteinase K was added and the samples were lysed overnight at 56°C. The next day, half of the lysed samples were removed to a new tube (taking care to avoid the fat at the top), treated with RNase A (100 mg/ml) (Qiagen) for 5 min, then purified through DNeasy columns. Seventy percent ethanol was substituted for Buffer AW2 in the final wash, and DNA was eluted in 50 μl of sterile water (Invitrogen, Carlsbad, CA). The concentration and quality of the DNA was measured by NanoDrop and by electrophoresis in 1% agarose.

Array CGH Hybridization and Data Analysis

Labeling and hybridization of Agilent 105K oligonucleotide CGH arrays was performed according to the manufacturer's protocol for Human Genome CGH 105A Oligo Microarray Kit, v.5.0 (Agilent Technologies, Santa Clara, CA). Briefly, 1 μg of patient DNA and 1 μg of a pooled male DNA reference (Promega, Madison, WI) was digested with *Alu I* and *Rsa I* restriction enzymes (Promega, Madison, WI) for 2 hr, then labeled with Cy5-dUTP (tumor) and Cy3-dUTP (reference) using the Agilent Genomic DNA Enzymatic Labeling Kit for 2 hr at 37°C followed by 14–18 hr at room temperature. Unincorporated nucleotides

were removed using Microcon YM-30 spin filter units (Millipore, Billerica, MA) and incorporation and yield was measured with the NanoDrop Spectrophotometer. Labeled tumor and reference DNAs were combined, annealed with COT-1 DNA (Invitrogen, Carlsbad, CA) and 10× Blocking Agent (Agilent) for 30 min at 37°C after boiling, then hybridized to Agilent 105A arrays for 40 hr at 65°C according to the manufacturer's instructions. After hybridization, arrays were washed according to Procedure B (which includes an ozone blocking wash) and scanned using an Agilent Scanner (G2565BA). Files were extracted using Agilent Feature Extraction software v.9.5 with the default CGH protocol. Extracted arrays with a DRL Spread <0.3 were included in the analysis (average DRLS = 0.19).

CGH Analytics software v.4.0 (Agilent Technologies) was used for copy number analysis, employing the ADM2 algorithm (threshold 5) with Fuzzy Zero and Centralization corrections to minimize background noise. A minimum of three consecutive probes were required to define a region as amplified or deleted. The data were also filtered by requiring a minimum absolute average log2 ratio of 0.58. All data were inspected visually using the interactive view. Log2 ratios >1 (2-fold) were considered amplified and log2 ratios >2 (4-fold) highly amplified, log2 ratios <0.8 were considered hemizygous and log2 ratios <1.8 homozygous deletions. The probes were sourced from and mapped to the NCBI Genome Build 36 (March 2006 assembly). Agilent expression array files for the tumors were also imported into DNA Analytics 4.0 and were used to examine expression of individual candidate genes and for joint CGH-expression analysis of amplified and deleted genomic regions.

RESULTS

Clinical/Pathological Features

This analysis included 46 tumors from 45 individuals. Tumor and patient characteristics are outlined in Table 1. Of the 46 tumors, 8 were benign (6 lipomas, 1 myelolipoma, and 1 hibernoma), 21 were WDLS (14 lipomatous, 2 sclerotic, 3 mixed sclerotic/lipomatous, and 2 mixed sclerotic/inflammatory), and 17 were DDLS. Thirty-two tumors were primary tumors and 14 were local recurrences. Since the initial diagnosis, 22 patients have experienced a recurrence [10/21 (48%) WDLS and 12/17 (71%) DDLS]. The retroperitoneum (n = 28, 61%) was the most prevalent site of presentation, followed by the extremities (n = 10, 22%). The average age at initial diagnosis was 60 years old (median 58, range 32–89). The average size of the tumors was 19 cm (median 15 cm, range 5–45 cm). The male to female ratio was 21:25. Five tumor samples were collected after patients underwent neoadjuvant chemotherapy (11%). Of the 17 DDLS, one tumor presented in a metachronous fashion, i.e. a WDLS that transformed after 5 years into a DDLS; while all of the other DDLS presented in a synchronous fashion, i.e. the WD and DD components were both present at the time of initial diagnosis. The average follow-up from the time of surgery was 25.9 months (range, 1.6–63.4 months). At the time of this analysis, all patients with benign fatty tumors had no evidence of disease (NED). Of the patients with a WDLS (21), 20 had NED and 1 was alive with disease (AWD). Of the patients with a DDLS (17), 6 had NED, 4 were AWD, and 7 have died of disease (DOD).

Overall Array CGH Findings

An overview of the DNA copy number changes detected by the 105K oligonucleotide array CGH for the lipomas (F3–F52, n = 7), hibernoma (F75), WDLS (F101–F141, n = 21), and DDLS (F501–F540, n = 17) is outlined in Table 2. The original aCGH data have been submitted to the public database Cangem (http://www.cangem.org/).

The seven lipomas and the one hibernoma showed very few genetic aberrations, all of which were low level (Table 2). In the benign fatty tumors, the most common event visible by aCGH was the partial loss of chromosome arm 13q.

Copy number aberrations (CNAs) were far more numerous in the 38 WD and DDLS than in the benign fatty tumors (Table 2). The WDLS had an average of 11.1 CNAs and the DDLS had an average of 22.7 CNAs (Table 2), counting amplification of 12q13-q15 as a single CNA. Only one DDLS (F510) demonstrated aberrations on chromosome arm 12q alone. Amplifications were more numerous than deletions; however, 7/17 DDLS had at least one deleted region compared to only 2/21 WDLS (P = 0.05).

Well-Differentiated and De-Differentiated Liposarcomas

Chromosome 12

A detailed array CGH analysis of 25 genes located in the 12q13.2-12q23.1 region is

TABLE 1. Clinical and Pathological Description of the Tumors

Sample	Histology	Origin of sample	Sample location	Sample size (cm)	Gender	Age at initial diagnosis	Number of recurrences since initial diagnosis	Current status
F3	Lipoma	Primary	Arm	11	F	48	0	NED
F5	Lipoma, intermuscular	Primary	Leg	15	M	84	0	NED
F6	Lipoma	Primary	Supraclavicular	12	M	57	0	NED
F7	Lipoma	Primary	Arm	6	F	78	0	NED
F8	Lipoma	Primary	Pelvis	18	M	59	0	NED
F51	Myelolipoma	Primary	RP	12	F	51	0	NED
F52	Lipoma	Primary	RP	13	F	60	0	NED
F75	Hibernoma	Primary	RP	8	F	41	0	NED
F101	WDLS	Recurrent	RP	10	M	68	3	AWD
F102	WDLS	Primary	Leg	20	F	49	0	NED
F106	WDLS	Primary	Arm	16	F	44	0	NED
F107	WDLS (sclerotic)	Recurrent	Pelvis	10	M	56	1	NED
F108	WDLS	Primary multifocal	RP	18	M	74	0	NED
F109	WDLS	Recurrent	Leg	9	F	62	1	NED
F113	WDLS	Primary	RP	25	F	47	0	NED
F114	WDLS	Primary	Leg	12	M	56	0	NED
F115	WDLS	Primary	Leg	33	F	34	0	NED
F116	WDLS (lipomatous/sclerotic)	Primary	RP	28	F	57	0	NED
F118	WDLS (lipomatous/sclerotic)	Primary	RP	45	F	50	0	NED
F120	WDLS	Primary	Abdomen	44	F	62	1	NED
F121	WDLS	Recurrent	Groin	12	M	55	>5	NED
F122	WDLS	Recurrent	Scapula	8	M	41	>10	NED
F123	WDLS	Primary	RP	15	F	57	0	NED
F124	WDLS	Primary	RP	15	F	69	0	NED
F125	WDLS (sclerotic)	Recurrent	RP	14	F	56	1	NED
F126	WDLS	Primary	Leg	28	M	80	0	NED
F128	WDLS (lipomatous/sclerotic)	Recurrent	RP	10	M	63	1	NED
F132	WDLS (sclerosing/inflammatory)	Primary	RP	40	M	71	1	NED
F141	WDLS (sclerosing/inflammatory)	Recurrent	RP	15	M	71	1	NED
F501	DDLS	Recurrent	RP	11	F	33	7	DOD
F502	DDLS	Recurrent	Abdomen	18	F	32	3	AWD
F503	DDLS	Primary	RP	31	M	66	3	DOD
F505	DDLS	Primary	RP	15	F	66	1	DOD
F507	DDLS	Recurrent	RP	15	F	60	2	DOD
F508	DDLS	Primary	RP	29	F	54	0	NED
F509	DDLS	Primary	RP	32	F	70	1	DOD
F510	DDLS	Primary	RP	30	M	76	1	DOD
F514	DDLS	Primary	Leg	6	M	89	1	NED
F515	DDLS	Primary	RP	27	M	73	0	DOD
F516	DDLS	Primary	RP	27	F	50	0	NED
F519	DDLS	Recurrent	RP	5	F	82	2	NED
F520	DDLS	Recurrent	Groin	20	M	51	2	AWD
F521	DDLS	Recurrent	RP	5	M	57	2	AWD
F530	DDLS	Primary	RP	42	M	43	0	NED
F534	DDLS	Primary	RP	24	F	67	1	AWD
F540	DDLS	Primary	RP	15	M	86	0	NED

Clinical and pathological description of the samples that were used in the aCGH analysis.
WDLS, well-differentiated liposarcoma; DDLS, de-differentiated liposarcoma; RP, retroperitoneum; NED, no evidence of disease; AWD, alive with disease; DOD, died of disease.

presented (Table 3), as is a penetrance plot summarizing the chromosomal aberrations (Fig. 1a). The corresponding RNA expression values of the LSs for this region are listed (Supporting Information Table S1). As expected, the 12q13-q15 region was amplified for at least one location in all of the LSs. The three peaks of amplification in this region were centered at *CDK4*, *HMGA2*, and *MDM2*. *CDK4* was amplified in a slightly lower percentage of WDLS (86%, 18/21) as

TABLE 2. DNA Copy Number Changes in Tumor Samples

Sample	Histology	Origin of sample	Sample location	DNA copy number gains (log2 ratio >1) by aCGH (italics indicates log2 ratio >2)	DNA copy number losses (log2 ratio <0.8) by aCGH (italics indicates log2 ratio <1.8)
F3	Lipoma	Primary	Arm		13q13.3(LHFP)-qter
F5	Lipoma, intermuscular	Primary	Leg		13q13.3(LHFP)-q21.3
F6	Lipoma	Primary	Supraclavicular		
F7	Lipoma	Primary	Arm		13q13.3(DCLK1)-q21.33
F8	Lipoma	Primary	Pelvis		6q13(RIMS1)-qter, 10q22.1-pter, 10q22.2-q22.3, 13
F51	Myelolipoma	Primary	RP		
F52	Lipoma	Primary	RP		
F75	Hibernoma	Primary	RP		
F101	WDLS	Recurrent	RP	12q13-q15, 12q21.33, 12q23.1, 12q23.2, Xp22.2	
F102	WDLS	Primary	Leg	1q21-q24, 12q14.1, *12q13-q15*, 12q21.2, 12q21.31, 12q24.22	
F106	WDLS	Primary	Arm	12q12, *12q13-q15*, 12q21.2, *12q21.31*, *12q21.33*, 12q23.1, 17p13.1	
F107	*WDLS (sclerotic)*	*Recurrent*	*Pelvis*	*5p15.33(TERT), 12q13-q15, 12q15-q21.1, 12q21.2, 12q21.31, 12q21.32, 12q21.33, 12q22, 12q23.3-q24.11, 12q24.12*	
F108	WDLS	Primary multifocal	RP	*12q13-q15, 12q15-q21.1, 12q21.2, 12q21.31, 12q21.32,* 12q21.33, *21q21.1, 21q22.12 (RUNX1*), 21q22.12, 21q22.2, 21q22.3*	1q25.2 (ABL2)-qter
F109	WDLS	Recurrent	Leg	1q21-q24, *12q13-q15*, *12q21.31-q21.33*, 12q22, *12q23.1*, *12q23.2, 12q24.32*	
F113	WDLS	Primary	RP	1q21-q24, 1q25.1, *12q13-q15*, 12q21.1, 12q21.2, 12q23.3, 12q24.22	
F114	WDLS	Primary	Leg	1q21.1-q25.2, 12q13-q15, 12q21.2-q21.31, 12q21.32-q21.33, 12q22-q23.3, 12q24.12, 12q24.23, 16q15.3-q21.1	
F115	*WDLS*	*Primary*	*Leg*	*1q21-q24, 1q25.1-q25.2, 12q13-q15, 12q21.1, 12q21.31, 12q22, 12q23.1, 12q23.3, 12q24.12, 12q24.21-q24.22*	
F116	WDLS (lipomatous/sclerotic)	Primary	RP	*1q21-q24*, *1q25.1*, 1q25.2, *6q23.1*, 6q23.3, 6q24.2, 6q27, 11p15.4-pter, 11p15.2, 11p13, *12q13-q15*, *12q21*, *12q22*, *12q23.2*, 14q31.3-q32.12, *14q32.13-q32.2 (DLK1)*, 14q32.2-qter, 18q21.1-qter	
F118	WDLS (lipomatous/sclerotic)	Primary	RP	*8p23.1*, *8p22*, *8p21.2*, *12q12*, *12q13-q15*, *12q21.2*, *12q21.33*, *12q22, 12q23.2*, 12q23.2, 14q32.12-q32.2	
F120	WDLS	Primary	Abdomen	8q12.3, 8q13.3, 8q24.21 (DDEF1*), *12q13-q15, 12q21.1-q21.2*, *12q21.31*, 12q21.32, 12q23.1, *12q23.3*, 19p13.2, *19q13.2*, 19q13.33, 22q11.23	

(Continued)

TABLE 2. DNA Copy Number Changes in Tumor Samples (Continued)

Sample	Histology	Origin of sample	Sample location	DNA copy number gains (log2 ratio >1) by aCGH (italics indicates log2 ratio >2)	DNA copy number losses (log2 ratio <0.8) by aCGH (italics indicates log2 ratio <1.8)
F121	WDLS	Recurrent	Groin	*1q24.2*, *1q25.1*, *2p16.3*, 6q22.1-q23.2, 6q24.1, 6q24.2, 6q24.3, 8q12.1, 8q21.12-q21.13(PKIA), 8q21.2, *12q13-q15*, *12q21.31*, *12q23.1*, *12q24.11 (FOXN4)*, *12q24.12*, 14q12, 14q23.2 (HSPA2), 15q21.3, 15q25.2, 15q26.2, 21q21.2, 21q22.13-q22.3	
F122	WDLS	Recurrent	Scapula	1q21.2, *1q24.1-q24.2*, 1q24.3-q25.1, 1q31.1, *12q13.12*, *12q13-q15*, *12q21.1*, *12q21.2-q21.32*, 16q12.2, 16q21 (CDH8), *18q12.3*, *18q21.1 (SMAD2,7)*, 18q21.2 (SMAD4*-DCC*)	
F123	WDLS	Primary	RP	*12q13-q15*, *12q21.2*, *12q21.32*, 15q25.2, 15q25.3 (NTRK3*), 15q26.3	
F124	WDLS	Primary	RP	12p12.3 (LMO3), 12q12, *12q13-q15*, 12q21.2, 12q21.33, *12q23.1*, 14q32.12-qter, 15q25.3-qter	
F125	WDLS (sclerotic)	Recurrent	RP	1q24.3, *3q13.31*, *3q13.33*, *4p16.3 (FGFR3)*, 4p16.1, 4p15.32, *6q25.1*, 7p14.3-pter, 8q22.1, *8q24.13*, *12q13-q15*, *12q21.1*, *12q21.31*, *18p11.31*, *19q13.12*, *19q13.2*, 21q22.3	
F126	WDLS	Primary	Leg	4p15.32-p15.32, 4p15.2, 12q13-q15, 12q23.2-q23.3	1p12-p34.2, 17p12
F128	WDLS (lipomatous/sclerotic)	Recurrent	RP	1p13.3, 1p13.2, 1p12, 1q21.2, 1q41-q42.11, 1q42.2, 9q22.2-q22.31, *12p13.32 (KCNA1)*, *12q13-q15*, *12q21.1*, 12q21.31, *12q21.33*, *12q22*, 12q23.1, *12q24.12*, *12q24.23*, *12q24.31*, 13q22.3	
F132	*WDLS (sclerosing/inflammatory)*	*Recurrent*	*RP*	*4q27 (CCNA2), 4q31.21, 4q21.22 (HHIP*), 4q32.1, 6q21, 6q22.31, 12q13.11 (SLC38A4), 12q13-q15, 12q21.1, 12q21.2, 12q21.31, 12q21.33, 12q24.23*	
F141	*WDLS (sclerosing/inflammatory)*	*Recurrent*	*RP*	*1q24.1, 3q23, 4q27 (CCNA2), 4q31.21, 4q21.22 (HHIP*), 4q32.1, 6q21, 6q22.31, 6q23.3, 6q25.3, 12q13.11 (SLC38A4), 12q13-q15, 12q21.1, 12q21.2, 12q21.31, 12q21.33, 12q24.23*	
F501	DDLS	Recurrent	RP	1p36.66, 1p36.23, 1p36.13, *1p35.1*, 4p16.3, 4p16.2, 4p15.31, 6q22.1, 6q23.2, *6q23.3*, 6q24.1, 6q25.1, *12q13-q15, 12q21.1(KCNC2*), 12q21.31(PPFIA2*), 12q21.33, 12q22, 12q23.1, 12q23.3*,	

(Continued)

TABLE 2. DNA Copy Number Changes in Tumor Samples (Continued)

Sample	Histology	Origin of sample	Sample location	DNA copy number gains (log2 ratio >1) by aCGH (italics indicates log2 ratio >2)	DNA copy number losses (log2 ratio <0.8) by aCGH (italics indicates log2 ratio <1.8)
				14q32.11, 14q32.12-q32.13, 14q32.2, 14q32.33	
F502	DDLS	Recurrent	Abdomen	2p23.2, 8p11.22(WHSC1L1, FGFR1), 8p11.22-qter, *12q13-q15*, *12q21*, *12q21.31*, *12q21.33*, *12q23.1*, 15q21.1, 15q21.2, 15q23-q24.2, 16q22.2, 16q23.1, 16q23.3-q24.1, 19q12-q13.2, *22q13.32-q13.33*	1p13.2-1p22.2, 3p12.1-3p22.1, 8p11.22-p22
F503	*DDLS*	*Primary*	*RP*	*2q34(ERBB4*), 3p24.3-pter, 5p15, 6q23.1-q24.3, 7p15.2(HOX), 8p22, 8q21.12-q21.13, 8q23.3, 9q21.13, 9q21.2-q21.31, 10p14, 11q12.1, 11q13.4, 11q14.3, 11q22.2, 12p12.33, 12p13.32, 12p13.2, 12p13.1, 12p12.3, 12p12.2, 12p12.1, 12p11.23, 12q12, 12q13-q15, 12q21.1, 12q21.2, 12q21.3, 12q22, 12q23.1, 12q24.11, 12q24.32, 13q22.1, 13q31.1, 15q22.32-q23, 15q26.2-qter, 19p13.3, 19p13.11-p13.2, 20p13*	*2p25.3, 3p12.1-p24.3, 4q25-q34.3, 6p22.1, 8p23.3, 8q21.13, 8q21.3-q23.1, 8q24.11-q24.13, 9p21.3(CDKN2A/B)-pter, 9q22.2, 9q22.32-q34.12, 9q34.2(RXRA)-qter, 11q14.3-q22.1, 11q22.3-qter, 12p13.2, 13q12.11-q21.32, 15q14-q21.3, 15q24.1-q25.1, 17p13.3, 20p11.21-p13, 20q12.32-qter, Xp22.33, Xq21.1*
F505	DDLS	Primary	RP	*1q21.3*, *1q21.2*, *1q24.1*, *1q24.2*, *1q24.3*, 1q31.1, 1q32.1, *1q44*, *4p14*, *6q22.2*, 6q22.31, *6q23.2*, *6q23.2*, *6q23.3-q24.3*, *6q25.2*, *7p21.1*, 7q22.1, *8q21.12(PKIA*)*, *9p13.2*, *9q21.11*, *11p11.2*, 11q13.1, 11q25, 12p13.32-pter, 12p13.31, *12q13-q15*, *14q13.1(EGLN3)*, *14q21.2*, *14q21.3*, 14q31.1, 15q24.2-q26.1, *15q26.1-qter*, *16q21(CNOT1)*, 16q21, *16q22.2-q22.3*, *16q23.1(CHST6)*, *16q24.3*, *19q13.43(ZNF cluster)*, 22	1q31.3-q43, 9p21.1-p24.1, 11q14.1(DLG2), 15q21.1-q21.2
F507	DDLS	Recurrent	RP	*1q21.2*, *1q21.3*, *1q22*, *1q23.1*, *1q23.2*, *1q23.3*, *1q24.1*, *1q24.3*, *1q25.1*, *1q25.2*, *5p15.33(TERT)*, 5p15.1, *12q13-q15*, *12q21.1*, *12q21.2*	3p12.1-p22.1, 4q, 5p15.33, 11, *11p11.2(CHST1)*, 13, 14, 18p, 20p, Xq
F508	DDLS	Primary	RP	1q24.2, 6q27, *12q13-q15*, *12q21.1*, *12q21.2*, *12q21.31*	
F509	*DDLS*	*Primary*	*RP*	*2q24.3, 2q32.1, 6q27, 11p12, 11p11.2, 12q13-q15, 12q21.2, 12q21.31, 14q24.2, 14q32.2, 14q32.33, 19q13.41*	
F510	DDLS	Primary	RP	*12q13-q15*, 12q21.2, *12q21.31*, 12q21.32, 12q22, 12q23.1	
F514	DDLS	Primary	Leg	*1p32.1*, *1p31.3*, *1q24.3*, *1q32.2*, 2q32.2, 4q34.1, *6p24.2(NEDD9)*, 6p21.1, *8p11.22-p11.23*, *9q21.1*, *12q13-q15*, *12q21.1*, *12q21.2*,	

(Continued)

TABLE 2. DNA Copy Number Changes in Tumor Samples (Continued)

Sample	Histology	Origin of sample	Sample location	DNA copy number gains (log2 ratio >1) by aCGH (italics indicates log2 ratio >2)	DNA copy number losses (log2 ratio <0.8) by aCGH (italics indicates log2 ratio <1.8)
				12q21.31, *12q21.32*, *12q21.33*, *12q23.1*, 19p13.3, 22q13.31	
F515	DDLS	Primary	RP	*1p32.1-p32.2*, *1q21.3*, *1q22*, *1q23.2-q23.3*, *1q24.1*, *1q24.2*, *1q23.3*, *1q31.3*, 1q41, *1q42.12(PARP1)*, *2q36.1(PAX3)*, 3p25.2, *8q11.22*, 8q11.23, 8q21.1(IMPAD1), *8q13.2*, 8q21.3, 8q24.21, *9q31.2*, *10p13*, *12q13-q15*, *12q21.2*, *12q21.31*, *12q23.1*, *12q24.12*, *14q12*, *14q12-q13.1*, *14q13.2(PSMA6)*, 16q12.3, 18q12.3, 18q21.2, *20q11.23*, *20q12*	9p24.2, 9p23, 9p21.3(CDKN2A)
F516	*DDLS*	*Primary*	*RP*	*3q24-q25.1*, *3q26.1*, *3q26.31(NLGN1)*, *6q16.1-q21*, *6q22.31*, *6q24.2(PLAGL1)-q25.1*, *6q25.3*, *12q13-q15*, *12q21*, *12q23.1*, *13q13.1*, *13q13.3*, *13q14*, *13q21.2-q21.3*	
F519	DDLS	Recurrent	RP	2q24.1-q31.1, 3q29, 5p, *7p22.3*, 7p22.2, *7q11.21*, 7q11.22, 7q21.11, 7q21.12, 7q21.2, 7q21.3, 7q22.2(MLL5), 7q31.1, 8q21.12(PKIA), *8q22.3*, 10q11.22, 10q22.2-q23.1, 10q24.31, 10q24.32-q25.3, 10q26.12(TACC2), *12p13.32*, *12p13.31*, 12p12.3, *12p12.1*, *12p11.22-p12.1*, *12p11.22*, *12p11.21(BICD1*)*, *12q12*, *12q13.12*, *12q13-q15*, *12q21.31*, *12q21.33*, *12q22*, *12q23.1*, *12q23.3-qter*, *15q15.1*, *18q21.33-qter*, *19q12*, *19q12-q13.11*, *19q13.42-qter*	8p23.2-pter, 11q14.1, 11q14.2, 11q21, 11q22.3-q23.3, 11q24.1-qter, 15q14-q15.1, 15q15.1-q21.1, 15q21.2, 15q26.2-qter
F520	DDLS	Recurrent	Groin	*1p32.1-p32.2*, *1q23.2-q23.3*, *1q24.3*, *12q13-q15*, *12q21.32-q21.33*	
F521	DDLS	Recurrent	RP	*1q23.2*, *1q24.3*, *4p15.32*, *4q28.3*, 6q22.31, *6q23.3-q24.1*, *6q24.3-q25.1*, *6q25.2*, *10p15.2*, *10p12.31*, *10p21.1-q12.2*, *10p11.22*, 11p15.4, *11p15.1*, 11p14.3, *11p14.2(BBOX1*)*, *12q13-q15*, *12q21.1*, *12q21.2*, *12q23.2*, *12q23.3*, *12q24.12(CUTL2)*, *12q24.23*, *12q24.31(ZNF664)*, *14q12*, 14q13.2(TITF1), *14q24.1*, *14q24.3*, *14q31.1*, *20q13.12*	7p14.2(EEPD1)
F530	DDLS	Primary	RP	5p13.3, 7p15.1-q15.2, 9q21.1, *12q13-q15*, *12q21*, 12q22, *12q23.2*, 12q24, 16q23.3, 19p13.3	

(Continued)

TABLE 2. DNA Copy Number Changes in Tumor Samples (Continued)

Sample	Histology	Origin of sample	Sample location	DNA copy number gains (log2 ratio >1) by aCGH (italics indicates log2 ratio >2)	DNA copy number losses (log2 ratio <0.8) by aCGH (italics indicates log2 ratio <1.8)
F534	DDLS	Primary	RP	2q13, 2q35, 2q37.1, 3p25.3, 4q13.3, 5p15.33(TERT), 6q14.2, 7p15.1-p15.2, 7p15.3, 7p22.2, 12p13.32, 12p13.2, 12p12.3, 12p11.1, *12q13-q15*, 12q21.2, 12q23.1, 12q24.12, 12q23.2, 12q23.3, 12q24.12, 12q24.31	
F540	DDLS	Primary	RP	12q13-q15, 16q22.1, 16q22.3	

An overview of the DNA copy number changes detected by the 105K oligonucleotide array CGH for the lipomas (F3–F52, $n = 7$), hibernoma (F75), WDLS (F101–F141, $n = 21$), and DDLS (F501–F540, $n = 17$). High-level amplification (log2 ratio > 2) and homozygous deletions (log2 ratio < 1.8) are in italics. If only a single gene is implicated by an amplification or deletion, it is listed in parenthesis after the location. Breaks within a gene are marked with an asterisk.

compared to the DDLS (100%), while *HMGA2* and *MDM2* were amplified in a slightly higher percentage of WDLS as compared to the DDLS [*HMGA2*: 100% WDLS, 88% DDLS (15/17); *MDM2*: 100% WDLS, 94% DDLS (16/17)]. *HMGA2* was frequently truncated by amplification in both the WD and DDLS. The DDLS were more likely than the WDLS to have amplification levels greater than 32 copies (log2 ratio >4) at *CDK4* (35% vs. 10%), *HMGA2* (24% vs. 10%), and *MDM2* (65% vs. 29%) (Data not shown).

The genes surrounding *CDK4* and *MDM2* (55.7–56.6 Mb), which may have prognostic and therapeutic implications, were amplified to varying degrees in the different tumors (Table 3). The genes just proximal and distal to *CDK4*, such as *STAT6* (signal transducer and activator of transcription 6, interleukin-4 induced), *B4GALNT1* (β-1,4-*N*-acetyl-galactosaminyl transferase 1), *OS9* (osteosarcoma amplified 9, endoplasmic reticulum lectin), *CENTG1* (*AGAP2*, ArfGAP with GTPase domain, ankyrin repeat and PH domain 2), *TSPAN31*, *METTL1* (methyltransferase like 1), and *XRCC6BP1* (XRCC6 binding protein 1) were frequently coamplified in both the WD and DDLS. Other than *GLI1* (GLI family zinc finger 1, 12q13.3), we did not identify any of the genes surrounding *CDK4* as being amplified in the DDLS alone. Similarly, amplification of the *MDM2* region, as well as 12q21-q23, was highly complex. A ~224 Kb region containing the genes *FRS2* (fibroblast growth factor receptor substrate 2), *CCT2* (chaperonin containing TCP1, subunit 2), *LRRC10* (leucine rich repeat containing 10), and *BEST3* (bestrophin 3) was frequently amplified in both the WD and DDLS, often after an interval of normal copy number at *CPM* (carboxypeptidase M) and *CPSF6* (cleavage and polyadenylation specific factor 6). The genes immediately distal to *BEST3*, *RAB3IP* (RAB3A interacting protein), and *CNOT2* (CCR4-NOT transcription complex, subunit 2) were often amplified although in fewer samples. RNA expression correlated well with amplification for *FRS2*, *CCT2*, *RAB3IP*, and *CNOT2*, but not for *BEST3* (no data for *LRRC10*). Additionally, an individual 12q21 region containing *CCDC131* (*ZFC3H1*, zinc finger, C3H1-type containing), *GLIPR1* (GLI pathogenesis-related 1), *BBS10* (Bardet-Biedl syndrome 10), *ZDHHC17* (zinc finger, DHHC-type containing 17), *KITLG* (KIT ligand), and *WDR51B* (*POC1B*, POC1 centriolar protein homolog B) were the targets of focal amplification and overexpression in 18–32% of the LSs. Finally, 15 (39%) LSs had focal amplification at 12q23.1. The smallest region of overlap (SRO) centered on *ELK3* (ELK3, ETS-domain protein). This amplification also correlated with gene overexpression. None of the amplifications from *MDM2* to *ELK3* correlated with the de-differentiated phenotype.

Chromosome 1

Amplification of chromosome 1 was found in both WD and DDLS. Although approximately equal percentages of WD and DDLS had at least one region of amplification on chromosome 1, we saw a clear difference in the location and level of

TABLE 3. 12q Regional Gains in Liposarcomas

A detailed array CGH analysis of the amplification of 25 genes in the q13.2-q23.1 region of chromosome 12. Black box, Log2 ratio $>$ 2.0; gray box, Log2 ratio $>$ 1.0 and $<$ 2.0; black/gray stripped box represents a likely gene breakage. WDLS (F101–F141) are homogenous lipomatous tumors unless qualified by a *sclerotic, ^mixed lipomatous and sclerotic, and °mixed sclerotic and inflammatory.

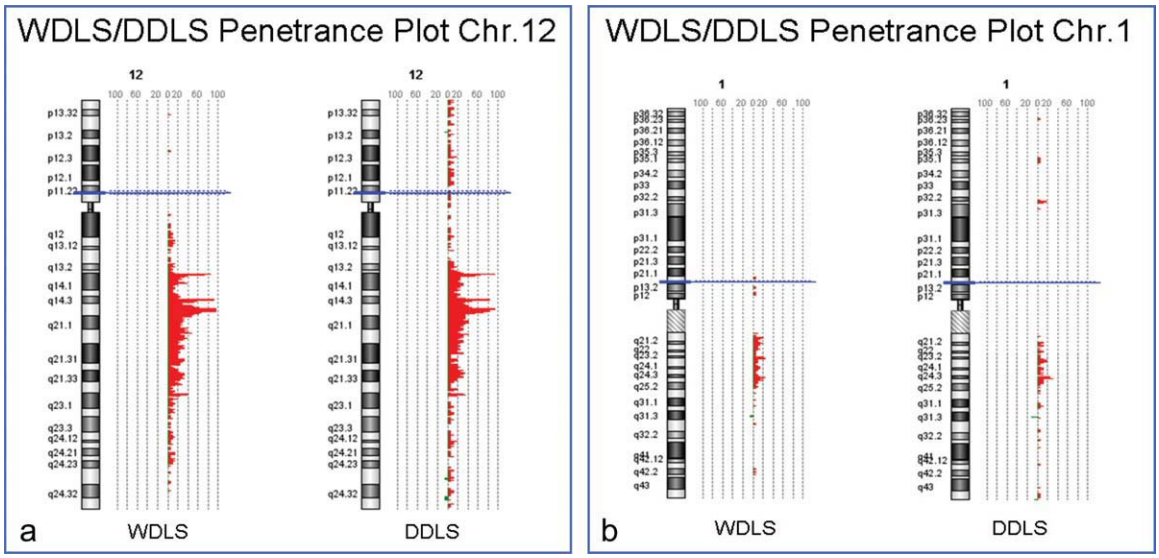

Figure 1. Penetrance plots of copy number changes in the LS tumors (WD and DD). Red bars depict percentage of tumors that had an amplification in the corresponding region of the chromosome. (a) Chromosome 12; (b) chromosome 1.

amplifications between WD and DDLS (Table 4; Fig. 1b). Four DDLS (24%) had a focal amplification of 1p32.2 at the *JUN* oncogene while no WDLS showed this alteration. In tumor F514, the *JUN* amplicon was just 407 Kb and contained only *JUN*. *JUN* expression correlated only moderately well with amplification, possibly due to poor hybridization to the single probe for *JUN* on the RNA arrays (Supporting Information Table S1).

At least one region from 1q21-q24 was amplified in nine WDLS (43%) and eight DDLS (47%). As compared to the WDLS, the amplicons of this area in the DDLS were more likely to be high level and discontinuous. The most frequently amplified region of 1q in both the WD and DDLS was centered at 1q24.3 within the *DNM3* (dynamin 3) gene (170,003,784—170,864,586 Mb). A total of 7/21 WDLS (33%) and 6/17 DDLS (35%) had amplification of an ~1 Mb region centered at *DNM3*. The level of amplification was higher in the DDLS with 5/17 having high-level amplification as compared to only 1/21 WDLS. Two micro-RNAs, miR-214 and miR-199a2, map in the *DNM3* gene at the site of highest amplification. Expression of the miRNAs (AK021543) correlated with amplification in 5/6 LSs that contain high-level amplification (Supporting Information Table 1).

A ROAST of the AK021543 mRNA was performed to identify the specific targets of these miRNAs. A ROAST is a procedure in the Rosetta analysis program that searches for genes with correlated or anticorrelated expression levels. This identified *CDKN1B/p27/Kip1* (cyclin-dependent kinase inhibitor 1B) as a potential target in the LSs. mRNA for *CDKN1B* was anticorrelated to the AK021543 probe for miR-214 and miR-199a2 (correlation value, −0.63; *P*-value, 0.00015). Looking at the matched values (Supporting Information Table S1), the amplification of miR-214 and miR-199a2 was reflected in a lower value for *CDKN1B*.

Additional chromosome 1 regions that were amplified in a significant number of samples are listed in Table 4. Expression of *MCL1*, *PIGM*, *ATF6*, and *BLZF1* correlated significantly with amplification (Supporting Information Table S1).

Chromosome arm 6q

Amplifications of chromosome bands 6q23-q24 in the WD and DDLS are summarized in Table 4. 6q23-q24 was amplified in 24% of the LSs at three subregions: at 6q23.3 near *MAP3K5*, at 6q24.1 (no genes), and at 6q24.3 near *SASH1/UST/MAP3K7IP2* (SAM and SH3 domain containing 1/uronyl-2-sulfotransferase/TAB2, TGF-β activated kinase 1/MAP3K7 binding protein 2). Amplifications were more frequent in the DDLS; amplification of *MAP3K5* occurred in 4/17 (24%) of the DDLS and in 1/21 (5%) of WDLS. Another common amplicon was located at *MAP3-K7IP2* which also occurred in 5/38 (13%) of the LSs. Other genes with focal amplifications on 6q

TABLE 4. 1p, 1q, and 6q Regional Gains in Liposarcomas

		1p32.2		1q21.1	1q23.2	1q23.2	1q24.2	1q24.3	1q24.3	1q24.3	1q		6q	6q23.2	6q23.2	6q23.3	6q23.3	6q24.3
		JUN		MCL1	PIGM	ATF6	BLZF1	VAMP4	MIR199A,214 DNM3	PIGC	ANY		ANY	CTGF	TCF21	MAP3K5	IFNGR1	MAP3K7IP2
		59.0 Mb		148.8 Mb	158.2 Mb	160.0 Mb	167.6 Mb	169.9 Mb	170.3 Mb	170.6 Mb				132.3 Mb	134.2 Mb	136.9 Mb	137.5 Mb	149.6 Mb
Sample																		
F101	WDLS																	
F102	WDLS																	
F106	WDLS																	
F107*	WDLS																	
F108	WDLS																	
F109	WDLS																	
F113	WDLS																	
F114	WDLS																	
F115	WDLS																	
F116^	WDLS																	
F118^	WDLS																	
F120	WDLS																	
F121	WDLS																	
F122	WDLS																	
F123	WDLS																	
F124	WDLS																	
F125*	WDLS																	
F126	WDLS																	
F128^	WDLS																	
F132°	WDLS																	
F141°	WDLS																	
F501	DDLS																	
F502	DDLS																	
F503	DDLS																	
F505	DDLS																	
F507	DDLS																	
F508	DDLS																	
F509	DDLS																	
F510	DDLS																	
F514	DDLS																	
F515	DDLS																	
F516	DDLS																	
F519	DDLS																	
F520	DDLS																	
F521	DDLS																	
F530	DDLS																	
F534	DDLS																	
F540	DDLS																	

Log2 ratio > 2.0
2.0 < Log2 ratio > 1.0
Likely Gene Breakage
* Sclerotic
^ Mixed Lipomatous and Sclerotic
° Mixed Sclerotic and Inflammatory

Regional chromosomal gains in chromosome arms 1p, 1q, and 6q that were noted in the liposarcoma samples. Black box, Log2 ratio > 2.0; gray box, Log2 ratio >1.0 and < 2.0; black/gray stripped box represents a likely gene breakage. WDLS (F101–F141) are homogenous lipomatous tumors unless qualified by a *sclerotic, ^mixed lipomatous and sclerotic, and °mixed sclerotic and inflammatory.

included *CTGF* (connective tissue growth factor) and *TCF21* (transcription factor 21) at 6q23.2, and *IFNGR1* (interferon γ receptor 1) at 6q23.3. The expression of *CTGF* was also increased in several nonamplified LSs (11 WD and 9 DDLS).

Micro-RNAs in the 12q, 1q, and 6q Amplicons

miR-26a2, located in the *CDK4* amplicon was amplified in 16 of 17 (94%) of the DDLS and in 19 of 21 (90%) of the WDLS. miR-616, located proximally in intron 1 of *DDIT3* (DNA-damage-inducible transcript 3), was much less frequently amplified (in 2/17 DDLS and 2/21 DDLS). miR-617 and miR-618, located in the *LIN7A* (lin-7 homolog A) locus at 12q21.31, were amplified in 2/17 DDLS and 5/21 WDLS. None of the miRNAs that were located on 12q appear to be a target of focal gains or amplifications.

On chromosome arm 1q, there were 10 miRNAs mapping to the ~30 Mb amplified region between 1q21 and 1q25. Most did not appear to

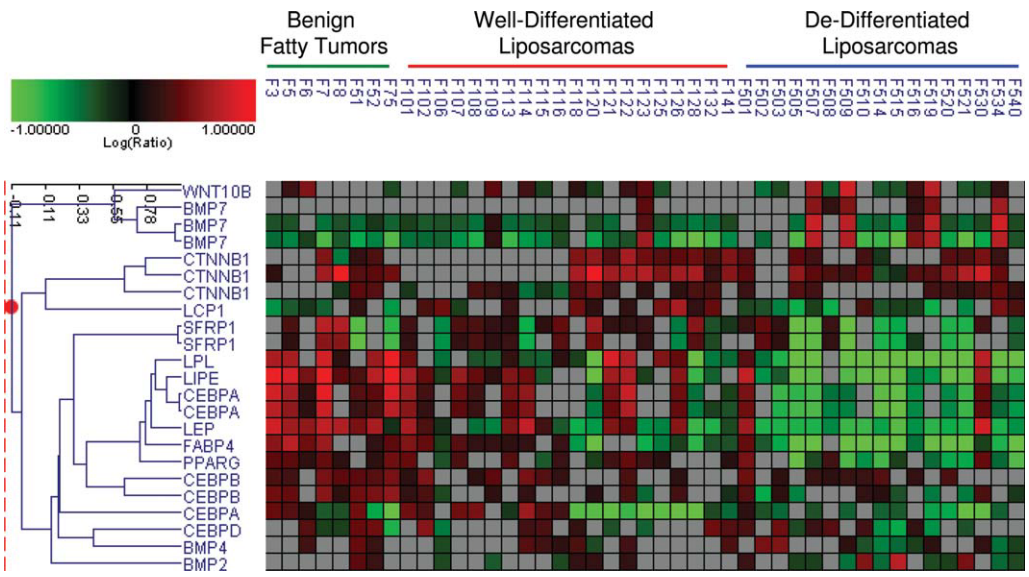

Figure 2. Supervised clustering: 2-D clustering of 45 fatty tumors based on the expression pattern of selective genes associated with adipogenesis. Length of dendrogram arm depicts degree of association of the 16 genes based on their expression pattern in the fatty tumors. Tumor samples (top); individual genes (left). Red, increased expression; green, decreased expression. Color intensity correlates with degree of expression as compared to the cRNA mixed reference pool.

be the targets of amplification. miR-214 and miR-199a2, both located in intron 14 of the *DNM3* gene at 1q24.3, were amplified in multiple samples (6/17 DDLS and 7/21 WDLS) and localized to the region of maximal amplification on chromosome arm 1q (Table 4). The level of amplification in the DDLS samples ranged from 2-fold in F520 to 20-fold in F521. Analysis of the expression of both miR-214 and miR199a2, contained in a single probe on the Agilent 4x44K expression arrays (AK021543/HEMBA1001803), indicated that amplification and expression correlated in 5/6 samples that had high-level amplification. In the DDLS without correlated expression of miR-214 and miR-199a2 (F507), the surrounding genes *VAMP*, *DNM3*, *PIGC*, and *C1orf9* (chromosome 1 open reading frame 9) all had upregulated expression. miR-548a2 at chromosome band 6q23.2, distal to *MYB* (v-myb myeloblastosis viral oncogene homolog), was not amplified in any of the samples.

RNA Expression Analysis of Genes Involved in the Adipocyte Differentiation Pathway

The expression profiles of 37 LSs and 8 benign fatty tumors were evaluated for genes intrinsic to adipocyte differentiation and lipogenesis. Representative genes are depicted (Fig. 2). Log2 ratios for these genes and for genes in the 12q, 1p, 1q, and 6q amplicons are shown (Supporting Information Table S1). Almost all of the DD samples lacked expression of selective lipogenic markers, including *LPL* (lipoprotein lipase), *LEP* (leptin), *FABP4* (aP2, fatty acid binding protein 4, adipocyte), and *LIPE* (lipase, hormone-sensitive). In addition, most of the DD samples showed loss of expression of the adipogenic transcription factors *CEBPA* [CCAAT/enhancer binding protein (C/EBP)] and *PPARG* (peroxisome proliferator-activated receptor γ). This explained the loss of lipogenic markers and indicated that an arrest in adipogenesis is occurring upstream of these factors. In an attempt to identify where the arrest in adipogenesis occurred, we examined the gene expression of several factors that regulate adipogenesis, including *BMP 2*, *4*, and 7 (bone morphogenetic protein 2, 4, 7), *WNT10b* (wingless-type MMTV integration site family 10b), *SFRP1*, *CTNNB1* [catenin (cadherin-associated protein), β1], *CEBPD*, *CEBPB*, and *CEBPG* (Fig. 2) (Rosen and MacDougald, 2006; Gesta et al., 2007). In some cases, the expression of factors that oppose adipocyte differentiation, such as *BMP2* and *BMP7*, were elevated and the expression of factors that promote adipogenesis [*BMP4* and *SFRP1* (secreted frizzled-related protein 1)] were lower in the DD samples.

SFRP1, which maps to 8p11.21, is of particular interest. SFRP's are factors that antagonize WNT proteins to promote adipogenesis (Bennett et al., 2002). 8/17 DDLS had very low expression of

SFRP1 (log 2 ratio <-1) while only 3/20 WDLS had low expression (Fig. 2, Supporting Information Table S1). This suggests that loss of *SFRP1* expression and possibly overexpression of the WNT signaling pathway may be a factor in adipocyte de-differentiation.

Clinical Correlates

A slight gender difference was noted regarding the age of tumor presentation. Female patients developed tumors at an earlier age; they accounted for 10/12 of the tumors which developed in patients who were $\leq$50 years old. In contrast, male patients accounted for 9/12 tumors which developed in patients $\geq$70 years old ($P = 0.0123$). *CCDC131* amplifications (12q21.1) preferentially occurred in recurrent lesions (3 primary, 8 recurrent; $P = 0.0076$). *GLI1* and *JUN* (1p32.2) amplifications did not occur within the same tumors and were only noted in the DD samples (F509, F510, F516, F519, and F508, F514, F515, F520, respectively). Finally, all 6q amplifications were noted in retroperitoneal lesions; however, only 32% of the retroperitoneal LSs had 6q amplifications.

DISCUSSION

To begin our analysis, we performed aCGH on seven lipomas and one hibernoma. None of the benign fatty tumors in this analysis harbored gains in the region of 12q13-q15. However, we did identify frequent losses in chromosome arm 13q. Partial deletions of 13q have been well documented in lipomas and atypical lipomatous tumors alike (Dahlen et al., 2003). The deletion of 13q often involves the area surrounding *RB1*. Our analysis indicated variable deletions in this region that often included *RB1* (13q14.2). However, the gene expression of *RB1* was not particularly low in these tumors.

Chromosomal CNAs were far more numerous in the WD and DDLS than in the benign fatty tumors (Table 2). Amplifications were more numerous than deletions; however, 7/17 DDLS had at least one deleted region compared to only 2/21 WDLS ($P = 0.05$). This suggests that de-differentiation in some cases may result from losses of critical genes rather than gains. These losses do not appear to target any one chromosomal region. However, three DDLS (F503, F505, and F515) had a hemizygous loss of *CDKN2A* (cyclin-dependent kinase inhibitor 2A) which correlated to lower gene expression (data not shown).

Amplifications of 12q are commonly seen in both WD and DDLS (Horvai et al., 2009; Snyder et al., 2009). In our analysis, 100% of the LSs had at least one region between 12q13-q15 that was amplified. The DDLS tended to have amplification levels in these areas of greater than 32 copies. *CDK4* was amplified in 100% of the DDLS, but in only 86% (18/21) of the WDLS. Conversely, the amplification peaks surrounding *HMGA2* and *MDM2* were more frequently amplified in the WDLS as compared to the DDLS (100% vs. 88% and 100% vs. 94%, respectively). This suggests that the *MDM2* amplicon has a role in the formation of well-differentiated tumors and possibly de-differentiated tumors, but other mechanisms exist that can induce de-differentiation, possibly amplifications in *CDK4*.

The use of a high-resolution oligonucleotide array allowed for the detailed analysis of the *MDM2* and *CDK4* amplicons. Although the amplification of both of these genes appeared to be relatively consistent between the WD and DDLS, the genes incorporated into their amplicons varied amongst the different tumors. *GLI1* and *STAT6* are notable genes incorporated into the *CDK4* amplicon that were preferentially amplified in the de-differentiated samples. Of these, *GLI1* was only amplified in the DDLS as compared to the WDLS. *GLI1* was amplified in 4 DDLS, three of which with high levels of amplification had matched overexpression. GLI1 is a transcription factor for the sonic hedgehog (SHh) pathway. The Hh pathway, through mutations in smoothened (SMO) and/or overexpression of *GLI*, can activate MDM2 and promote TP53 ubiquination (Abe et al., 2008). In addition, active Hh signaling negatively regulates the normal process of adipogenesis (Zehentner et al., 2000; Spinella-Jaegle et al., 2001). Activity of the Hh pathway through GLI1 may precipitate a maturation arrest in adipogenesis and serve as an excellent target for clinical inhibition in a subset of LSs as numerous targeted inhibitors to this pathway are being developed.

Much like the *CDK4* amplicon, the *MDM2* amplicon was highly complex and displayed variation. In this amplicon, the presence of *CCT2*, a member of the chaperonin containing TCP1 complex TRiC, is of interest. Our analysis also identified *BBS10* as being amplified in the tumors (WD >DD). *BBS10* is located on chromosome 12 (12q21.2) but is not associated with the

MDM2 or *CDK4* amplicons. BBS10 has sequence homology to the CCT proteins and can complex with CCT2 (Seo et al., 2010). Both the CCT and BBS proteins have significant ties to adipocyte differentiation through PPARG signaling (Marion et al., 2009). In early adipogenesis, BBS10 is involved in the formation of a transient primary cilium that can facilitate WNT and Hh signaling (Marion et al., 2009). Down-regulation of BBS10 expression abrogates the cilium formation and promotes preadipocyte differentiation through PPARG signaling (Marion et al., 2009). Noted over-expression of CCT2 and BBS10 in LS may facilitate formation of the primary cilium and/or stabilize its presence allowing for Hh and Wnt signaling at the expense of PPARG and CEBPA function and terminal adipocyte differentiation. In addition, *POC1B* (WDR51B; 12q21.33), is also amplified (WD >DD). POC1B plays a role in primary ciliogenesis, possibly through the stabilization of basal bodies (Pearson et al., 2009).

Abnormalities in 6q23 and 1q23, along with amplifications in 1p32, are often associated with LSs (Chibon et al., 2002; Horvai et al., 2009; Snyder et al., 2009). Target genes in 1q23 have yet to be established. However, enhanced signaling of the Jun N-terminal kinase (JNK) pathway in LS either through amplifications/overexpression of the *JUN* oncogene (1p32.2) or *MAP3K5*/*ASK1* (6q23.3) has been proposed to arrest adipogenesis by interfering with the activity of PPARG and CEBPB (Mariani et al., 2007; Snyder et al., 2009). In our analysis, 1p32 and 6q23 were amplified in 32% of the LSs. Coamplification occurred in only one tumor (F508). 8/17 (47%) DD tumors had either an amplification of 1p32 (*JUN*) or 6q23 at the *MAP3K5* locus. Although 3/21 WDLS had an amplification at 6q23, only one involved *MAP3K5* (F141); the other WDLS had amplifications centered at *IFNGR1* or *MAP3K7IP2*. In all but one tumor (F141, *MAP3K5*), amplifications in *JUN* or *MAP3K5* were noted in the DD samples. This is slightly different then what has been previously described in which amplifications of both *JUN* and *MAP3K5* were noted in both the WD and DD sections of synchronously presenting tumors (Horvai et al., 2009). Our analysis did not evaluate the paired WD and DD components of the same tumor. Rather, the WD tumors we analyzed had yet to develop a DD component. The disparity in these observations in which *JUN* and *MAP3K5* amplifications are noted in well and de-differentiated components of synchronously presenting tumors but not in WDLS without a DD component argues for a causative role of these genes in arresting adipogenesis. Also, in our analysis, amplifications of *GLI1* (12q13.3), *JUN* (1p32.2), and *MAP3K5* (6q23.3) were mutually exclusive. 13 tumors had amplifications in any one of these genes. With the exception of F141 (*MAP3K5*), all of these amplifications occurred in DDLS. In total, 12/17 (71%) of the DDLS had an amplification in either *GLI1*, *JUN*, *or MAP3K5* ($P = 0.0001$).

Along these lines, significant decreases in the expression of *LPL*, *LEP*, *aP2/FABP4*, *CEBPA*, and *PPARG* were noted in our samples (Fig. 2, Supporting Information Table S1). These changes, consistent with a maturation arrest in adipogenesis, were characteristic of the de-differentiated samples. Interestingly, 4/20 WD samples also had a severe loss of lipogenic markers (F120, F128, F132, and F141). These samples have not had a long clinical follow-up. It is therefore possible that this profile will subsequently identify those patients with well-differentiated tumors who are at high risk for developing future de-differentiated disease. Further follow-up of our sample population may be revealing in this regard. These data also suggest that selective well-differentiated tumors harbor a population of cells that is undergoing, or at least programmed to undergo, continued de-differentiation. Isolation of this cellular population from WD tumors may provide insight into the suspected mesenchymal/pre-adipocyte cell that undergoes de-differentiation.

Further evaluation of the genes associated with adipogenesis identified a decrease in expression of *CEBPA* as compared to *CEBPB*, which is also consistent with a block in adipogenesis (Fig. 2, Supporting Information Table S1). Numerous samples, both WD and DDLS, had this characteristic gene expression pattern in the absence of *JUN*, *MAP3K5*/*ASK1*, or *GLI1* amplification. It is possible, that in these samples, *JUN* amplification or activation is occurring through mechanisms not detectable by aCGH as previously proposed (Snyder et al., 2009). For example, five DDLS samples had low expression of *DACH1* (log2 ratio <-1), three of which did not have amplification of *JUN* or *MAP3K5* (Supporting Information Table S1). DACH1 is an inhibitor of JUN-induced growth and is considered to be a tumor suppressor gene (Wu et al., 2007). No WDLS showed this expression pattern. Loss of expression without homozygous deletion may be occurring by aberrant methylation and/or other methods. Alternatively, it suggests that

mechanisms other than AP-1 signaling, such as mediators of WNT and Hh signaling, are involved in blocking adipogenesis.

Differential miRNA expression has been documented in human sarcomas (Subramanian et al., 2008; Sarver et al., 2010)}. Differential miRNA expression has also been documented in the regulation of adipogenesis (Ortega et al., 2010). In our analysis, 7/21 WDLS (33%) and 6/17 DDLS (35%) had amplification of an ~1 Mb region centered at *DNM3* (1q24.3). Two micro-RNAs, miR-214 and miR-199a2, map in the *DNM3* gene at the site of highest amplification. Expression of the miRNAs (AK021543) correlated with amplification.

ROAST analyses indicated that *CDKN1B/ p27/ Kip-1* expression was inversely correlated to the expression of miR-214 and miR-199a2. CDKN1B is an important inhibitor of the cell cycle that is controlled by a variety of transcriptional and post-translational mechanisms (Sherr and Roberts, 1999). Micro-RNAs have been shown to negatively regulate CDKN1B in glioblastoma, prostate, and breast cancer cell lines (Galardi et al., 2007; Gillies and Lorimer, 2007; le Sage et al., 2007). Our observations suggest that miR-214 and miR-199a2 may down regulate CDKN1B in WD and DDLS.

The overall effect of miRNAs on gene expression and protein translation is relatively mild, often supplementing other regulatory processes (Baek et al., 2008; Selbach et al., 2008). In our analysis, several DD samples had *JUN* or *MAP3K5* and miRNA214/199a2 coamplification. *CDKN1B* expression is also a target of the AP-1 family of transcription factors and is negatively regulated by JUN and FOS (Khattar and Kumar, 2010). In these samples miR-214/199a2 may further exacerbate the AP-1 associated down-regulation of *CDKN1B*. This may accentuate the aggressive behavior of certain LSs by potentiating cellular proliferation especially in samples that have *CDK4* or *MDM2* amplifications.

Several interesting clinical caveats were noted in this analysis. For the most part, females represented the majority of those patients who develop fatty tumors prior to the age of 50 years old, while the majority of patients who developed tumors after the age of 70 years old were men. This is of interest as a single nucleotide polymorphism (SNP309) has been identified in the *MDM2* promoter that results in increased expression of *MDM2* RNA levels (Bond et al., 2006). Interestingly, this region of the promoter coincides to the binding site for estrogen. It is thought that SNP309 alters the effect of estrogen on tumorigenesis. This in turn would explain the gender differences noted in our patient population regarding the age of onset of tumor development. As LSs appear to be in part dependent on *MDM2* amplification and activity, the presence of SNP309 may increase the formation of fatty tumors in estrogen producing females. As noted in our cohort, this would predict that women would develop LSs at a younger age and continue to do so until they reach menopause.

Another interesting correlate is that all of the 6q amplifications occurred in retroperitoneal tumors. This observation suggests that a subset of retroperitoneal LSs develop under the influence of unique genetic triggers. The developmental and clinical significance of this observation should be evaluated in a larger cohort of patients. However, a unique chromosomal abnormality inherent to retroperitoneal LSs may allow for the further substratification of LSs when developing and clinically testing novel inhibitors.

REFERENCES

Abe Y, Oda-Sato E, Tobiume K, Kawauchi K, Taya Y, Okamoto K, Oren M, Tanaka N. 2008. Hedgehog signaling overrides p53-mediated tumor suppression by activating Mdm2. Proc Natl Acad Sci USA 105:4838–4843.

Baek D, Villen J, Shin C, Camargo FD, Gygi SP, Bartel DP. 2008. The impact of microRNAs on protein output. Nature 455:64–71.

Barretina J, Taylor BS, Banerji S, Ramos AH, Lagos-Quintana M, Decarolis PL, Shah K, Socci ND, Weir BA, Ho A, Chiang DY, Reva B, Mermel CH, Getz G, Antipin Y, Beroukhim R, Major JE, Hatton C, Nicoletti R, Hanna M, Sharpe T, Fennell TJ, Cibulskis K, Onofrio RC, Saito T, Shukla N, Lau C, Nelander S, Silver SJ, Sougnez C, Viale A, Winckler W, Maki RG, Garraway LA, Lash A, Greulich H, Root DE, Sellers WR, Schwartz GK, Antonescu CR, Lander ES, Varmus HE, Ladanyi M, Sander C, Meyerson M, Singer S. Subtype-specific genomic alterations define new targets for soft-tissue sarcoma therapy. Nat Genet 42:715–721.

Bennett CN, Ross SE, Longo KA, Bajnok L, Hemati N, Johnson KW, Harrison SD, MacDougald OA. 2002. Regulation of Wnt signaling during adipogenesis. J Biol Chem 277:30998–31004.

Bond GL, Hirshfield KM, Kirchhoff T, Alexe G, Bond EE, Robins H, Bartel F, Taubert H, Wuerl P, Hait W, Toppmeyer D, Offit K, Levine AJ. 2006. MDM2 SNP309 accelerates tumor formation in a gender-specific and hormone-dependent manner. Cancer Res 66:5104–5110.

Chibon F, Mariani O, Derre J, Malinge S, Coindre JM, Guillou L, Lagace R, Aurias A. 2002. A subgroup of malignant fibrous histiocytomas is associated with genetic changes similar to those of well-differentiated liposarcomas. Cancer Genet Cytogenet 139:24–29.

Coindre JM, Pedeutour F, Aurias A. 2009. Well-differentiated and dedifferentiated liposarcomas. Virchows Arch 456:167–179.

Dahlen A, Debiec-Rychter M, Pedeutour F, Domanski HA, Hoglund M, Bauer HC, Rydholm A, Sciot R, Mandahl N, Mertens F. 2003. Clustering of deletions on chromosome 13 in benign and low-malignant lipomatous tumors. Int J Cancer 103:616–623.

Dal Cin P, Kools P, Sciot R, De Wever I, Van Damme B, Van de Ven W, Van den Berghe H. 1993. Cytogenetic and fluorescence in situ hybridization investigation of ring chromosomes

characterizing a specific pathologic subgroup of adipose tissue tumors. Cancer Genet Cytogenet 68:85–90.
Dalal KM, Kattan MW, Antonescu CR, Brennan MF, Singer S. 2006. Subtype specific prognostic nomogram for patients with primary liposarcoma of the retroperitoneum, extremity, or trunk. Ann Surg 244:381–391.
Eilber FC, Brennan MF, Eilber FR, Dry SM, Singer S, Kattan MW. 2004a. Validation of the postoperative nomogram for 12-year sarcoma-specific mortality. Cancer 101:2270–2275.
Eilber FC, Eilber FR, Eckardt J, Rosen G, Riedel E, Maki RG, Brennan MF, Singer S. 2004b. The impact of chemotherapy on the survival of patients with high-grade primary extremity liposarcoma. Ann Surg 240:686–695; discussion 695–697.
Fletcher CD, Akerman M, Dal Cin P, de Wever I, Mandahl N, Mertens F, Mitelman F, Rosai J, Rydholm A, Sciot R, Tallini G, van den Berghe H, van de Ven W, Vanni R, Willen H. 1996. Correlation between clinicopathological features and karyotype in lipomatous tumors. A report of 178 cases from the Chromosomes and Morphology (CHAMP) Collaborative Study Group. Am J Pathol 148:623–630.
Galardi S, Mercatelli N, Giorda E, Massalini S, Frajese GV, Ciafre SA, Farace MG. 2007. miR-221 and miR-222 expression affects the proliferation potential of human prostate carcinoma cell lines by targeting p27Kip1. J Biol Chem 282:23716–23724.
Gesta S, Tseng YH, Kahn CR. 2007. Developmental origin of fat: Tracking obesity to its source. Cell 131:242–256.
Gillies JK, Lorimer IA. 2007. Regulation of p27Kip1 by miRNA 221/222 in glioblastoma. Cell Cycle 6:2005–2009.
Henricks WH, Chu YC, Goldblum JR, Weiss SW. 1997. Dedifferentiated liposarcoma: A clinicopathological analysis of 155 cases with a proposal for an expanded definition of dedifferentiation. Am J Surg Pathol 21:271–281.
Horvai AE, DeVries S, Roy R, O'Donnell RJ, Waldman F. 2009. Similarity in genetic alterations between paired well-differentiated and dedifferentiated components of dedifferentiated liposarcoma. Mod Pathol 22:1477–1488.
Italiano A, Bianchini L, Keslair F, Bonnafous S, Cardot-Leccia N, Coindre JM, Dumollard JM, Hofman P, Leroux A, Mainguene C, Peyrottes I, Ranchere-Vinee D, Terrier P, Tran A, Gual P, Pedeutour F. 2008. HMGA2 is the partner of MDM2 in well-differentiated and dedifferentiated liposarcomas whereas CDK4 belongs to a distinct inconsistent amplicon. Int J Cancer 122:2233–2241.
Kattan MW, Leung DH, Brennan MF. 2002. Postoperative nomogram for 12-year sarcoma-specific death. J Clin Oncol 20:791–796.
Khattar E, Kumar V. 2010. Mitogenic regulation of p27(Kip1) gene is mediated by AP-1 transcription factors. J Biol Chem 285:4554–4561.
le Sage C, Nagel R, Egan DA, Schrier M, Mesman E, Mangiola A, Anile C, Maira G, Mercatelli N, Ciafre SA, Farace MG, Agami R. 2007. Regulation of the p27(Kip1) tumor suppressor by miR-221 and miR-222 promotes cancer cell proliferation. EMBO J 26:3699–3708.
Mariani O, Brennetot C, Coindre JM, Gruel N, Ganem C, Delattre O, Stern MH, Aurias A. 2007. JUN oncogene amplification and overexpression block adipocytic differentiation in highly aggressive sarcomas. Cancer Cell 11:361–374.
Marion V, Stoetzel C, Schlicht D, Messaddeq N, Koch M, Flori E, Danse JM, Mandel JL, Dollfus H. 2009. Transient ciliogenesis involving Bardet-Biedl syndrome proteins is a fundamental characteristic of adipogenic differentiation. Proc Natl Acad Sci USA 106:1820–1825.
Matushansky I, Hernando E, Socci ND, Matos T, Mills J, Edgar MA, Schwartz GK, Singer S, Cordon-Cardo C, Maki RG. 2008. A developmental model of sarcomagenesis defines a differentiation-based classification for liposarcomas. Am J Pathol 172:1069–1080.
Ortega FJ, Moreno-Navarrete JM, Pardo G, Sabater M, Hummel M, Ferrer A, Rodriguez-Hermosa JI, Ruiz B, Ricart W, Peral B, Fernandez-Real JM. 2010. MiRNA expression profile of human subcutaneous adipose and during adipocyte differentiation. PLoS One 5:e9022.
Pearson CG, Osborn DP, Giddings TH Jr., Beales PL, Winey M. 2009. Basal body stability and ciliogenesis requires the conserved component Poc1. J Cell Biol 187:905–920.
Persson F, Olofsson A, Sjogren H, Chebbo N, Nilsson B, Stenman G, Aman P. 2008. Characterization of the 12q amplicons by high-resolution, oligonucleotide array CGH and expression analyses of a novel liposarcoma cell line. Cancer Lett 260:37–47.
Rieker RJ, Weitz J, Lehner B, Egerer G, Mueller A, Kasper B, Schirmacher P, Joos S, Mechtersheimer G. 2009. Genomic profiling reveals subsets of dedifferentiated liposarcoma to follow separate molecular pathways. Virchows Arch 456:277–285.
Rosen ED, MacDougald OA. 2006. Adipocyte differentiation from the inside out. Nat Rev Mol Cell Biol 7:885–896.
Sarver AL, Phalak R, Thayanithy V, Subramanian S. 2010. S-MED: Sarcoma microRNA expression database. Lab Invest 90:753–761.
Selbach M, Schwanhausser B, Thierfelder N, Fang Z, Khanin R, Rajewsky N. 2008. Widespread changes in protein synthesis induced by microRNAs. Nature 455:58–63.
Seo S, Baye LM, Schulz NP, Beck JS, Zhang Q, Slusarski DC, Sheffield VC. 2010. BBS6, BBS10, and BBS12 form a complex with CCT/TRiC family chaperonins and mediate BBSome assembly. Proc Natl Acad Sci USA 107:1488–1493.
Sherr CJ, Roberts JM. 1999. CDK inhibitors: Positive and negative regulators of G1-phase progression. Genes Dev 13:1501–1512.
Shimoji T, Kanda H, Kitagawa T, Kadota K, Asai R, Takahashi K, Kawaguchi N, Matsumoto S, Hayashizaki Y, Okazaki Y, Shinomiya K. 2004. Clinico-molecular study of dedifferentiation in well-differentiated liposarcoma. Biochem Biophys Res Commun 314:1133–1140.
Singer S, Socci ND, Ambrosini G, Sambol E, Decarolis P, Wu Y, O'Connor R, Maki R, Viale A, Sander C, Schwartz GK, Antonescu CR. 2007. Gene expression profiling of liposarcoma identifies distinct biological types/subtypes and potential therapeutic targets in well-differentiated and dedifferentiated liposarcoma. Cancer Res 67:6626–6636.
Snyder EL, Sandstrom DJ, Law K, Fiore C, Sicinska E, Brito J, Bailey D, Fletcher JA, Loda M, Rodig SJ, Dal Cin P, Fletcher CD. 2009. c-Jun amplification and overexpression are oncogenic in liposarcoma but not always sufficient to inhibit the adipocytic differentiation programme. J Pathol 218:292–300.
Spinella-Jaegle S, Rawadi G, Kawai S, Gallea S, Faucheu C, Mollat P, Courtois B, Bergaud B, Ramez V, Blanchet AM, Addmant G, Baron R, Roman-Raman S. 2001. Sonic hedgehog increases the commitment of pluripotent mesenchymal cells into the osteoblastic lineage and abolishes adipocytic differentiation. J Cell Sci 114(Pt 11):2085–2094.
Sreekantaiah C, Karakousis CP, Leong SP, Sandberg AA. 1992. Cytogenetic findings in liposarcoma correlate with histopathologic subtypes. Cancer 69:2484–2495.
Subramanian S, Lui WO, Lee CH, Espinosa I, Nielsen TO, Heinrich MC, Corless CL, Fire AZ, van de Rijn M. 2008. MicroRNA expression signature of human sarcomas. Oncogene 27:2015–2026.
Trombetta D, Mertens F, Lonoce A, D'Addabbo P, Rennstam K, Mandahl N, Storlazzi CT. 2009. Characterization of a hotspot region on chromosome 12 for amplification in ring chromosomes in atypical lipomatous tumors. Genes Chromosomes Cancer 48:993–1001.
Wu K, Liu M, Li A, Donninger H, Rao M, Jiao X, Lisanti MP, Cvekl A, Birrer M, Pestell RG. 2007. Cell fate determination factor DACH1 inhibits c-Jun-induced contact-independent growth. Mol Biol Cell 18:755–767.
Zehentner BK, Leser U, Burtscher H. 2000. BMP-2 and sonic hedgehog have contrary effects on adipocyte-like differentiation of C3H10T1/2 cells. DNA Cell Biol 19:275–281.

Appendix 2:

PTEN dosage is essential for neurofibroma development and malignant transformation.

PTEN dosage is essential for neurofibroma development and malignant transformation

Caroline Gregorian[a,1], Jonathan Nakashima[a,1], Sarah M. Dry[b,c], P. Leia Nghiemphu[d], Kate Barzan Smith[a], Yan Ao[e], Julie Dang[b], Gregory Lawson[f], Ingo K. Mellinghoff[a,2], Paul S. Mischel[a,b,c], Michael Phelps[a,c,3], Luis F. Parada[g], Xin Liu[a,b], Michael V. Sofroniew[e], Fritz C. Eilber[a,c,h], and Hong Wu[a,c,3]

[a]Department of Molecular and Medical Pharmacology, [b]Department of Pathology and Laboratory Medicine, [c]Institute for Molecular Medicine, [d]Department of Neurology, [e]Department of Neurobiology, [f]Division of Laboratory Animal Medicine, [h]Division of Surgical Oncology, University of California, Los Angeles, CA 90095; and [g]Department of Developmental Biology, University of Texas Southwestern Medical Center, Dallas, TX 75390-9133

Contributed by Michael Phelps, September 11, 2009 (sent for review March 30, 2009)

Patients with neurofibromatosis type 1 (NF1) carry approximately a 10% lifetime risk of developing a malignant peripheral nerve sheath tumor (MPNST). Although the molecular mechanisms underlying NF1 to MPNST malignant transformation remain unclear, alterations of both the RAS/RAF/MAPK and PI3K/AKT/mTOR signaling pathways have been implicated. In a series of genetically engineered murine models, we perturbed RAS/RAF/MAPK or/and PTEN/PI3K/AKT pathway, individually or simultaneously, via conditional activation of *K-ras* oncogene or deletion of *Nf1* or *Pten* tumor suppressor genes. Only K-Ras activation in combination with a single *Pten* allele deletion led to 100% penetrable development of NF lesions and subsequent progression to MPNST. Importantly, loss or decrease in PTEN expression was found in all murine MPNSTs and a majority of human NF1-associated MPNST lesions, suggesting that PTEN dosage and its controlled signaling pathways are critical for transformation of NFs to MPNST. Using noninvasive in vivo PET-CT imaging, we demonstrated that FDG can be used to identify the malignant transformation in both murine and human MPNSTs. Our data suggest that combined inhibition of RAS/RAF/MAPK and PTEN/PI3K/AKT pathways may be beneficial for patients with MPNST.

in vivo PET imaging | peripheral nerve sheath tumor | tumor suppressor

Neurofibromatosis type 1 (NF1) is one of the most common inherited disorders with an estimated birth incidence of 1 in 2,500. An autosomal dominant disorder, NF1 is clinically characterized by peripheral neurofibromas (NF), café-au-lait spots, axillary freckling, optic nerve gliomas, and hamartomas of the iris. NFs are benign peripheral nerve sheath tumors that develop as cutaneous or s.c. masses, deep soft tissue lesions, plexiform NFs, or intraneural tumors (1–4).

NF1 patients carry approximately a 10% lifetime risk of developing malignant peripheral nerve sheath tumors (MPNSTs) compared to less than 0.1% in the general population (5, 6). MPNSTs are malignant soft tissue sarcomas with particularly poor survival rates. The molecular mechanisms behind the malignant transformation of NF into MPNST remain unclear. Although NF1 is the most important known risk factor for the development of MPNST and the loss of the second copy of the *NF1* allele is found in MPNST cells possibly contributing to malignant transformation, loss of both *NF1* alleles is not sufficient for malignant transformation of benign NFs (5).

Mutations in the *NF1* tumor suppressor gene are believed to be one of the earliest events contributing to peripheral nerve tumor development in NF1 patients. Neurofibromin, the protein product of *NF1*, is a RAS-GTPase-activating protein (RAS-GAP) that negatively regulates RAS activity (1, 7, 8). Recent studies demonstrate a role of neurofibromin in controlling mammalian target of rapamycin (mTOR), indicating the involvement of PI3K/AKT/mTOR pathway in the etiology of NF1 (9–11). Although no mutations have been identified in the RAS- and PI3K-controlled pathways, both the RAS/MAPK and PI3K/AKT/mTOR signaling pathways may play critical roles in the development of NF1-related tumors.

The murine homolog for *Nf1* has been knocked out via homologous recombination (12). $Nf1^{-/-}$ mice die during embryogenesis due to cardiac development failure, while $Nf1^{+/-}$ mice show no hallmark of the human NF1 phenotype (13, 14). Chimeric mice bearing $Nf1^{-/-}$ cells develop plexiform NFs, suggesting that *Nf1* loss of heterozygosity (LOH) or NF1 gene dosage is essential for NF1 initiation. However, no dermal NFs were reported (15). *Nf1* conditional knockout mice were since generated by multiple groups. Schwann cell- and astrocyte-specific ablation of *Nf1* leads to plexiform NFs, confirming loss of NF1 expression is sufficient for formation of tumors with pathological features of NFs, whereas MPNST development may require alterations of additional genes or signaling pathways. In the search for pathways responsible for the malignant transformation, $Nf1^{+/-}$ mice were crossed onto *p53* null background. Although neither *p53* null nor heterozygous mice develop MPNSTs, mice with mutations in both genes do develop soft tissue tumors resembling MPNSTs (15, 16). In addition, genetic studies also suggest that other cell types, such as $Nf1^{+/-}$ mast cells or fibroblasts, may also be critical for disease development (17–19).

Since the RAS/RAF/MAPK and PI3K/AKT/mTOR are the two major signaling pathways involved in tumorigenesis of both the peripheral and central nervous systems (7), we reasoned that perturbation of these pathways, individually and in combination, may be a more efficient way of modeling human NF1 and its associated MPNST development. By creating a series of mouse models harboring conditionally deletable *Pten* (20) or *Nf1* allele (21) and conditionally activatable mutant $LSL\text{-}K\text{-}ras^{G12D}$ alleles (22), we demonstrated that loss of expression of *Pten*, the second most frequently mutated tumor suppressor gene in all human cancers, in combination with K-RAS activation, led to the development of NFs with 100% penetrance, followed by MPNST transformation. Importantly, MPNST development correlates with loss of PTEN expression in both our murine model as well as human NF1 patients and can be visualized via noninvasive [^{18}F]-2-fluoro-2-deoxy-D-glucose positron emission tomography (FDG-PET) imaging.

Author contributions: C.G., J.N., I.K.M., X.L., M.V.S., F.C.E., and H.W. designed research; C.G., J.N., S.M.D., P.L.N., K.B.S., Y.A., J.D., and G.L. performed research; S.M.D., M.P., L.F.P., and F.C.E. contributed new reagents/analytic tools; C.G., J.N., S.M.D., P.L.N., K.B.S., Y.A., G.L., I.K.M., P.S.M., X.L., M.V.S., F.C.E., and H.W. analyzed data; and C.G., J.N., S.M.D., P.L.N., K.B.S., I.K.M., P.S.M., M.V.S., F.C.E., and H.W. wrote the paper.

The authors declare no conflict of interest.

Freely available online through the PNAS open access option.

[1]C.G. and J.N. contributed equally to this work.

[2]Present address: Department of Neurology and Human Oncology and Pathogenesis Program, Memorial Sloan-Kettering Cancer Center, New York, NY 10065.

[3]To whom correspondence may be addressed. E-mail: hwu@mednet.ucla.edu or mphelps@mednet.ucla.edu.

This article contains supporting information online at www.pnas.org/cgi/content/full/0910398106/DCSupplemental.

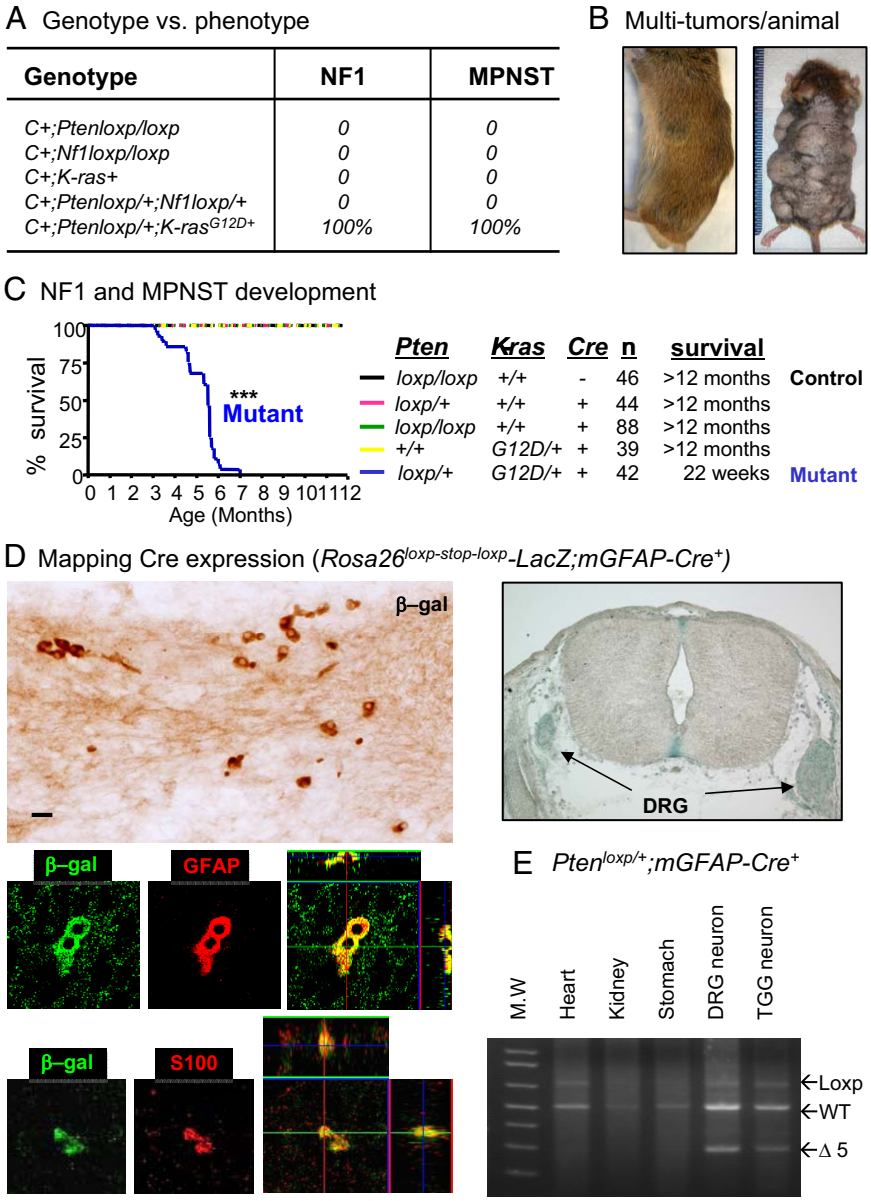

Genotype	NF1	MPNST
C+;Ptenloxp/loxp	0	0
C+;Nf1loxp/loxp	0	0
C+;K-ras+	0	0
C+;Ptenloxp/+;Nf1loxp/+	0	0
C+;Ptenloxp/+;K-ras^{G12D+}	100%	100%

Fig. 1. Genotypes and phenotypes of mice generated. (*A*) Overview of genotype and phenotype of mice generated. (*B*) Representative photo of a mutant mouse bearing multiple tumors. Additional tumors were revealed upon removal of body hair (right; ranging from two to 25 per animal). Ruler ticks, 1 mm. (*C*) Kaplan Meier curve for duration of survival of mice with five genotypes. The mortality rate of *mGFAP-Cre*$^{+}$;*Pten*$^{loxp/+}$;*LSL-K-ras*$^{G12D/+}$ mice (mutant in blue; $P <$ 0.01) was significantly earlier than that of control (black). Genetic composition, number of mice, and mean survival are shown on the right. (*D*) Mapping Cre expression. Left, colocalization of β-gal^{+} cells with endogenous GFAP and S100 expression on E13.5 embryo; right, X-gal staining of DRG of E13.5 embryo. (*E*) PCR genotype for *Pten* exon 5 excision (Δ5) in adult DRG and TGG neurons *C+*, *mGFAP-Cre*$^{+}$.

Results

Conditional Deletion of *Pten* and Activation of *K-ras* Leads to NF and MPNST Development. To genetically test the contribution of PTEN/PI3K/AKT and RAS/RAF/MAPK pathways in NF and MPNST development, we crossed the *Pten* (*Pten*$^{loxp/loxp}$) (20) or the *Nf1* conditional deletion allele (*Nf1*$^{loxp/loxp}$) (23) and the *K-ras* conditional activatable allele (*LSL-K-ras*$^{G12D/+}$) (22) with *mGFAP-Cre*$^{+}$ mice (line 77.6). The resulting mice with *Pten* or *Nf1* single gene conditional deletion or *K-Ras* activation were tumor-free with normal life spans and indistinguishable from their wild-type (WT) littermates (Fig. 1*A*). Therefore, K-RAS activation and NF1 or PTEN loss alone are not sufficient for NF1 development even though both K-RAS activation and NF1 loss can activate the mTOR pathway (9–11).

A single activated *K-ras* allele or *Nf1* deleted allele was then introduced into the *Pten* heterozygous background (*mGFAP-Cre*$^{+}$;*Pten*$^{loxp/+}$). Although *mGFAP*-Cre^{+};*Nf1*$^{loxp/+}$;*Pten*$^{loxp/+}$ compound heterozygous animals showed no tumor development, the resulting *mGFAP-Cre*$^{+}$;*Pten*$^{loxp/+}$;*LSL-K-ras*$^{G12D/+}$ mice developed multiple visible s.c. tumors with 100% penetrance, starting from postnatal 4 months (Fig. 1 *B* and *C*; n = 42). These tumors varied in size and location with the majority located on the back and sides of the animal body (Fig. 1*B*). When exposed, almost all of the nodules were locally confined and solid. Detailed histopathological analyses demonstrated that each mutant mouse carried more than one lesion with pathological features indistinguishable from human NFs, including the plexiform NF characteristic of NF1 patients, and MPNSTs (Fig. S1). Murine and human NFs are comprised of a mixture of cell

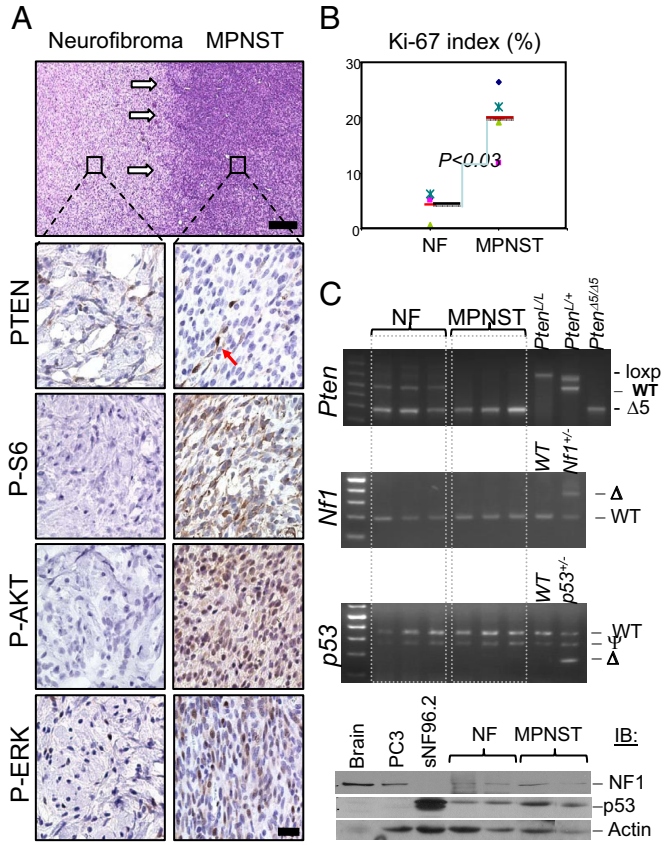

Fig. 2. PTEN loss is critical for malignant transformation of benign NF in mice. (*A*) Lesions containing both benign NFs and MPNSTs were harvested from mutant mice and subjected to immunohistochemical analysis (white arrows indicate ''transition zone'' from benign NF to MPNST). Compared to benign NF, MPNSTs showed marked reduction in immunoreactivity for PTEN in tumor cells, with PTEN$^+$ stained endothelial cells as an internal positive control (arrow). MPNSTs also show intensive staining with antibodies specific for surrogate markers of activated PI3K/AKT (P-AKT, P-S6) and RAS/MAPK (P-ERK) pathways. [Scale bars, 150 μm (H&E) and 25 μm (IHC).] (*B*) MPNST tumors have higher Ki-67 labeling index than NF tumors ($P < 0.03$). (*C*) Upper three panels: PCR analysis of NF and MPNST tumor DNA from *mGFAP-Cre*$^+$;*Pten*$^{loxp/+}$;*LSL-K-ras*$^{G12D/+}$ mice, indicating loss of *Pten* WT allele and retaining of both *p53* and *Nf1* genes in MPNST lesions; lower panel, Western blot analysis showing NF1 and p53 proteins in NF and MPNST samples. PC3 and sNF96.2 are human cell lines used here as controls that are null for p53 and NF1, respectively.

types, including Schwann cells, mast cells, perineural cells, and fibroblasts (18, 24), and we thus tested for these cells in the murine tumors. Special stains or antibodies known to be positive in murine and human NFs (18, 24), including the Schwann cell marker S100, mast cell markers toluidine blue, or c-Kit showed classic staining patterns for NFs (Fig. S2). In addition, benign NFs had fewer numbers of Ki-67$^+$ cells, whereas MPNST lesions showed an increased Ki-67 labeling index (Fig. S2 and Fig. 2*B*). Importantly, MPNST lesions were found in 100% of mutant mice when followed for 7 months. However, when mutant mice were killed at 12 weeks of age, multiple small foci of benign NFs and plexiform NFs were found without any MPNSTs, indicating that progression from NFs to MPNST is likely a time-dependent event. This result suggests that *Pten* haploinsufficiency, i.e., loss of one allele of the *Pten* tumor suppressor gene, is critical for NF initiation caused by K-Ras activation.

Mapping the NF Initiating Cells in *mGFAP-Cre*$^+$;*Pten*$^{loxp/+}$;*LSL-K-ras*$^{G12D/+}$ Model. The cell-of-origin of NF is a subject of current debate. Although several recent studies agree that *Nf1*-null neural crest cells are not the NF-initiating cells, they differ as to what particular glial differential stage gives rise to the neoplastic lesions (25). To define the NF-initiating cells in our model, we crossed *mGFAP-Cre 77.6* line with the *Rosa26*$^{loxp\text{-}stop\text{-}loxp}$-*LacZ* reporter mouse (26). *mGFAP-Cre*$^+$;*Rosa26*$^{loxp\text{-}stop\text{-}loxp}$-*LacZ* embryos were harvested from E12.5 to P0 and cryoprotected before staining with either X-gal or anti-β-gal antibody (Fig. 1*D*, upper panels). No *LacZ* expression could be detected at E12.5, 0.5–1 days before the onset of endogenous GFAP expression (25). On the other hand, Cre expression could be detected in E13.5 intercostal nerve (left) and dorsal root ganglions (DRG; right). Detailed fluorescent immunohistochemistry analysis (27) further confirmed that all β-gal expressing cells also expressed endogenous GFAP and S100 expression (Fig. 1*D*, lower left panels; Fig. S3), suggesting that the oncogenic initiation event in our model begins at the stage between Schwann precursor and immature Schwann cells (25). Cre expression could be detected throughout embryogenesis and in adult peripheral nerve tissues, such as DRG and trigeminal ganglion (TGG) neurons, as indicated by PCR-aid genotype analysis (Fig. 1*E*) and immunohistochemistry staining. Collectively, this analysis suggest that Schwann precursor or immature Schwann cells are the cell-of-origin in *mGFAP-Cre*$^+$;*Pten*$^{loxp/+}$;*LSL-K-ras*$^{G12D/+}$ model.

***Pten* LOH Correlates with MPNST Transformation in the NF Murine Model.** Since all MPNSTs are developed within existing NF in *mGFAP-Cre*$^+$;*Pten*$^{loxp/+}$;*LSL-K-ras*$^{G12D/+}$ mice, we focused our attention on the "transition zone" between NF and MPNST lesions. As shown in the upper panel of Fig. 2*A*, a benign lesion (left) is clearly separated from MPNST (right; white arrows) within the same tumor mass. Pathologically, NFs showed relatively uniform, ovoid to spindle-shaped cells, many with tapered ends, intermixed with collagen fibers and mast cells (Figs. S1 and S2). In contrast, MPNSTs showed a marked increase in cellularity, moderate to severe nuclear pleomorphism (cellular anaplasia), obvious mitoses, including atypical mitoses (Fig. S2) and focal areas of necrosis. These histological features, particularly that of MPNSTs arising from preexisting NFs, are classic features of human NF1-associated MPNSTs (3, 28).

Importantly, loss of PTEN expression was detected in all (n = 15) MPNST tumors (Fig. 2*A*, second right; arrow points to a PTEN$^+$ blood vessel). P-AKT and P-S6 levels, two surrogate markers for PTEN-controlled PI3K pathway activation, were also elevated in MPNST lesions (Fig. 2*A*, lower right panels). The corresponding NFs, from which the MPSNT developed, showed relatively normal PTEN expression with no significant increase in P-AKT or P-S6 levels (Fig. 2*A*, lower left panels). P-ERK expression could be detected in both lesions, although significantly increased in MPNSTs (Fig. 2*A*, bottom panels). Consistent with the malignant nature of MPNST and with previous reports in humans (29), the proliferation index, as measured by Ki-67 staining (Fig. S2), was significantly higher than that seen in NF (Fig. 2*B*; $P < 0.03$), suggesting that PTEN controls NF to MPNST malignant transformation, at least in part, via its role in negatively regulating cell proliferation.

Loss of PTEN expression in MPNSTs could be due to either genetic loss of the second *Pten* allele, mutations that destabilize PTEN protein, or epigenetic silencing of *Pten* mRNA expression. To determine the molecular mechanisms involved in loss of PTEN expression, we first tested whether the WT allele of *Pten* was lost during tumor progression (LOH) by PCR analysis. As shown in Fig. 2*C*, the WT allele of *Pten* is completely deleted in three independent NF1-associated MPNST lesions (Fig. 2*C*, top panel). On the other hand, we did not detect obvious defects, either by PCR or via Western blot analysis, in *Nf1* and *p53* genes, although we cannot rule out possible interstitial deletions or point mutations (Fig. 2*C*, lower three panels). This study clearly

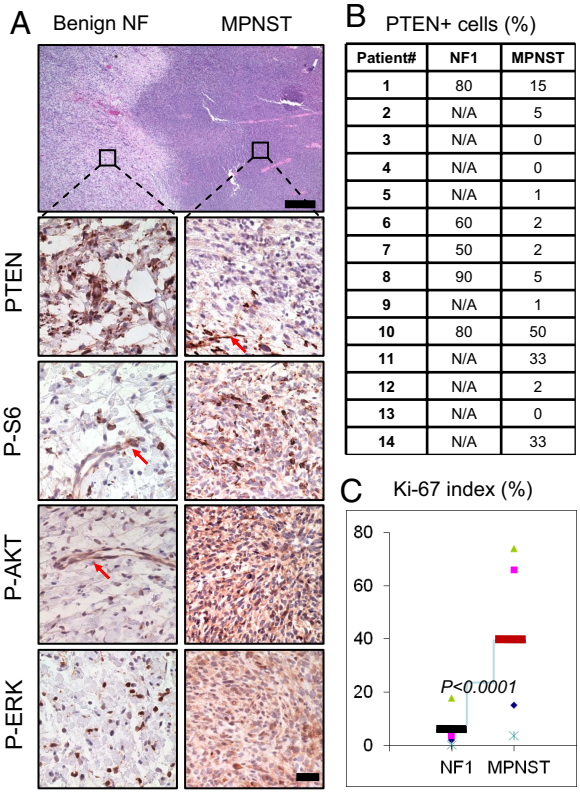

Patient#	NF1	MPNST
1	80	15
2	N/A	5
3	N/A	0
4	N/A	0
5	N/A	1
6	60	2
7	50	2
8	90	5
9	N/A	1
10	80	50
11	N/A	33
12	N/A	2
13	N/A	0
14	N/A	33

Fig. 3. Decreased PTEN expression in human NF1-associated MPNSTs. (*A*) Histological and immunohistological analyses of transition zone of human NF1-MPNST lesions demonstrate reduced PTEN expression (second right panel; arrows indicates PTEN$^+$ vascular endothelial cells) and activated PI3K and RAS/MAPK pathways. [Scale bars, 150 μm (H&E) and 25 μm (IHC).] (*B*) Summary of PTEN IHC staining results, presented as percentages of PTEN$^+$ tumor cells, of 14 NF1 patients with MPNST lesions. N/A, only MPNST samples are available. (*C*) Human MPNST tumors have higher Ki-67 labeling index than NF tumors ($P < 0.0001$).

demonstrates that *Pten* LOH is critical for the malignant transformation of NF to MPNST in this mouse model.

Reduction of PTEN Expression in Human MPNSTs. The correlation of *Pten* loss and MPNST development in our NF murine model prompted us to investigate whether PTEN expression is similarly reduced in the transition of human NFs to MPNST. For this, we surveyed the status of PTEN in human NF1-associated high grade MPNSTs and if possible the associated NF from which they arose (for details, please see *Materials and Methods*). As was seen in the murine model, marked reduction of PTEN protein levels was detected in all human MPNSTs samples examined (Fig. 3*A*; $n = 14$). Detailed quantitative analysis showed less than 20% PTEN positive tumor cells in 11 of 14 samples (Fig. 3*B*), with tumor vascular endothelial cells retaining PTEN staining and thus serving as an internal positive control (Fig. 3*A*, arrows). Similar to the murine model, increased P-S6, P-AKT, and P-ERK levels (Fig. 3*A*, lower right panels) were detected in the human MPNST samples. All corresponding NFs ($n = 5$) demonstrated higher PTEN expression levels, as well as low and sporadic P-S6, P-AKT, and P-ERK staining patterns (Fig. 3*B*, lower left panels). In addition, human MPNSTs had significantly increased Ki-67 proliferation index (Fig. 3*C*; $P < 0.0001$). These observations suggest that, similar to the murine model, reduced PTEN expression may be important for the malignant transformation of NFs to MPSNTs in human NF1 patients.

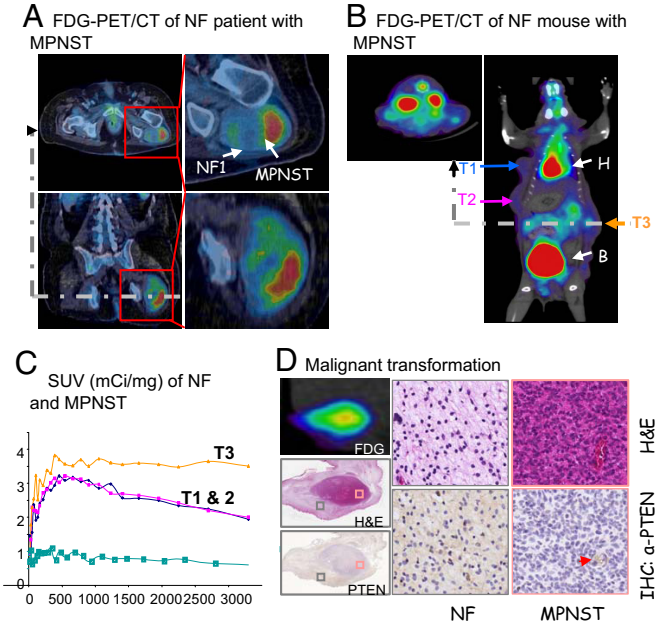

Fig. 4. Noninvasive in vivo imaging of MPNSTs transformation within NF lesions. (*A*) FDG-PET/CT image of a NF1 patient with MPNST. (*B*) FDG-PET/CT image of a NF mouse with MPNST. *mGFAP-Cre*$^+$;*Pten*$^{loxp/+}$;*LSL-K-ras*$^{G12D/+}$ mouse with three independent tumors, T1 and T2 are NF with low FDG intake, while T3 has increased FDG intake. (*C*) The FDG-PET SUVs, measured from the ROI for each tumor, compared to baseline uptake (blue) measured from limb muscle without tumor. (*D*) Correlation of FDG uptake, H&E staining, and PTEN expression (left panels) in a NF lesion (gray boxed sample area, middle panels) with MPNST transformation (red boxed sample area, right panels). Red arrow points to PTEN$^+$ vessel. T, tumor; H, heart; B, bladder.

Differentiating NF from MPNST Using Noninvasive PET/CT Imaging. Currently the diagnosis of MPNST is made pathologically. Unfortunately, targeted needle core biopsies are often not technically possible or falsely negative due to the heterogeneous nature of these tumors. Noninvasive modalities that can reliably differentiate NF from MPNST would significantly contribute to the management of NF1 patients. Recently, FDG-PET has been shown by us and other investigators to be a promising noninvasive modality with the potential to differentiate malignant from benign tumors (30, 31). Fig. 4*A* shows FDG-PET/CT images of a NF1 patient with a left gluteal MPNST arising within a NF lesion. The MPNST component of the tumor demonstrated high FDG uptake (standardized uptake value SUVmax of MPNST = 6.3 g/mL), which represents 4.85-fold increase over NF region (SUVmax of the NF = 1.3 g/mL).

Similar to the human studies, we also monitored MPNST malignant transformation in our NF murine model using noninvasive in vivo PET imaging in conjunction with CT. While MPNSTs could be sensitively detected with FDG ($n = 10$), similar to human MPNSTs, benign NF lesions were low or negative for FDG ($n = 29$). Fig. 4*B* showed a mouse with three independent lesions, two NFs with low FDG uptake (T1 and T2) and one MPNST with higher FDG uptake (T3; expressed as SUV in Fig. 4*C*). Importantly, malignant transformation can be positively confirmed on FDG-positive NFs by high cellularity, loss of PTEN expression (Fig. 4*D*), high proliferation index, necrosis, and massive angiogenesis (Fig. S4*A*). The percentage of animals with detectable FDG^{low} and FDG^{high} lesions appears to be age-dependent, similar to our histopathological analysis (Fig. S4*B*). These data suggest that noninvasive FDG-PET imaging may be used longitudinally to follow the NF to MPNST malignant transformation in animal models, as well as to provide

a valuable and noninvasive/nonlethal diagnostic strategy to assess potential therapeutic response.

Discussion

The transition from benign NF to MPNST represents the most lethal complication of NF1. Currently, there are no treatment strategies that prevent this transformation. Here, we describe a mouse model for NF and MPNST, which recapitulates the essential clinical features observed in human NF1 and NF-associated MPNSTs. Our study demonstrates the importance of PTEN loss in the NF to MPNST transformation. This finding provides support for potential therapeutic strategies that are both rational and selective.

Although *RAS* or *PTEN* mutations per se have not been identified in human NFs, several reports support the alterations of RAS or PTEN controlled signaling pathways in NF and MPNST development. A recent study showed that five of six human MPNST samples contain a hypermethylated PTEN promoter (32), providing a mechanistic explanation of loss of PTEN expression observed in our study. Several groups have identified constitutive RAS activation as a result of NF1 or NF2 deletion (33–36). Previous studies have also shown that RAS activity and its downstream effectors are elevated in the cortex and hippocampus of $NF1^{+/-}$ mice (37, 38). Furthermore, the learning deficits in $Nf1^{+/-}$ mice can be rescued by decreasing RAS function either genetically (crossing with the $K\text{-}Ras^{+/-}$ heterozygote) or pharmacologically (treated with farnesyltransferase inhibitors of Ras) (37, 39). Although mice with oncogenic *N-Ras* expression in nerve and neural crest-derived cells mimic two main symptoms of human NF1 and/or NF2, namely pigmentary abnormality and dermal NFs, plexiform NF, Schwannoma, astrocytoma, and pheochromocytoma were not detected (40). Since the three forms of Ras, (H, K, N) are expressed in different cells, this could explain the absence of some of these tumor types in our model and the presence of various other tumors.

Mutations in the *NF1* tumor suppressor gene is inherited as an autosomal-dominant trait, suggesting a possible gene dosage effect. In fact, haploinsufficiency is apparently enough to bring about many of the clinical manifestations seen in NF1 patients. However, the development of MPNST in NF1 individuals requires acquisition of additional genetic aberrations, whether it is inactivation of *TP53*, *CDKN2A*, or amplification of platelet-derived growth factor receptor or epidermal growth factor receptor (18, 41–43). Reminiscent of the malignancies seen in NF1 patients, compound heterozygous mice for both *Nf1* and *p53* develop MPNSTs with full penetrance (15, 16). In addition, as NF1 has a spectrum of specific tumors, modifying genes and epigenetic phenomena have been shown to play a role in modulating *Nf1*-associated tumor susceptibility (44, 45).

Consistent with multigene targets hypothesis, when we crossed the same *mGFAP-Cre* line to conditional knockout *Pten* (46) or *Nf1* or constitutively activate *K-ras* (this study), we did not observe any tumor development. However, NFs and MPNSTs were found in compound $mGFAP\text{-}Cre^{+};Pten^{loxp/+};LSL\text{-}K\text{-}ras^{G12D/+}$ mice. Interestingly, NFs had *Pten* expression, while MPNSTs within the NF lesions had lost the WT allele of *Pten*. When human samples were tested for PTEN expression, the results matched those found in mice, demonstrating that PTEN loss or PI3K/AKT activation is the rate-limiting step in murine and human NF1 malignant transformation and the development of MPNST.

Distinguishing MPNST from benign NFs is often difficult, particularly in patients with NF1. Optimal clinical management rests on correct pretreatment classification. Patients with benign NFs can either be followed with serial imaging or undergo nerve sparing surgery. Patients with MPNST require radical resection, radiation therapy, and frequently, chemotherapy. Currently, histologic features alone determine diagnosis. However, even targeted needle core biopsies can be inaccurate and are often not technically possible. Diagnostic methods that will reliably differentiate between MPNST and benign NFs would be essential in the management of these tumors. Our parallel comparison of mouse model and human patients indicates that FDG-PET can distinguish benign NF from MPNST with high sensitivity and specificity. Our study further suggests that such a noninvasive functional imaging strategy may serve as a valuable modality to assess potential therapeutic response.

Materials and Methods

Animals. $mGFAP\text{-}Cre^{+};Pten^{loxp/loxp}$ line was generated previously (21) and crossed to $LSL\text{-}Kras^{G12D/+}$ mice (26) on a C57, 129/BALB/c background. Since $LSL\text{-}K\text{-}ras^{G12D/G12D}$ mice are embryonically lethal (27), $Pten^{loxp/loxp};LSL\text{-}Kras^{G12D/+}$ males were backcrossed to $mGFAP\text{-}Cre^{+};Pten^{loxp/+}$ females to produce experimental animals. Similarly, $Nf1^{loxp/loxp}$ mice (47) were crossed with $mGFAP\text{-}Cre^{+};Pten^{loxp/loxp}$, and compound heterozygous animals were backcrossed with $mGFAP\text{-}Cre^{+};Pten^{loxp/loxp}$ mice to produce experimental animals. Mice were observed daily for evidence of illness or tumor formation. If palpable tumors exceeded 1.5 cm in diameter or interfered with feeding and grooming, mice were killed. Animals were housed in a temperature-, humidity-, and light-controlled room (12-h light/dark cycle), and allowed free access to food and water. All experiments were conducted according to the research guidelines of the University of California, Los Angeles (UCLA) Chancellor's Animal Research Committee.

Polymerase Chain Reaction. *Pten*, *Nf1*, or *p53* deletion, *K-ras* activation, and Cre expression were evaluated by PCR using genomic DNA from tail clip biopsy as described previously using standard techniques (14, 47, 48). PCR was performed in 20-μL reactions using standard procedures for 40 cycles; each cycle consisted of denaturing at 94 °C for 30 s, annealing at 60 °C for 1 min 30 s, and extension at 72 °C for 1 min, followed by a single 5-min extension at 72 °C. The PCR products were resolved on 2% agarose gels.

Histology and Immunohistochemistry of Tissue Sections. All tumors were graded according to World Health Organization (WHO) histopathological criteria (32). IHC staining was performed on age-matched control and mutant sections. Five-micrometer sections that were prepared from paraffin-embedded blocks were placed on charged glass slides. The slides were deparaffinized with xylene and rehydrated in descending grades (100–70%) of ethanol. The endogenous peroxidase activity was inactivated in 3% hydrogen peroxide (H_2O_2). After washing in deionized water, antigen retrieval was performed by incubating the slides in 0.01 M citric acid buffer (pH 6.0) at 95 °C for 13.5 min. Slides were then allowed to cool for 30 min in citric acid buffer. After washing in deionized water, the slides were then transferred to either PBS (pH 7.4) or TBST for 5 min. For DAB staining, slides were first blocked with 5% normal goat serum, then incubated with primary antibody overnight at 4 °C. Following three 5-min washes in either PBS or TBST, slides were incubated with biotinylated secondary antibody (1:200; Biogenex) for 30 min at room temperature. Amplification was performed with a horseradish peroxidase system (Vectastain ABC kit, PK-6100; Vector Laboratories) using a liquid DAB peroxidase substrate (HK130–5K; Biogenex). Slides were counterstained in Gill's hematoxylin, dehydrated, cleared, and coverslipped. Negative control slides were run without primary antibody. Primary antibodies used were rabbit anti-PTEN (1:100, 9552; Cell Signaling), mouse anti-PTEN (1:100, 9556; Cell Signaling), rabbit anti-pAKT (1:50, 3787; Cell Signaling), pERK, pS6, S100beta (1:100, 9101 and 2215; Cell Signaling and 1:400, Z0311; Dako).

To map Cre-expressing cells, embryos were cryoprotected in buffered 30% sucrose overnight, and 20-μm frozen sections were prepared. Bright field and fluorescence immunohistochemistry were performed as described previously (27) using biotinylated secondary antibodies (Vector Laboratories), biotin-avidin-peroxidase complex (Vector Laboratories), and diaminobenzidine (Vector Laboratories) as the bright field developing agent or Alexa Fluor-tagged secondary antibodies Alexa 488 (green), Alexa 568 (red) (Invitrogen). Primary antibodies were: Rabbit anti-β-gal (1:200 or 1:6,000; Millipore), rat anti-GFAP (1:500; Zymed Laboratories), sheep anti-S100 (1:200; QED Bioscience). Stained sections were examined and photographed using bright field and fluorescence microscopy (Zeiss) and scanning confocal laser microscopy (Leica).

microPET/CT Imaging and Analysis. microPET/CT imaging was performed with a microPET FOCUS 220 PET scanner (Siemens Preclinical Solutions) and micro-

CAT II CT scanner (Siemens Preclinical Solutions) with UCLA Chancellor's Animal Research Committee approval. Briefly, mice are anesthetized with isofluorane 15 min before receiving ^{18}F-fluoro-D-glucose (200 μCi ^{18}FDG per mouse) via tail vein. The mice are then placed in the imaging chamber and imaged over 1 h in the microPET scanner, followed by a 10-min microCAT scan for anatomical localization. PET images were analyzed with the AMIDE software. Regions of interest (ROIs) were manually drawn on the area of tumor with maximal tracer uptake at 1 mm in diameter. Activity concentrations were quantified as SUVs normalized to injected dose per weight of mouse (mCi/g).

Human NF1-MPNST Analysis. Following UCLA IRB approval for studies on human MPNSTs, the UCLA Sarcoma and Pathology databases were used to identify patients with NF1 who underwent surgical treatment for a MPNST. Slides from the selected cases were reviewed. Whenever possible, we chose cases in which we could identify a MPNST arising from the associated NF and selected sections demonstrating a transition from NF to MPNST. Anonymously labeled sections for immunohistochemistry studies, as detailed above, were prepared by the UCLA Department of Pathology Translational Pathology Laboratory. Additionally, an H&E slide was made from each block to confirm the diagnosis.

ACKNOWLEDGMENTS. We thank members of our laboratories for helpful comments on the manuscript. C.G. and K.B.S. are predoctoral trainees supported by USHHS Ruth L. Kirschstein Institutional National Research Service Award no. T32 CA09056. J.N. is supported by National Cancer Institute (NCI) P50 (P50 CA086306) Career Development Award. This work is supported by the following grants and awards: Miriam and Sheldon Adelson Program (to H.W. and X.L.), National Institutes of Health Grants NS057624 (to M.V.S.) and NS50151 (to P.S.M.), Brain Tumor Funders' Collaborative (to P.S.M., I.K.M., and H.W.), University of California, Los Angeles' Jonsson Comprehensive Cancer Center Foundation (to F.C.E. and S.M.D.), American Cancer Society and National Institutes of Health Grant P50NS052606 (to L.F.P.), Brain Tumor Society Award (to X.L.), and Henry Singleton Brain Cancer Research Program and a James S. McDonnell Foundation Award (to H.W. and P.L.N.).

1. Ferner RE, et al. (2007) Guidelines for the diagnosis and management of individuals with neurofibromatosis 1. *J Med Genet* 44:81–88.
2. Listernick R, Louis DN, Packer RJ, Gutmann DH (1997) Optic pathway gliomas in children with neurofibromatosis 1: Consensus statement from the NF1 Optic Pathway Glioma Task Force. *Ann Neurol* 41:143–149.
3. Ferner RE (2007) Neurofibromatosis 1. *Eur J Hum Genet* 15:131–138.
4. Williams VC, et al. (2009) Neurofibromatosis type 1 revisited. *Pediatrics* 123:124–133.
5. Ferner RE, Gutmann DH (2002) International consensus statement on malignant peripheral nerve sheath tumors in neurofibromatosis. *Cancer Res* 62:1573–1577.
6. Evans DG, et al. (2002) Malignant peripheral nerve sheath tumours in neurofibromatosis 1. *J Med Genet* 39:311–314.
7. Zhu Y, Parada LF (2002) The molecular and genetic basis of neurological tumours. *Nat Rev Cancer* 2:616–626.
8. Dasgupta B, Li W, Perry A, Gutmann DH (2005) Glioma formation in neurofibromatosis 1 reflects preferential activation of K-RAS in astrocytes. *Cancer Res* 65:236–245.
9. Dasgupta B, Yi Y, Chen DY, Weber JD, Gutmann DH (2005) Proteomic analysis reveals hyperactivation of the mammalian target of rapamycin pathway in neurofibromatosis 1-associated human and mouse brain tumors. *Cancer Res* 65:2755–2760.
10. Johannessen CM, et al. (2008) TORC1 is essential for NF1-associated malignancies. *Curr Biol* 18:56–62.
11. Johannessen CM, et al. (2005) The NF1 tumor suppressor critically regulates TSC2 and mTOR. *Proc Natl Acad Sci USA* 102:8573–8578.
12. Gutmann DH, Giovannini M (2002) Mouse models of neurofibromatosis 1 and 2. *Neoplasia* 4:279–290.
13. Brannan CI, et al. (1994) Targeted disruption of the neurofibromatosis type-1 gene leads to developmental abnormalities in heart and various neural crest-derived tissues. *Genes Dev* 8:1019–1029.
14. Jacks T, et al. (1994) Tumour predisposition in mice heterozygous for a targeted mutation in Nf1. *Nat Genet* 7:353–361.
15. Cichowski K, et al. (1999) Mouse models of tumor development in neurofibromatosis type 1. *Science* 286:2172–2176.
16. Vogel KS, et al. (1999) Mouse tumor model for neurofibromatosis type 1. *Science* 286:2176–2179.
17. Bajenaru ML, et al. (2003) Optic nerve glioma in mice requires astrocyte Nf1 gene inactivation and Nf1 brain heterozygosity. *Cancer Res* 63:8573–8577.
18. Zhu Y, Ghosh P, Charnay P, Burns DK, Parada LF (2002) Neurofibromas in NF1: Schwann cell origin and role of tumor environment. *Science* 296:920–922.
19. Yang FC, et al. (2008) Nf1-dependent tumors require a microenvironment containing Nf1$^{+/-}$ and c-kit-dependent bone marrow. *Cell* 135:437–448.
20. Lesche R, et al. (2002) Cre/loxP-mediated inactivation of the murine Pten tumor suppressor gene. *Genesis* 32:148–149.
21. Zhu Y, et al. (2005) Early inactivation of p53 tumor suppressor gene cooperating with NF1 loss induces malignant astrocytoma. *Cancer Cell* 8:119–130.
22. Tuveson DA, et al. (2004) Endogenous oncogenic K-ras(G12D) stimulates proliferation and widespread neoplastic and developmental defects. *Cancer Cell* 5:375–387.
23. Zhu Y, et al. (2001) Ablation of NF1 function in neurons induces abnormal development of cerebral cortex and reactive gliosis in the brain. *Genes Dev* 15:859–876.
24. McLaughlin ME, Jacks T (2002) Thinking beyond the tumor cell: Nf1 haploinsufficiency in the tumor environment. *Cancer Cell* 1:408–410.
25. Carroll SL, Ratner N (2008) How does the Schwann cell lineage form tumors in NF1? *Glia* 56:1590–1605.
26. Soriano P (1999) Generalized lacZ expression with the ROSA26 Cre reporter strain. *Nat Genet* 21:70–71.
27. Faulkner JR, et al. (2004) Reactive astrocytes protect tissue and preserve function after spinal cord injury. *J Neurosci* 24:2143–2155.
28. Ferner RE (2007) Neurofibromatosis 1 and neurofibromatosis 2: A twenty first century perspective. *Lancet Neurol* 6:340–351.
29. Lin BT, Weiss LM, Medeiros LJ (1997) Neurofibroma and cellular neurofibroma with atypia: A report of 14 tumors. *Am J Surg Pathol* 21:1443–1449.
30. Benz MR, et al. (2009) Quantitative FDG-PET accurately characterizes peripheral nerve sheath tumors as malignant or benign. *Cancer*, in press.
31. Ferner RE, et al. (2008) [^{18}F]2-fluoro-2-deoxy-D-glucose positron emission tomography (FDG PET) as a diagnostic tool for neurofibromatosis 1 (NF1) associated malignant peripheral nerve sheath tumours (MPNSTs): A long-term clinical study. *Ann Oncol* 19:390–394.
32. Weiss SW, Goldblum JR (2008) *Soft Tissue Tumors* (Elsevier, Philadelphia), 5th Ed.
33. Bollag G, et al. (1996) Loss of NF1 results in activation of the Ras signaling pathway and leads to aberrant growth in haematopoietic cells. *Nat Genet* 12:144–148.
34. Basu TN, et al. (1992) Aberrant regulation of ras proteins in malignant tumour cells from type 1 neurofibromatosis patients. *Nature* 356:713–715.
35. DeClue JE, et al. (1992) Abnormal regulation of mammalian p21ras contributes to malignant tumor growth in von Recklinghausen (type 1) neurofibromatosis. *Cell* 69:265–273.
36. Murray SK, Breau RH, Guha AK, Gupta R (2004) Spread of prostate carcinoma to the perirectal lymph node basin: Analysis of 112 rectal resections over a 10-year span for primary rectal adenocarcinoma. *Am J Surg Pathol* 28:1154–1162.
37. Li W, et al. (2005) The HMG-CoA reductase inhibitor lovastatin reverses the learning and attention deficits in a mouse model of neurofibromatosis type 1. *Curr Biol* 15:1961–1967.
38. Costa RM, et al. (2001) Learning deficits, but normal development and tumor predisposition, in mice lacking exon 23a of Nf1. *Nat Genet* 27:399–405.
39. Costa RM, et al. (2002) Mechanism for the learning deficits in a mouse model of neurofibromatosis type 1. *Nature* 415:526–530.
40. Saito H, Yoshida T, Yamazaki H, Suzuki N (2007) Conditional N-rasG12V expression promotes manifestations of neurofibromatosis in a mouse model. *Oncogene* 26:4714–4719
41. Levy P, et al. (2004) Molecular profiling of malignant peripheral nerve sheath tumors associated with neurofibromatosis type 1, based on large-scale real-time RT-PCR. *Mol Cancer* 3:20.
42. Castle B, Baser ME, Huson SM, Cooper DN, Upadhyaya M (2003) Evaluation of genotype-phenotype correlations in neurofibromatosis type 1. *J Med Genet* 40:e109.
43. Stemmer-Rachamimov AO, et al. (2004) Comparative pathology of nerve sheath tumors in mouse models and humans. *Cancer Res* 64:3718–3724.
44. Easton DF, Ponder MA, Huson SM, Ponder BA (1993) An analysis of variation in expression of neurofibromatosis (NF) type 1 (NF1): Evidence for modifying genes. *Am J Hum Genet* 53:305–313.
45. Reilly KM, et al. (2004) Susceptibility to astrocytoma in mice mutant for Nf1 and Trp53 is linked to chromosome 11 and subject to epigenetic effects. *Proc Natl Acad Sci USA* 101:13008–13013.
46. Gregorian C, et al. (2009) Pten deletion in adult neural stem/progenitor cells enhances constitutive neurogenesis. *J Neurosci* 29:1874–1886.
47. Zhu Y, Parada LF (2001) Neurofibromin, a tumor suppressor in the nervous system. *Exp Cell Res* 264:19–28.
48. Freeman DJ, et al. (2003) PTEN tumor suppressor regulates p53 protein levels and activity through phosphatase-dependent and -independent mechanisms. *Cancer Cell* 3:117–130.